The Beta Beam

E. Wildner, C. Hansen, E. Benedetto, E. Jensen, T. Stora, T. Melo Mendonca, and V. Vlachoudis
CERN, Geneva, Switzerland

E. Bouquerel
Institut Pluridisciplinaire Hubert Curien, Université de Strasbourg, CNRS/IN2P3, Strasbourg, France

M. Marie-Jeanne, P. Balint, C. Fourel, J. Giraud, J. Jacob, T. Lamy, L. Latrasse, P. Sortais, and T. Thuillier
Laboratoire de Physique Subatomique et de Cosmologie,
Université Joseph Fourier Grenoble, CNRS/IN2P3,
Institut National Polytechnique de Grenoble, Grenoble, France

F. Debray, C. Trophime, S. Veys, and C. Daversin
Laboratoire National des Champs Magnétiques Intenses,
CNRS, Université Joseph Fourier, Grenoble, France

V. Zorin, I. Izotov, and V. Skalyga
Institute of Applied Physics, Nizhny Novgorod, Russia

A. Chancé and J. Payet
CEA, IRFU, SACM, Gif-Sur-Yvette, France

G. Burt and A. C. Dexter
Lancaster University, Lancaster, United Kingdom

V.L. Kravchuk,[*] T. Marchi,[†] M. Cinausero, F. Gramegna, G. De Angelis, and G. Prete
INFN, Laboratori Nazionali di Legnaro, Legnaro , Italy

G. Collazuol and M. Mezzetto
Physics Department, Padova University and Istituto Nazionale di Fisica Nucleare, Padova, Italy

E. Vardaci, A. Di Nitto, A. Brondi, G. La Rana, R. Moro, and V. Palladino
Dipartimento di Scienze Fisiche dell'Universitá di Napoli and Istituto Nazionale di Fisica Nucleare, Napoli, Italy

N. Gelli
Istituto Nazionale Fisica Nucleare, Sezione di Firenze, Sesto Fiorentino, Firenze, Italy

M. Mazzocco and C. Signorini
Dipartimento di Fisica dell'Universitá di Padova and Istituto Nazionale di Fisica Nucleare, Padova, Italy

T.Y. Hirsh
Weizmann Institute of Science, Rehovot, Israel and
Soreq NRC, Yavne, Israel

M. Hass
Weizmann Institute of Science, Rehovot, Israel

D. Berkovits
Soreq NRC, Yavne, Israel

A. Stahl, M. Schaumann, and J. Wehner,
Aachen University, Germany

(Dated: September 1, 2012)

'Beta Beams' produce collimated pure electron (anti-) neutrino beams by accelerating beta active ions to high energies and having them decay in a race track shaped storage ring of 7 km circumference, the Decay Ring. EUROnu Beta Beams are based on CERN infrastructures and existing machines. Using existing machines may be an advantage for the cost evaluation, however, this choice is also constraining the Beta Beams. The isotope pair of choice for the Beta Beam is ^{6}He and ^{18}Ne. However before the EUROnu studies one of the needed isotopes, ^{18}Ne, could not be produced in rates that satisfy the needs for physics reach of the Beta Beam. Therefore, studies of alternative beta emitters, ^{8}Li and ^{8}B, with properties interesting for a Beta Beam have been proposed and have been studied within EUROnu. These alternative isotopes could be produced by using a small storage ring, in which the beam traverses a target, creating the ^{8}Li and ^{8}B isotopes. This Production Ring, the injection Linac and the target system have been evaluated. Measurements of the cross-section of the reactions to produce the Beta Beam isotopes show interesting results. A device to collect the produced isotopes from the target has been developed and tested. However, the obtained rates of the ^{8}Li and ^{8}B, using the Production Ring for production of ^{8}Li and ^{8}B, is not yet, according to simulations, giving the rates of isotopes that would be needed. Therefore, a new method of producing the ^{18}Ne isotope has been developed and tested giving good production rates. The baseline presented for the Beta Beam is therefore now to use the ^{6}He and ^{18}Ne isotopes for neutrino production. A 60 GHz ECRIS prototype, the first in the world, was developed and tested with contributions from EUROnu. The Beta Beam has to take into account the modifications of the injectors planned in view of LHC-upgrades. The Decay Ring lattices for the ^{8}Li and ^{8}B have been developed, the lattice for ^{6}He and ^{18}Ne has been optimized also to ensure the high intensity ion beam stability.

PACS numbers: 25.55.-e, 29.30.Hs,25.70.-z, 25.70.Hi, 25.70.Lm, 29.20.-c, 29.38.Gj, 29.20.D, 29.20.dk, 29.20.Ej, 14.60.Pq

CONTENTS

* kravchuk@lnl.infn.it
† Also at Physics Department, Padova University.

I. OVERVIEW

The idea to produce neutrinos and antineutrinos from beta decay of radioactive isotopes circulating in a race track shaped storage ring originated in 2002 [1]. Beta Beams produce pure ν_e or $\bar{\nu}_e$ beams depending on if the accelerated isotope is a β^+ or a β^- emitter. The neutrino energy depends on the Q-value of the beta decay and of the chosen relativistic γ boost of the stored isotopes. The neutrino spectrum is well known from the electron spectrum and the reaction energy value, Q, is in the order of 10 MeV for the isotopes presently considered for Beta Beams.

To design a Beta Beam facility needs taking into account the neutrino interaction cross-sections and the beam divergence change with Q-values and with the γ-boost of the ions. From this we get we get a merit factor of γ/Q. Consequently, if we choose to increase the neutrino energy by increasing the Q-value of the chosen radioactive isotopes, the required neutrino fluxes from the accelerators will increase approximately with Q due to the fact that we need a longer baseline. Beta Beam physics reach is thus limited by the maximum number of charges that can be accelerated and stored in the accelerators, assuming that the isotopes can be produced in sufficient quantities. By choosing higher γ-boosts, the beam divergence is smaller and the flux of neutrinos in the detector would be better; on the other hand the longer decay times at higher γ require higher circulating currents in the decay ring or longer straight sections. It will also increase the cost of the accelerator. The cost of a Beta Beam facility depends to a large extent on the decay ring size and the choice of magnet technology. Therefore it is beneficial to reduce the arcs, where neutrinos are sent in different directions and thus not useful.

A Beta Beam facility, using the isotope pair ^{6}He/^{18}Ne and a baseline from CERN to Fréjus in France has been studied within the European Framework Program 6, the FP6 EURISOL Design Study (2005-2009) [2]. The studied scenario is based on CERN infrastructure and machines and on existing technologies. To use existing machines and infrastructure for the acceleration of the beta active isotopes is advantageous, however it is also constraining the facility (the machines are not designed for the Beta Beam and co-existence with other physics programs has to be considered in addition). The EUROnu project made it possible to address some crucial aspects of the Beta Beam: isotope production and end to end simulations of the performance and stability of the high intensity ion beams. After the EURISOL Design Study there was an estimated significant deficit in the production of ^{18}Ne. Therefore the EUROnu Beta Beam proposal was based on a new idea to produce neutrinos from the decay of ^{8}Li and ^{8}B with an internal target in a production ring [3]. The concept was studied within EUROnu see section III A and the conclusion was that, for the time being, the technology issues are major and that a redirection of the research was necessary. Another approach was then put forward during the study, namely to produce the ^{18}Ne Isotopes using a molten salt loop target at CERN ISOLDE [4]. Research and measurements ^{18}Ne Isotope production rates from the molten salt target, together with the already performed experiments for the production of ^{6}He, now makes the option of using the isotope pair ^{6}He/^{18}Ne the baseline option for the Beta Beam. The detector would be placed in the Fréjus tunnel, 130km from CERN.

For an optimal sensitivity of the Beta Beam facility to the θ_{13} angle and CP violating phase, a total throughput

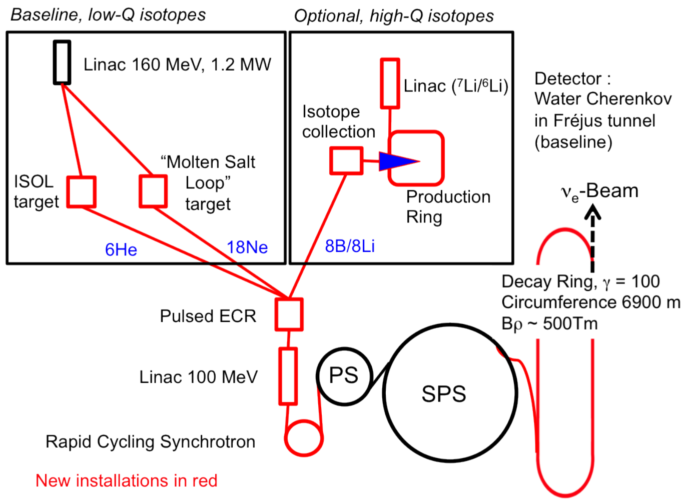

Figure 1. Layout of the CERN Beta Beam. Two beta emitting isotope pairs are considered: ^{6}He/^{18}Ne (low-Q) and ^{8}Li/^{8}B (high-Q) for $\nu_e/\bar{\nu}_e$ production respectively. The Decay Ring has similar dimensions for the two isotope pairs. The inclination angle is 0.6° for a neutrino beam pointing at the Fréjus detector and 3° for a neutrino beam from CERN to Gran Sasso in Italy, or Canfranc in Spain.

of $1.1 \cdot 10^{19}$ neutrinos and $2.9 \cdot 10^{19}$ anti-neutrinos was generally assumed over a running period of 10 years (200 days/year, 50% efficiency). In turn, a top-down approach results in the need for production of about $3.3 \cdot 10^{13}$ ^{6}He radioactive atoms and $2.1 \cdot 10^{13}$ 18Ne atoms per second, taking into account efficiency coefficients along the accelerator chain. Even if the production of ^{18}Ne is a factor of 2 low, the experiment can run longer for the isotope lacking production and still give good physics reach. Today we know that the oscillation angle θ_{13} is relatively large ($sin^2 2\theta_{13}$ is determined to be 0.092 ± 0.016 (stat) ± 0.005 (sys) [5]) and the sensitivity of the Beta Beam to the CP violating phase for this specific value of θ_{13} is now the important performance measure. If, for large θ_{13}, the suppression factor in the detector can be relaxed, these rates may be increased by a redistribution of the ions in the machines (larger number of less intense bunches).

The Beta Beam isotopes are accelerated in an ion Linac after being collected in a charge breeding ECR source. The ionized isotopes then pass through a Rapid Cycling Synchrotron (RCS) [6], the CERN PS synchrotron and the last acceleration stage before the Decay Ring (DR) is the CERN SPS. The Decay Ring [7] would have a circumference of 6900 m and a straight section length of almost 2700 m. The main bending magnet field is 6 T. Consequently superconducting technology is necessary. The presently studied CERN scenarii are shown in figure 1. To use an existing facility for acceleration saves costs for construction of new machines. However it also constrains the scenario in many ways. A considerable part of the efforts spent to make the Beta Beam a solid option for neutrino production deals with the integration of the Beta Beam into the CERN accelerator complex. In the baseline option we have taken an upgraded Linac 4 as proton driver also for production of ^{6}He; this option is used in the costing analysis. An existing SPL may be used for the ^{6}He production but it would not be necessary.

Studies of collective effects i the SPS and in the PS have only started. The Decay Ring work is more advanced. This machine, since not yet constructed, can still be improved and use modern approaches and technology. The PS and the SPS are already today receiving high intensity beams and approach levels of irradiation that need special attention for the longevity of the equipment. Therefore measures are needed to make sure that a Beta Beam can be integrated in the physics program.

Beta Beams are based on the acceleration of beta active isotopes. The life time of the chosen isotopes should be such that we get a sufficient number of decays at high relativistic γ, in the Decay Ring, but as few as possible at the beginning of the acceleration, where decays are not not useful, decay times shorter (the relativistic γ is low). The optimum overall life-time is given by the chosen acceleration scenario and is usually in the order of a second in the ion rest frame. Extraction of the ions from the production target and their transport into the charge breeder (ECR ion source) have to be fast to limit the decay losses. Isotopes generating hazardous waste products, that cannot be safely handled either at the production phase or after decay, would not be an acceptable choice. Isotope production giving a sufficient amount of radioactive ions for acceleration is one of the important challenges for Beta Beams.

Noble gases are chemically stable and therefore good candidates for Beta Beams. The charge-to-mass ratio of the ions has to be large enough for efficient acceleration. Highly charged ions induce space charge phenomena that have unwanted effects on the beam properties. A specific accelerator can accelerate fully stripped ions up to Z/A times its maximum proton energy, where A is the total number of nucleons and Z is the atomic number of the ion. New isotope production and extraction methods have to be specifically developed for Beta Beams.

Two isotope pairs with the required properties have been selected for studying a Beta Beam facility: ^{6}He/^{18}Ne and ^{8}Li/^{8}B for $\bar{\nu}_e/\nu_e$ production. ^{6}He and ^{18}Ne have Q-values of 3.5 MeV and 3.3 MeV, and decay times at rest of 0.8 s and 1.67 s respectively; in this context we refer to them as low-Q ions. The alternative ion pair, ^{8}Li and ^{8}B, has Q-values of 13.0 MeV and 13.9 MeV respectively. The high-Q ions give higher neutrino energy compared to the low-Q isotopes assuming the same ion γ-boost, $E < 2\gamma Q$. But as mentioned above, we need about 5 times higher ion intensities in the machines and collective effects in the accelerated beams may have greater impact on the beam. The production rate of the high-Q isotopes is still far from what is required to get reasonable physics reach for the Beta Beam: the ^{8}Li/^{8}B option still needs considerable research.

In figure 1 the layout for the two options ^{6}He/^{18}Ne and ^{8}Li/^{8}B are shown. The low-Q option, ^{6}He/^{18}Ne, is the Beta Beam that can be proposed as a possible option today. The CERN SPS allows a maximum γ-value of 150 (^{6}He) or 250 (^{18}Ne). The choice of energy, corresponding to a γ-value of 100, was made to optimize the physics reach at a baseline 130 km from CERN where the proposed MEMPHYS detector would be located. This detector in the Fréjus tunnel would be a Mton water Cherenkov.

It is of interest for a neutrino facility is to be able to use existing detectors at strategic distances for physics performance. In the present LAGUNA study [8], the Fréjus site is one of the studied options to place a neutrino detector. The Beta Beam has been laid out on the CERN site for the Fréjus option [9], see figure 2. The beam is extracted from the SPS and injected into the Decay Ring. The ring is oriented so that the neutrino beam is directed towards Fréjus in France.

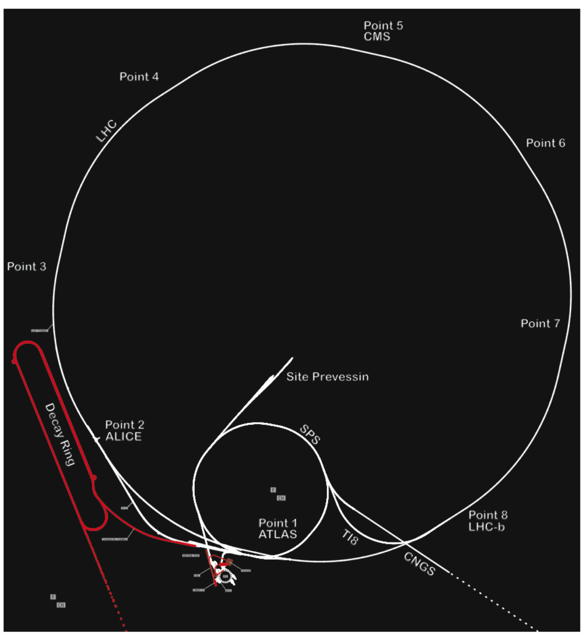

Figure 2. The CERN Beta Beam directed to Fréjus, the inclination angle of the Decay Ring is 0.6° for a neutrino beam pointing at the Fréjus detector.

II. THE PRODUCTION OF LOW-Q RADIO-ISOTOPES FOR THE BETA BEAMS

The demonstration of the technical feasibility of the production of the isotopes required for the beta beams has significantly progressed during the past years. Important developments have been made within the EURISOL-DS project [10]. Part of the study was dedicated to the production of the isotope pair ^{6}He/^{18}Ne, otherwise known as baseline ions, via the isotope separation on-line method (ISOL) [11].

Different production schemes have been proposed depending on the ion type. The production of ^{6}He has been successfully validated using the isotope separation online (ISOL) method [11], where the ions have been obtained with fast neutrons on a thick beryllium oxide target. Experimental tests performed at CERN-ISOLDE showed the validation of the production of 10^{14} ^{6}He/s with 100 μA, 1.4 GeV protons and an optimized geometry [12].

The production of the required 10^{13} ^{18}Ne/s was found to be more challenging and, thus, an alternative route consisting of a circulating loop of molten salt has been proposed [4]. Proton beams close to 1 MW power, from an upgraded Linac4 at CERN, would impinge a circulating molten NaF-based salt to produce extracted rates of 10^{13} ^{18}Ne/s. A first test on the feasibility of the production of ^{18}Ne has been performed at CERN-ISOLDE using a standard static target unit.

A new variant of a production scheme for light radioactive beams has been developed, using a high current deuteron beam and a sequential two-target irradiation. The primary target is essentially a neutron converter, providing a fast and possibly directed neutron source while the actual production takes place separately in a secondary target by fast neutron induced reactions. The efficiency of this setup results from complete separation of the two most major problems in radioactive ion beam production, namely, heat removal of the beam power and extraction of the radioisotopes from the target material.

By using porous, micro-fiber target materials, BeO for ^{6}He and B_4C for ^{8}Li production, respectively, high yields of these isotopes can be produced. This technique is also easily scalable and can thus serve as a firm basis for the utilization of ^{6}He and ^{8}Li as prime candidates for the "beta-Beam" concept.

A review of the progress achieved in the production of the baseline ions will be given in the following subsections.

A. Production of high intensity ^{6}He beams

The production of ^{6}He is obtained with fast neutrons on a beryllium oxide target through the ^{9}Be(n,α)^{6}He reaction, which benefits from high cross-sections over a wide neutron energy spectrum [13]. Neutrons in the 0.1-10 MeV range, of interest for ^{6}He production, are to a first approximation emitted in all directions from solid metal converters that will act as neutron spallation sources. Therefore, a conceptual layout of a dual converter-target assembly has been proposed. As shown in figure 3(a), the assembly is composed by a cylinder made of tungsten or tantalum in the centre of a concentric beryllium oxide production target. In addition, this layout has been adapted to integrate a mechanical support and water-cooling circuit to the converter in order to accommodate a beam of 100 kW, 1 GeV protons. Figure

3(b) shows a preliminary configuration which integrates these different elements.

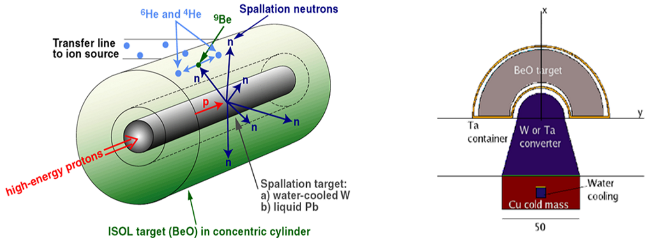

Figure 3. (a) Conceptual dual converter-target unit for 1 GeV protons [10]. (b) Unit with first engineering elements [14].

The validation of the required ^{6}He intensities for the β-beams has been performed with online tests at CERN-ISOLDE [12]. These tests have been performed using a standard ISOLDE unit, as shown in figure 4(a), that consisted of a tungsten neutron converter placed next to a cylindrical target oven containing beryllium oxide target material. This assembly is a simplified version of the optimized geometry developed for the beta beams shown in figure 3(a). The target material was composed by porous, small grained beryllium oxide sintered pellets of density of 2.1 g/cm^3. The pellets have been stacked in a standard 20 cm long and 2 cm diameter oven, which has been further connected to a versatile arc discharge ion source (VADIS) [15] via a water cooled transfer line.

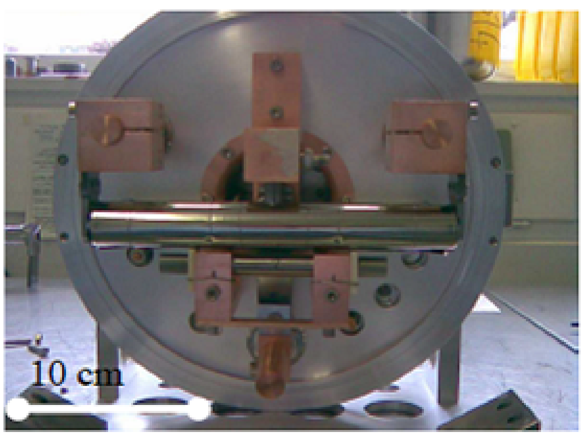

Figure 4. Configuration of the neutron converter (tungsten cylinder and beryllium oxide target used for online tests at CERN-ISOLDE).

The operation parameters, release properties and production ^{6}He yields have been monitored with pulsed 1.4 GeV protons delivered from the PSB accelerator. The extraction efficiency and deduced yields have been measured as a function of the target temperature in a range from 700 to 1400°C.A representative curve showing the release of ^{6}He at 1400°C is shown in figure 5(a). The shape of the curve originates from the diffusion and effusion processes in the production unit, from the beryllium oxide matrix up to the ion source. From the shape of the curve one can observe that ^{6}He is released from the production unit following a rising part and a subsequent decay after the short proton beam impact.

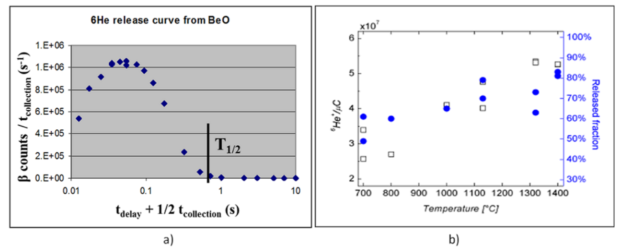

Figure 5. (a) Release curve obtained at 1400°C: time evolution of ^{6}He isotopes/s (black squares) released from the target unit in function of the time after their production at the proton beam impact. (b) Left side scale: experimentally measured yields (empty squares) for different target temperatures; right side scale: release fraction (full dots) determined from the release curves.

The deduced ^{6}He yields (shown in figure 5(b)) from the release curves at different target temperatures showed an in-target production that ranged from 2.6×10^{10} to 4.1×10^{10} ^{6}He/μC of incident protons, in excellent agreement with the calculated 2.8×10^{10} ^{6}He/μC and 2.4×10^{10} ^{6}He/μC using FLUKA and GEANT4, respectively [12]. Therefore, about 82% of the produced isotopes were released at a target temperature of 1400°C, which translates into a release efficiency of 57% at the foreseen beta beam facility [12]. One shall note that in the beta beams configuration, a similar neutron converter beryllium oxide target layout is proposed, with a water-cooled converter to dissipate the deposited beam power of an incoming 200 kW proton beam and a larger target allowing the interception of a larger fraction of the emitted neutrons.

B. Production of ^{18}Ne beams

The production of ^{18}Ne was found to be more challenging The production of ^{18}Ne can be performed by (p, X) (or $(^3He, X)$) reaction on Na, F or Mg targets [16]. The use of targets containing any of these elements would present several advantages on the production of Ne. Amongst the wide list of available molten salts, the best candidate to the present application would be sodium fluoride (NaF). However, the high melting point of this salt (995°C [17]) limits its applications and the use of a binary system containing NaF would be more advantageous.

An extensive list of molten salts is available in the literature due to their application as coolants in nuclear reactors [17, 18] and more recently in optics and solar cells. Two different binary systems have been first proposed as candidates for the production of ^{18}Ne: NaF:ZrF_4

(60:40 % mol) and NaF:LiF (39:61 % mol). Both mixtures present eutectics with melting points at 500°C and 649°C, respectively. A summary of relevant physico-chemical properties is listed in table I.

Table I. List of relevant physico-chemical properties exhibited by the $NaF:ZrF_4$ and NaF:LiF binary systems: composition, melting point (T_M), room temperature density and 900°C vapor pressure (P_{vapor}).

Salt	**Composition (% mol.)**	$\mathbf{T_M}$ **(°C)**	**Density (g/cm^3)**	$\mathbf{P_{vapor}}$ **(mmHg)**
$NaF:ZrF_4$	60:40	500	3.14	5
NaF:LiF	39:61	649	2.75	0.1

The choice of the salt composition has been made on a basis of thermal stability and low vapour pressure at operating temperatures. One shall note that the low vapor pressures of the salt are not only required to keep the stability of the system but it also avoids the change of the molten salt composition that can occur due to incongruent vaporization. Following these criteria, the systems $NaF:ZrF_4$ and NaF:LiF have been carefully investigated in order to obtain the most adequate salt to the present application.

For the synthesis of both binary systems, high purity NaF, ZrF_4 and LiF have been used as starting reactants. Due to the high reactivity of the starting materials, all handling was carried out in dry glove boxes, under argon atmosphere, to prevent oxide contaminations. The synthesis of the binary systems was obtained by mixing stoichiometric quantities of the starting reactants, which have been heated up to about ∼50-100°C above the melting points of each system. The composition and stoichiometry of the obtained salts has been carefully controlled using scanning electron microscopy (SEM) coupled to an energy dispersive x-ray (EDS) detector. The melting point of the mixtures has been identified via differential scanning calorimetry (DSC). Representative SEM micrographs of both binary systems are shown in figure 6.

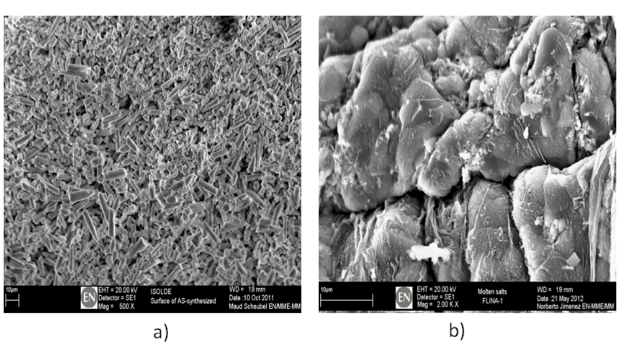

Figure 6. Representative SEM micrographs of the as-synthesized salts: a) $NaF:ZrF_4$, and b) NaF:LiF.

Following the synthesis and characterization, several annealing tests have been carried out to test the stability of proposed binary systems. These stability tests showed that the $NaF:ZrF_4$ system is unstable at the operating temperatures required for the circulating loop operation. This instability is due to high vapor pressure and high reactivity of ZrF_4, that leads to losses of material and consequent changes in its composition. In contrast, the lower vapor pressures and reactivity with air exhibited by the NaF:LiF system proved the suitability of this salt for its use in a circulating loop for the production of ^{18}Ne.

The first test to validate the production of ^{18}Ne from a molten NaF:LiF salt has been performed using a standard target unit at ISOLDE-CERN. The unit consisted of a 21.6 cm long and 2 cm diameter hexacylindrical container made of a special nickel-rich alloy (Haynes 242 [19]) as shown in the schematic representation of figure 7. The choice of the container material has been made accounting for the high reactivity and corrosive nature of the fluoride salts at high temperatures. Furthermore, the dimensioning of the salt target container has been performed accounting for the material and heat transfer properties.

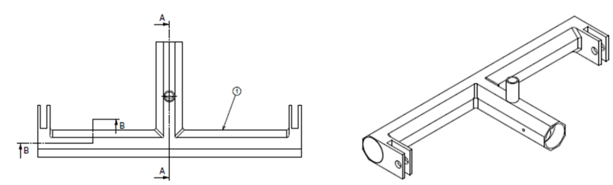

Figure 7. (left) Front view of the haynes target container. (right) 3D schematic representation of the container.

The metallic container was equipped with a temperature controlled condensation chimney with a helix allowing the condensation of less volatile elements. The container was filled with the NaF:LiF melt up to 3/4 of its volume allowing a free surface for the isotopes to diffuse out of the target. Figure 8 shows a picture of the target unit assembly used at ISOLDE for the molten salt tests. The unit was further connected to a versatile arc discharge ion source (VADIS) [15] via a temperature controlled transfer line, suited for the production of noble gases.

The release properties and production yields of ^{18}Ne have been assessed at CERN-ISOLDE with 1.4 GeV from the PSB accelerator. The extraction efficiency and deduced yields have been studied as a function of the target temperature and proton beam intensities. The target unit has been kept above its melting point during the experimental run.

Figure 9 shows representative data of the production yields of ^{18}Ne at different target temperatures and proton beam intensities. The efficiencies required to calculate the atom production from a measured beam intensity were determined previously with stable tracers. From the measured yields at different target temperatures, the

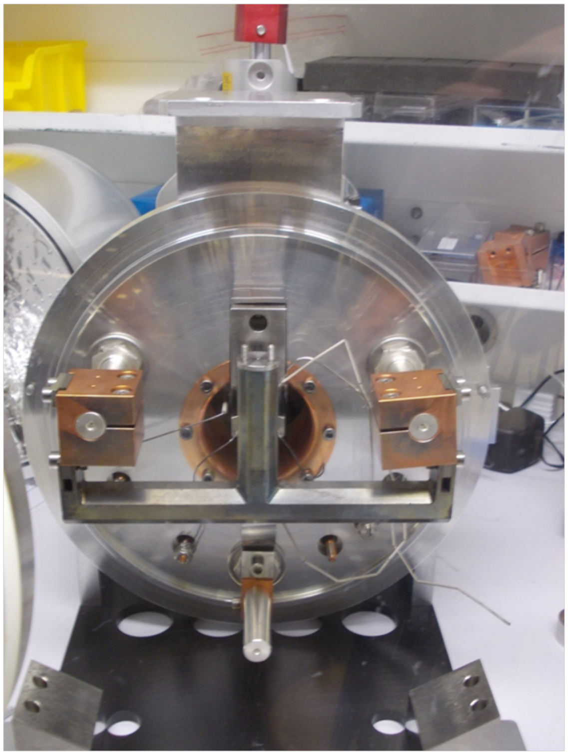

Figure 8. Picture of the molten salt static target unit used at ISOLDE.

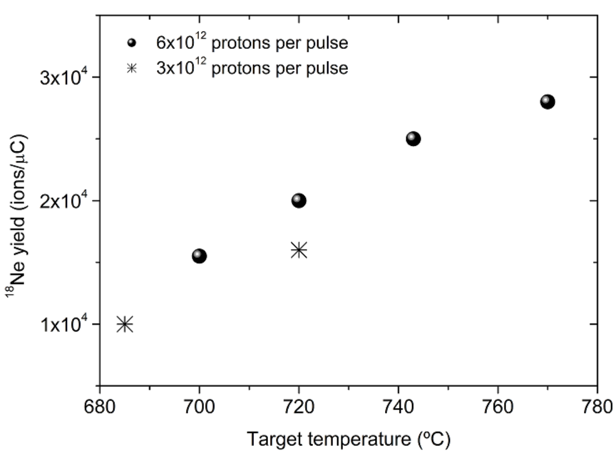

Figure 9. Experimentally measured yields for different target temperatures and different proton beam intensities.

^{18}Ne production varied from $1 \cdot 10^4$ to $3.3 \cdot 10^4$ ^{18}Ne/μC of incident protons. The present results validate the use of NaF-based salts in the production of ^{18}Ne as well as its use in a molten salt loop target. The circulating molten salt target will improve the diffusion time of ^{18}Ne and rates of $1 \cdot 10^{13}$ ^{18}Ne/s are expected for 160 MeV, 7 mA proton beam.

III. PRODUCTION OF THE HIGH-Q ISOTOPES

A. The Production Ring

To produce the ion pair ^{8}Li/^{8}B [3] proposes a compact synchrotron in which a 25 MeV Lithium ion beam circulates and interacts with a D or ^{3}He supersonic gas-jet target, to exploit the ^{7}Li(d,p)^{8}Li and ^{6}Li(3He,n)^{8}B reaction channels. The radioactive isotopes, produced at every passage through the target, are collected by a special device which stops and transports them to the charge-breeder ECR-source by a diffusion/effusion ISOL-like mechanism, for further acceleration through the Beta Beam complex.

The choice of reverse kinematics (projectile heavier than target) has the advantage that most of the primary beam can be recycled, the ^8Li being produced in a narrow cone in the forward hemisphere with a velocity close to the beam velocity. However, since the angular spread of for example ^8Li is confined in a cone of only 11 °, the amount of produced ions implanted for further re-acceleration in a properly positioned absorber will strongly depend on the angular distribution of the reaction products. Consequently, one requirement of the system above is the knowledge of the angular distribution of the produced isotopes.

The stored beam is expected to survive for several thousands of turns, corresponding to the production characteristic time for the target thickness proposed in [3] and according to this scheme, the ionization cooling [20, 21], provided by the target itself and a suitable RF system would be sufficient to compensate for Multiple Coulomb Scattering and energy straggling. First the ionization cooling mechanism is introduced, giving an estimation for the cooling potential for a Beta Beam Production Ring. The lattice design, [22], the ring parameters are then reported. Finally, the tracking simulations work [23] and the results in terms of emittance evolution and beam losses are presented. In the second part, technological solutions and challenges for the production ring, are discussed, with special attention to the requirements for the gas-jet target, the stable Li source, the RF cavity and the vacuum issues. Finally, when the feasibility of the proposal cannot be easily demonstrated and/or when we think it could be an interesting option to be considered, alternative solutions are identified and discussed.

1. *The Accelerator*

In order to produce 8Li and 8B from the reactions ^{7}Li(d,p)^{8}Li and ^{6}Li(3He,n)^{8}B, [3] proposes to use of a compact ring in which a Lithium beam is stored and interacts with a D or^{3}He supersonic gas-jet target. The small synchrotron has a circumference of about 10 m and the kinetic energy of the incoming beam is 25 MeV, giving a relativistic beta of about $\beta_r \sim 0.1$. The ions are injected as Li^{+1} at the target location via a charge-exchange method where the target itself is acting as a charge stripper. At 25 MeV, the circulating beam is fully stripped. The radioactive isotopes, produced at every passage through the target, are emitted in a narrow angular cone of about 8° (section III D). A special collection device (section III B), stops them and transports them to the charge-breeder ECR-source, for further acceleration through the Beta Beam complex. Due to the interaction with the target, the stored beam suffers of longitudinal and transverse emittance blow-up, induced by Multiple Coulomb Scattering and energy straggling. The beam degradation is kept under control with the ionization cooling mechanism provided by the target itself and a suitable RF system.

2. *The circulating beam*

The number of particles N circulating in the ring is given by

$$\frac{dN}{dt} = -\frac{1}{\tau}N + I_{source} \quad (1)$$

Following [3], in order to produce 10^{14} radioactive isotopes per second, the ^{7}Li ion source has to provide I_{source} = 160μA = 10^{15} ions/s. Being τ = 10^4 turns/f$_{rev}$ = 3 ms, the nuclear lifetime, after a few ms transient, there will be some 10^{12} ^{7}Li particles circulating in the ring. For the ^{8}B production, since the nuclear cross-section is a factor 10 smaller, these quantities have to be increased by the same factor.

3. *The Internal Target*

The circulating Li beam is interacting with the production target at every passage in the ring. According to [3] for the energies of interest, the cross-section for the nuclear reaction ^{7}Li(d,p)^{8}Li is about 100 mbarn, while for the ^{6}Li(3He,n)^{8}B reaction it is about 10 mbarn (see also [24, 25]).

The total cross-section, the sum of the nuclear elastic and inelastic reaction cross-sections, which causes the ejection of the particle from the beam, is typically of 1 barn for both ^{6}Li and ^{7}Li nuclei and, assuming a target thickness t = 0.277 mg/cm^2 [3], this corresponds to a nuclear beam lifetime of about $n = 104$ turns.

The blow-up due to Multiple Coulomb Scattering is evaluated using the Moliere rms angle equation:

$$\Theta_c = \sqrt{\langle\Theta^2\rangle} = \frac{14.1\mathrm{MeV}}{\beta_r cp} z\sqrt{\frac{t}{\chi_0}}[1 + 0.038\ln\frac{t}{\chi_0}] \quad (2)$$

where $\beta_r c, \gamma_r, p$ and z are the velocity, relativistic mass factor, momentum and charge of the incident ion and χ_0 is the radiation length.

The mean energy lost at the target is estimated via the Bethe-Bloch formula [26]:

$$\Delta E_{BB} = \langle\frac{dE_L}{dx}\rangle t \Rightarrow \quad (3)$$

$$\Delta E_{BB} = Kz^2\frac{Z}{A}\frac{1}{\beta_r^2}[\frac{1}{2}\ln\frac{2m_ec^2\beta_r^2\gamma_r^2T^m}{I^2} - \beta_r^2 - \frac{1}{2}\delta(\beta_r^2\gamma_r^2)]t \quad (4)$$

where A, Z and I are the target atomic mass, charge and mean excitation energy. The quantity

$$T_m = \frac{2m_ec^2\beta_r^2\gamma_r^2}{1 + 2\gamma_r m_e/M + (m_e/M)^2} \quad (5)$$

is the maximum kinetic energy which can be imparted to a free electron in a single collision, with m_e the electron mass and M the mass of the incident particle, and

$$K = 4\pi N_A r_e^2 m_e c^2 \quad (6)$$

is a constant, r_e the classical electron radius and N_A Avogadro's number.

For a target thickness of t = 0.277 mg/cm^2 [3], the average energy lost by a Lithium ion is 300 keV, value that needs to be restored by a strong RF system.

Energy fluctuations are assumed to have a Gaussian distribution, with an r.m.s. width of about $\sqrt{\langle\delta^2_{rms}\rangle}$ = 15 keV, as from Table 1 in [3]. Losses due to single large-scattering events [27] and by Intra-Beam Scattering are for the time being not included in the computations.

4. *Ionization Cooling*

The ionization cooling [20] is recently receiving large attention for the fast cooling of muons for a Neutrino Factory or a Muon Collider [21]. It is based on the principle that a beam traversing a material looses energy and only its longitudinal component is recovered in the RF cavities, with the net effect of a transverse emittance shrinking.

In analogy to synchrotron radiation damping, one can introduce [21] partition numbers, whose sum is invariant, to characterize the cooling rates in the three planes and define equilibrium emittances from the balance between the cooling terms and the heating ones.

The challenge of applying ionization cooling for low-energy ions resides in the strongly negative slope of the Bethe-Bloch formula [26] for the energies of interest. In particular, $(\delta E_{loss}/\delta p) < 0$ means that for an increase of particle momentum, the energy losses in the material becomes weaker, thus causing strong heating, instead of cooling, in the longitudinal plane. Longitudinal cooling can be achieved by introducing coupling with the horizontal plane via the dispersion and by using a wedge-shaped absorber in a dispersive region, but since the sum of the partition numbers is a constant (and in this case only slightly positive [28]), one can achieve longitudinal cooling only at expenses of the transverse one. Following the derivation of [21], and using parameters from [3, 22] for the Production Ring we find that [23] we have to introduce coupling in the transverse plane, in the region of the target, to achieve cooling on the longitudinal plane. This can be done by introducing a wedge shaped target and using the dispersion in the target area. However the total cooling power, which is the sum of the partition numbers in the three planes, cannot be changed.

The result of the analysis shows that for the case of the Production Ring for Beta Beam isotopes, using a ^{7}Li or ^6Li beam at 25 MeV impinging on a D or ^{3}He target, the cooling efficiency is very low, almost zero. This depends on the slope of the Bethe-Bloch equation and could be improved only by changing the beam energy, on which there is not much freedom since it is set to optimize the production cross-section. The practical meaning, for the Production Ring application, is that there is a very small margin for cooling and only in the case of perfect emittance exchange, achieved by coupling the longitudinal plane both with the horizontal and with the vertical, it will be possible to keep the beam size under control, as already pointed out in [28].

5. *The Proposed Lattice of the Production Ring*

The optics of the 12mÐlong production ring for the 25 MeV ^{7}Li ions (to produce ^{8}Li iso- topes) is shown in figure 10 and the design is well documented in [22].

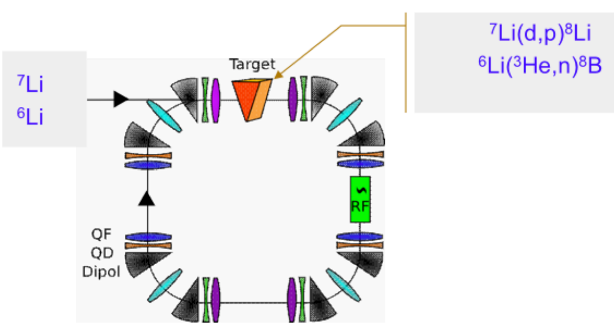

Figure 10. The production Ring

The ring has a two-fold symmetry: two of the straight sections have zero dispersion, in order to accommodate the RF cavity(ies), the other two, instead, have an horizontal dispersion of 50 cm, as required by the specifications for the production target, which will be installed in one of them. Table 1 summarizes the ring parameters.

For the simulations, the working point of (2.58,1.63) has been chosen. The horizontal β_x is for the moment of about 2.6 m at the target and leads to important beam blow-up due to Multiple Coulomb Scattering.

For particles with 'large' momentum offset (i.e. of the order of 1%), the large negative chromaticity may induce resonance crossing and losses. A first attempt to include sextupoles in the lattice to compensate the chromaticity led to dynamic aperture problems. A trade-off between the increase in tune spread and the reduction in dynamic aperture has to be found. Moreover, a large second order dispersion in the straight sections leads to a non-zero dispersion in the RF cavity for particles with a 1% momentum offset and to a 10% difference in the cooling section, which may need to be taken into account. This lattice, which still needs to be tuned for optimizing the cooling efficiency, is used to set-up tracking simulations and for identifying the parameters to reduce the blow-up ([29]).

6. *The code SixTrack for the Production Ring*

SixTrack [19] is a fully 6D, single-particle tracking code, based on high order truncation of Taylor expansion, which is widely used at CERN for dynamic aperture studies and for collimation. The code had to be adapted for the Production Ring simulations. The production target has been implemented in the code as a special element and the interaction with matter modeled by simple analytical formulas. Since SixTrack can only deal with protons, an equivalent proton beam is tracked, with the same rigidity (Bρ) and the same momentum $\Delta p_{RF}/p$ recovered at the RF-cavity. Before the interaction with the target, the proton energy is converted to the ^{7}Li equivalent and then back again after the target [22]. The equivalent proton energy is 19 MeV and the energy recovered at the RF cavity is ΔE_{RF}=0.22 MeV for the reference particle. The RF voltage and synchrotron phase, for an harmonic number h = 1, have been set to V = 860.6 kV and ϕ_s = 15°, from considerations of bucket height, but this can be further tuned. Furthermore, a few beam diagnostics elements have been included in SixTrack, e.g. the possibility to have the turn by turn r.m.s. emittance evolution in the three planes.

Since SixTrack is mainly used for LHC tracking and, since there is not much experience with low energy ma-

Table II. Beta-Beam requirements for the Production Ring

Production Ring Parameters		
Particle		^{7}Li
Kinetic energy	E_{BB}	300 keV
Relativistiv mass factor	γ_r	1.00383
Beam rigidity	Bρ	0.636 Tm
Circumference	C	12 m
Revolution frequency	f_{rev}	2.18 MHz
Transition γ	γ_t	3.58
Tune	$Q_{x,y}$	2.58, 1.63
Natural chromaticity	$Q'_{x,y}$	-3.67,-3.58
β @ target	$\beta^*_{x,y}$	2.62 m, 0.35 m
Dispersion @ target	$D^*_{x,y}$	0.523 m, 0 m
Target thickness	t_0	0.27 mg/cm^2
Target thickness	n_t	10^{19}atoms/cm^2
Energy loss @ target	E_c	25 MeV

chines, it was necessary to perform a benchmark with MADX and PTC. Beta functions and dispersion for one half of the ring, for a momentum offset of 1% has been calculated and results have beed compared. Even for this 'large' momentum offset, both MADX and SixTrack, which are using a truncated Taylor expansion, are in very good agreement with PTC, which is using the exact Hamiltonian.

For a rectangular target some expected blow-up in the momentum spread was found and indeed some cooling in the transverse plane up to about 300 turns. However when the momentum spread goes above 2% the transverse emmittances increase considerably. The particles are lost in the dispersive regions. The emittance blow-up in the transverse plane may have two explanations: the uncorrected chromaticity may cause resonance crossings and the large second order dispersion at the place where the emittance is computed generates an artificial emittance increase due to particles with non zero dispersion whose invariant is not correctly evaluated at this stage.If the analysis is restricted to 300 turns the values found in the simulations are in agreement with the analytical estimations for the transverse equilibrium emittances of ϵ_x=87.7 mm mrad and ϵ_y=11.7 mm mrad

7. *The choice of wedge-angle*

A wedge-shaped target in a dispersive region is used to transfer the cooling from the horizontal to the longitudinal plane. By linearizing the Bethe-Bloch formula, with respect to the target thickness variation Æt and the particle energy offset δE, one obtains:

$$E_{BB}(t, E_c) \approx \left.\frac{dE}{ds}\right|_{E_{c0}} t_0 + \left.\frac{dE}{ds}\right|_{E_{c0}} \Delta t + \left.\frac{\partial E}{\partial s}\right|_{E_{c0}} t_0 \Delta E_c \tag{7}$$

The first term is the mean energy lost by a beam of nominal energy E_{c0}, traversing a target of uniform thickness t_0, and it is the energy recovered in the RF-cavity by the synchronous particle. The second and third terms both depend on the particle momentum offset (δp/p):

$$\Delta E_c = E_c \frac{\gamma_r + 1}{\gamma_r} \frac{\Delta p}{p} \tag{8}$$

$$\Delta t = 2\rho \tan\frac{w}{2} \Delta x = 2\rho \tan\frac{w}{2} \Delta x D^* \frac{\Delta p}{p} \tag{9}$$

where ρ is the target density, w is the angle of the wedge and Δx is the horizontal offset, induced by the dispersion D^* at the target. By playing with the dispersion and the wedge-angle it is possible to compensate for the difference in mean loss value due to different particle energy and, in particular, to fully compensate for the losses dependence on the momentum offset if:

$$D^* tan\frac{w}{2} = \frac{1}{2\rho} \left(\frac{dE}{ds}\right)^{-1}_{E_{c0}} \frac{\gamma_r + 1}{\gamma_r} \frac{\partial}{\partial E_c} \left.\left(\frac{dE}{ds}\right)\right|_{E_{c0}} t_0 E_c \tag{10}$$

From these considerations, the angle necessary to keep a constant momentum spread, thus to have no blow-up in the longitudinal plane, is $w = 15°$, but, if one would chose this value, the blow-up in the horizontal plane would be too large and would lead to losses comparable to the zero-wedge case. Indeed, a $w = 6°$ angle is the best compromise between the blow-up in the horizontal and longitudinal planes (see [30] for more details).

For a $w = 6°$ angle, the momentum spread increase is smaller than in the case of a rectangular target ($w = 0°$), but this is obtained at the expense of a more important horizontal blow-up. In the vertical plane the cooling is the same as before, since there is no coupling. Increasing the wedge angle to as high as 12° leads again to strong losses, due to the uncontrolled horizontal blow-up. Even for the best case ($w = 6°$), after 900 turns 60% of the beam is lost in the machine. This has to be compared to the expected production rate, which generates a decrease of the circulating beam with a characteristic time of ∼104 turns. These results can be improved by minimizing the horizontal beta function value at the target position and by introducing coupling with the vertical dimension, to share the cooling power in the three planes.

8. *The primary ions source challenges*

According to [3], for the energies of interest for the ^{6}Li and ^{7}Li nuclei, the total cross-section is of the order of 1 barn. For the nuclear reaction ^{7}Li(d,p)^{8}Li, the cross section is about 100 mbarn at 25 MeV, see III D, meaning that 10% of the interacting particles will produce a useful isotope. Therefore, in order to reach the 10^{14}/s radioactive isotope flux from the production ring, as required from physics, one would need 10^{15}/s ^{7}Li particles injected. Assuming 100% transmission efficiency in the linac, this corresponds to 160 μA from the ^{7}Li source. Existing ECRIS only reach some $\sim 30\mu$A.

The primary ion intensity is not considered to be a show-stopper for the ^{8}Li production, since several sources could be added in parallel to feed the linac, and/or R&D has to be pushed.

For the ^{6}Li(^{3}He,n)^{8}B reaction, the cross section is less III C so more intensity should be provided from the source, which is challenging.

9. *The production Ring RF cavity*

By traversing the 0.27 mg/cm^2 thick internal target, the Lithium ions will loose about 300 keV [3]. This energy has to be restored by an RF cavity. Since the revolution frequency is ∼ 3MHz, and the harmonic number should be as small as possible, a low-frequency cavity is needed. Moreover, the cavity should be as compact as possible, because of the space constraints. The solution is to use an evacuated cavity with capacitive loading, in order to keep the size below 2m. A typical example at CERN is the bunch rotation cavity for ACOL (now used in the AD) which reaches 750 kV at 9.55 MHz [31]. It is a pulsed device dissipating 660 kW at full voltage. At 300 kV, operation in CW would be feasible.

10. Charge exchange injection

Particles are injected in the ring as Li^{1+} ions at the gas-jet target location, which will also act as a stripper, and the circulating ions will be fully stripped. The transfer line and the injection have to be designed, however the design will be simpler than for standard H^- injection systems, as the stripper will stay in the circulating beam being the target itself.

11. Beam scraper

In order to clean out large amplitude particles and have losses concentrated in one location, a beam scraper can be envisaged e.g. in the dispersive region opposite to the target.

12. Target

In order to produce a sufficient number of beta-emitters per second, the gas-jet target density should be extremely high. In [30] is shown that today existing gas-jet and cluster-jet target reach a maximum of 10^{15} atoms/cm^2, which is 4 orders of magnitude less than the thickness proposed in [3] and that the needed gas flows would be a problem for the vacuum in the Production Ring.

13. Discussion of possible solutions

The required 10^{19}atoms/cm^2 thick gas-jet target in the accelerator vacuum environment represents the most crucial issue for the feasibility of the Production Ring. Possible solutions have been investigated:

- Increasing the injected beam intensity, to reach the required ion production rate, is not feasible, since the proposed stable-ion sources are already at the limit of or beyond the available operational currents
- Living with a poor vacuum in the machine, which could be a solution as long as the residual gas is ÒthinÓ with respect to the jet-target, causes multipacting in the RF cavity and it is therefore not feasible.
- Separating the target by 'thin' windows causes a significant additional emittance growth and extra RF power to compensate for energy losses.
- Working at different energies is not an option, since 25 MeV is already the best compromise between good production cross-section (which decreases with increasing energy) and stripping efficiency.
- Running with a 'conventional' gas-jet target, with a 4 orders of magnitude lower thickness, decreases the production rate by the same amount. This is partly compensated by the increase in lifetime which will also increase the circulating beam current. The space charge limit is anyway at about 10^{12} ions/bunch therefore only a factor 10 can be gained. Moreover, since the energy lost and recovered in the RF cavity is smaller as well, the cooling rate is also lower by the same amount, therefore ionization cooling may not be efficient.
- Using already existing CERN rings, such as AD, ELENA or LEIR, deserves feasibility studies. They have a larger circumference which allows the storage of a higher number of ions, for the same space-charge constraints, and they are equipped with electron cooling, in case ionization cooling is weak. This solution is not as elegant as the one proposed in [3], but it may be considered if the production rates are high enough.
- Having a solid or liquid target allows to reach 10^{19} atoms/cm^2 target thickness. In this case it is preferable to have a Lithium target and a Deuterium or Helium beam (direct kinematic). This is for the time being our preferred option and it is under study.

14. Production ring Conclusions

We have analyzed in detail the proposal by [3] to use a compact ring with an internal target to produce ^{8}Li and ^{8}B isotopes for the Beta Beams. A preliminary ring design is available. The optics studies have been done for the ^{7}Li(d,p)^{8}Li inverse kinematics case, but they can be easily scaled to the other reactions. Due to the strongly negative slope of the Bethe Bloch function at the energies of interest for the isotopes production, the total budget of ionization cooling that can be achieved is very low, almost zero, therefore one should not expect sensitive emittance reduction but, in the best case, only control of the beam blow-up. 6D tracking tools are fully in place and predict what expected from analytical ionization-cooling considerations. SixTrack code allows us to see also the high order effects, e.g. chromaticity and second order dispersion, therefore the blow-up that is seen in the simulations is explained and could be corrected, although it is not so straightforward due to the small periodicity of the machine. The lattice requires careful tuning to maximize ionization-cooling efficiency and in particular the beta function at the target position needs to be reduced as much as possible. Coupling with the vertical plane should be introduced as well. Feasibility studies identified as a major issue the large thickness (10^{19}atoms/cm^2) required for the gas-jet target in a vacuum environment. The direct kinematics approach looks more feasible for the point of view of the target density, although the thin liquid-films technology (used as heavy-ion strippers and as targets in nuclear physics) is still in early R&D.

B. The Collection Device

1. ^2H (^7Li,^8Li) p. Validation for the ^8Li

The experiment was performed with ^{7}Li2$^+$ beam provided by the isochronous cyclotron of the Centre de Recherches du Cyclotron at Louvain-la-Neuve. The R&D work was organized in two phases: first, the design and construction of a collection device which will be validated with ^{8}Li, then the experimental study of the possible ways to extract ^{8}B from the collection device.

The inverse kinematics scheme was used. The ^{7}Li beam accelerated to 30 MeV by the cyclotron is sent on a gas cell filled with D_2 at about 150 mbar. After the energy losses in the foils in front of the gas the energy of the ^{7}Li beam is 24.9 MeV. The D_2 gas target is made of a Copper cylindrical cell, 17 mm in diameter and 15 mm in length, closed by two Tantalum windows 5 and 2 μ thick. The beam current is monitored by the scattering of the ^{7}Li beam on a gold foil installed just before the gas cell. The backscattered ions are detected by a Silicon detector (PIPS detector 300 μm thick) which is mounted at an angle of 166°. The typical beam intensity for the ^{8}Li runs is 10 pnA. In order to discriminate the production of the secondary particles, the beam was very well collimated with Ta collimators. The recoiling ^{8}Li are collected in a tantalum tube (d=28mm, l=112mm) in which they are slowed down by a set of 2 μm thick tantalum foils. A diffusion pipe (d=8mm, l=118mm) bring the ^{8}Li atoms to a cold plate in front of a telescope made of 2 plastic scintillators to detect the beta decay (see figure 11). A set of power supplies allowed heating this collection device in order to favor the diffusion of the ^{8}Li ions.

The production of ^{8}Li is measured by detecting β^- associated with the ^{8}Li β-decay (figure12). In order to identify the nature of the secondary particles produced in the runs, the beam is pulsed and the betas are registered during the beam-off period only.

The time structure of the ^{8}Li experiments is given in figure 13. During a total cycle of 6 s, the beam is on the target during 2 s. After a time interval of 5 ns, the measurement starts during 4 s.

In parallel, a second setup (without collection device and oven) is used to measure the overall production of

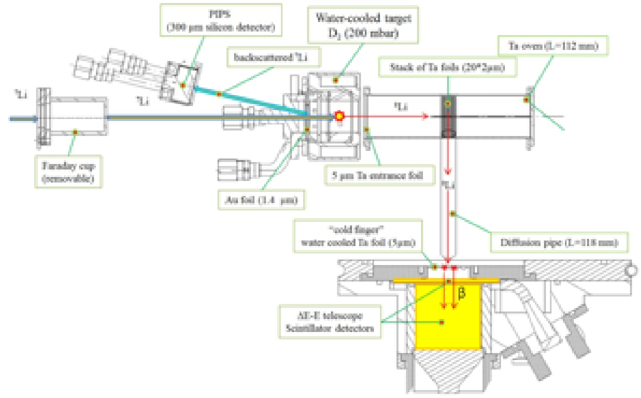

Figure 11. Experimental setup for the ^{8}Li runs.

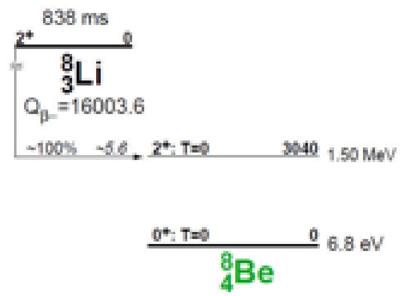

Figure 12. : Partial level scheme of the ^{8}Li decay.

^{8}Li and to check our detection system ('integral measurement'). See figure 14. The time structure is different; the beam is on the target during 2 s and afterwards the betas are detected during 8 s.

To decrease the production of other products induced by the^{7}Li beam we used degraders (Cu and Al foils, with respect of the Coulomb barrier value) See figure 14. To avoid any normalization factors and to keep the same geometry (dimensions, distances, angles) we used the same target unit in both cases. Figure 15 shows the decay curve of ^{8}Li obtained in the integral measurement. The obtained lifetime is very close to the value in the literature. The calculated efficiency of the detection system (the ratio between the amount of ^{8}Li we detect and the amount of ^{8}Li we produce in the target) is 27% with an uncertainty of 2%. This value can be explained knowing the geometry of our setup: we stop the Li8 nuclei in foils in front of the scintillators telescope and this gives us a geometrical efficiency around 31%.

The quantity of ^{8}Li produced during a run is calculated from the amount of backscattered beam, from the amplitude of the ^{8}Li exponential decay curve and from a factor which takes into account the time structure of the measurement. After the validation of our detection system we start measurements with the collection device with a oven. Usual decay curves at different temperatures are

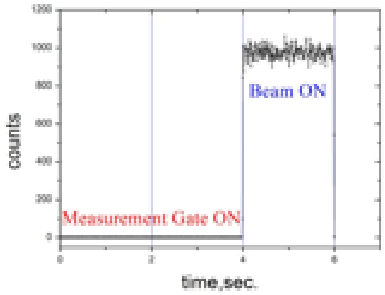

Figure 13. Time structure used in the experiment.

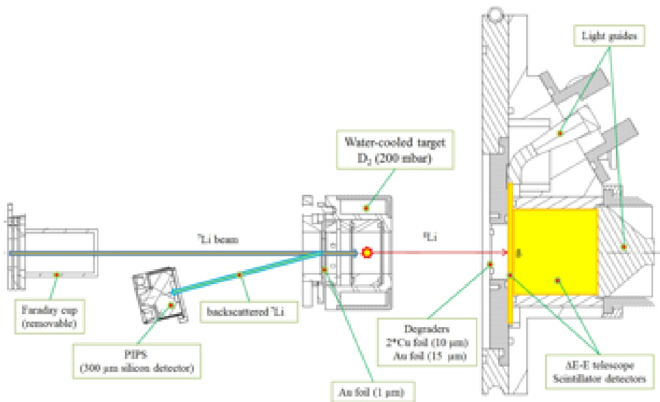

Figure 14. Experimental setup without collection device.

shown in figure 16 a and b.

2. ^{3}He (^{6}Li,^{8}B) n. B8 experiments

Knowing that the setup is working properly the ^{8}B measurements ia started. The ^{8}B nuclei are produced by the reaction ^{3}He (^{6}Li,^{8}B) n. The ^{6}Li beam accelerated to 32 MeV by the cyclotron is sent on a gas cell filled with ^{3}He at about 200 mbar. After the energy losses in the foils in front of the gas the energy of the ^{7}Li beam is 29.3 MeV. Once again, in order to be able to compute an extraction efficiency, we have first to know the amount of produced ^{8}B ions ('integral measurement'). The typical beam intensity for the ^{6}Li runs is 2 pnA (figure 17).

We want to try two completely different extraction schemes. In the first one, the ^{8}B are slowed down in a stack of heated Ta foils and we want to see whether the ^{8}B ions are able to escape as is the case with Li ions. In the second schema, the ^{8}B are slowed down in AlF_3 in which we could observe an exchange reaction B + AlF_3 -> Al + BF_3. BF_3 is a gas which can diffuse very easily up to the detection setup, if it is not dissociated by a too high temperature.

In the first case (stack of Ta foils) the extraction and

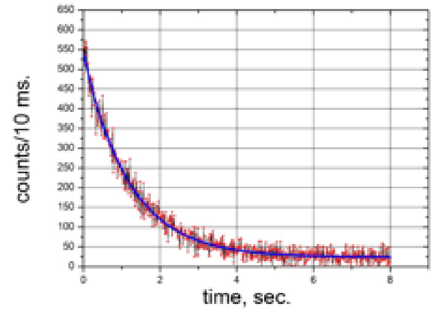

Figure 15. Decay of ^{8}Li (setup without the collection device). χ^2/n = $T_{1/2}$ = 826 ms in comparison with $T_{1/2}$ = 840 ms (from in literature adopted value).

diffusion of the ^{8}B ions is negligible and the decay curves are flat, consistent with a small random background (figure 18).

In the second case we fill the oven with AlF3 powder and heat the collection device to rise the effusion of BF_3. The most representative plots are shown in figure 19.

While the detected ^{8}B amount is negligible at 320 and 540 °C, ^{8}B is obviously produced and extracted at 440 °C. A possible explanation (which should be confirmed by additional measurements) is that at low temperatures the extraction efficiency is too low but at higher temperature the BF_3 molecule is broken, giving an optimum at around 440 °C. The observed extraction efficiency at 440 °C is 0.53±0.08 %. The most reasonable explanation of a so low efficiency is that a lot of BF_3 is lost before it will reach the detection system: the tightness of the setup to deliver the BF_3 up to a 'cold finger' cooled with liquid nitrogen should be improved. This experiment is planned for around December 2012.

C. ^{8}B cross section measurements

The EUROnu Beta Beam development needs measurements cross sections and angular distributions of the reaction products ^{8}B and ^{8}Li from the reactions:

- ^{3}He + ^{6}Li $->$ ^{8}B + n (subject of this paper)
- ^{7}Li + d $->$ ^{8}Li + p (see the paper of E. Vardaci *et al. ibid.* [32]).

The ^{8}B nucleus is considered as a neutrino source producing relatively high-energy neutrinos [33]:

- ^{8}B $->$ ^{8}Be + e^+ + ν_e (with the decay time of 0.77 s.)

The results of these measurements are necessary to design the tabletop accelerator and the other necessary equipment that will be used for the production of these

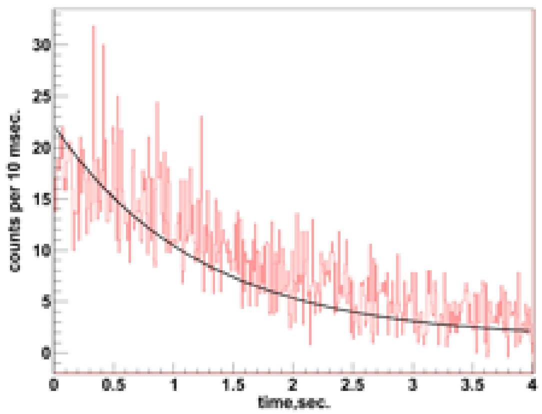

(a) 1450 °C

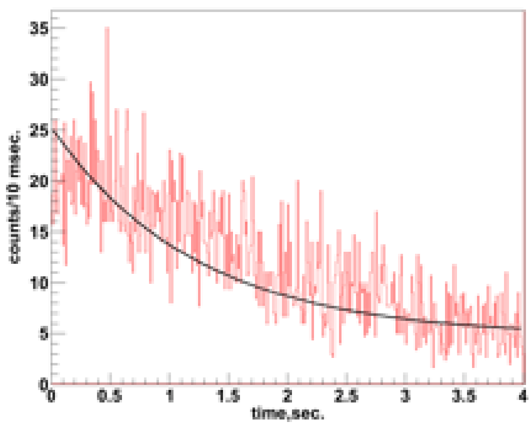

(b) 1650 °C

Figure 16. Decay of ^{8}B (setup with the collection device) at 1450 °C and 1650 °C. χ^2/n (1450°C) = 574.7/397 ; χ^2/n (1650°C)= 494.4/398

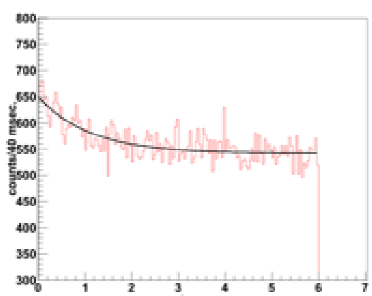

Figure 17. Decay of ^{8}B (setup without the collection device). $\chi^2/n = 596.9/597$ $T_{1/2} = 639$ ms in comparison with $T_{1/2} =$ 770 ms (from in literature adopted value).

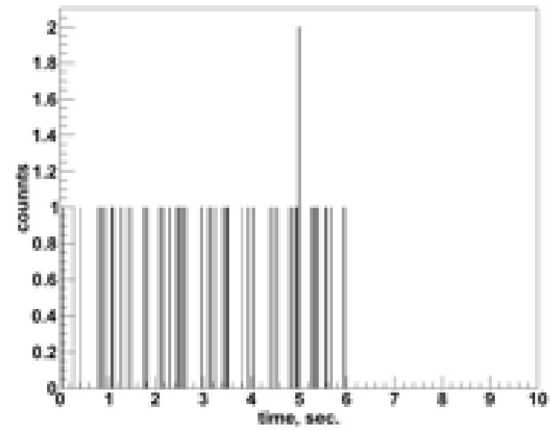

(a) 700 °C

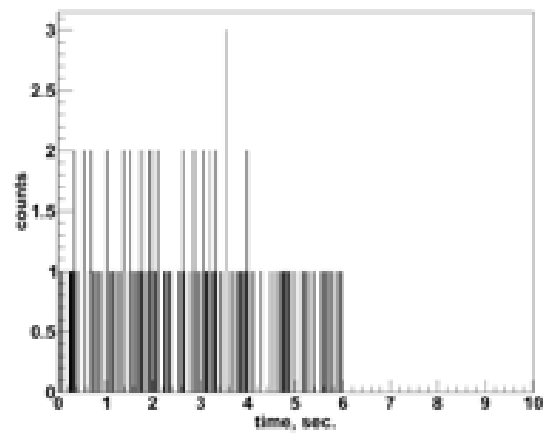

(b) 1700 °C

Figure 18. Decay of 8B (setup with the collection device) at 700 °C (a) and 1700 °C (b)

isotopes, in particular to assess the performance of an internal target that also serves as a stripper and an absorber for ionization cooling of the circulating beam proposed by C. Rubbia *et al.* [3].

The total cross section of the ^{8}B production in the ^{6}Li(^{3}He,n)^{8}B reaction was measured previously by using two different techniques. The results of the experiments using the measurement of the ^{8}B positron decay reported in [25] and considered in the original proposal of C. Rubbia *et al.* [3] demonstrate the total cross section with at least a factor of 3 smaller with respect to the results from the experiment using neutron time-of-flight method [34]. The results reported in [24] at the bombarding energies above 8 MeV are not in agreement with the work of the other groups. Moreover, uncertainties of some experimental results are reaching 15-20%. Therefore, our aim was to accurately measure absolute cross section and the angular distribution of ^{8}B produced in the ^{6}Li(^{3}He,n)^{8}B reaction by using the neutron-time-of-flight techniques employing the digital electronics, collecting high statistics and performing pulse-shape analysis (PSA).

1. *Experiment*

The experiment was done at the CN 7 MV Van De Graaff accelerator of Laboratori Nazionali di Legnaro.

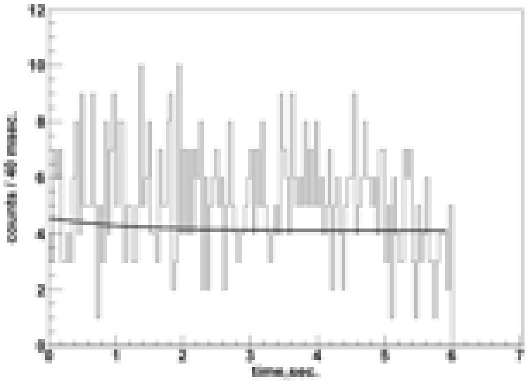

(a) 320°C

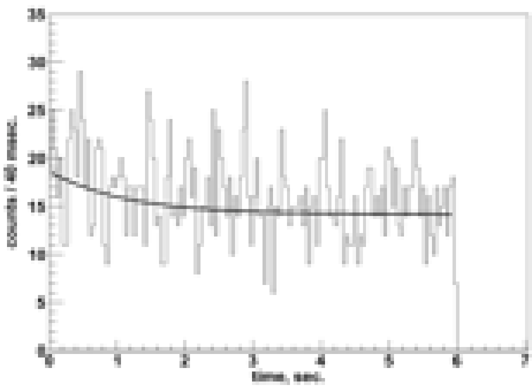

(b) 440 °C

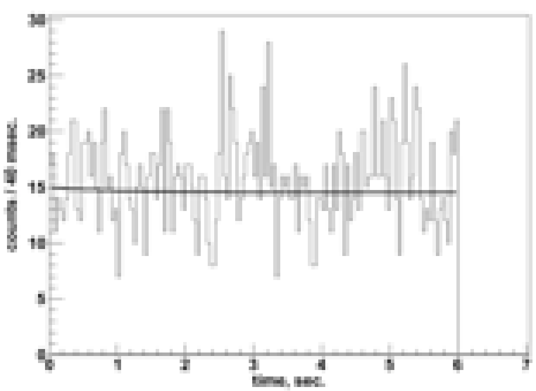

(c) 540 °C

Figure 19. Decay of 8B (setup with the collection device and AlF_3) at 320 °C (a), 440 °C (b) and 540 °C (c)

The $^6Li(^3He,n)^8B$ reaction was studied using a 6.1 MeV pulsed ^3He beam onto a LiF 500 $\mu g/cm^2$ thick target. The LiF target was 95% enriched in ^6Li and evaporated on a 500 $\mu g/cm^2$ thick Au backing. To minimize Li evaporation the target was cooled during the experiment and the gold backing was mounted towards the beam. The resulting beam energy after passing the Au and at the middle of the LiF target was 5.77 MeV The pulsed beam structure was characterized by a 333 ns repetition rate and a 2 ns time resolution.

The emitted neutrons were measured via the time-of-flight techniques by using 8 large volume BC501 liquid scintillation detectors of the RIPEN modular array [35] upgraded with digital electronics. The detectors were placed at the distance of 2 m from the target at the angles of 15, 23, 31, 39, 50, 80, 110 and 140 degrees. A ΔE (15 μm) - E (200 μm) Silicon Telescope placed inside the scattering chamber at 150 degrees and at the distance of 56.5 mm from the target was used to comtinuously monitor the current intensity through the elastically scattered ^3He particles on gold. Possible contaminations have been taken into account and their evaluation have been considered through appropriate measurements. In particular measurements of ^3He on ^7LiF, ^{12}C have been performed. In addition, a measurement with no target has been performed for background determination.

The scintillator and silicon detectors signals were recorded using two CAEN V1720 digitizers (12 bit, 250 Ms/s) in the 8 channels VME version communicating with a standard PC via a VME bridge (CAEN V1718). The software used for the data acquisition is a customized version of CAEN WaveDump, able to handle and synchronize two or more digitizers. Three different kinds of information are expected to be obtained processing the scintillator signals: the energy release of the impinging particles, its time of flight and the pulse shape discrimination between neutrons and gammas. Data are processed using algorithms able to perform RC/CR filters and Constant Fraction Discriminator (CFD) emulator. A proper baseline subtraction is computed from the raw data.

Energy calibration of the BC501 detectors was done using ^{137}Cs, ^{60}Co and ^{88}Y gamma sources. Silicon detectors calibration was performed using a triple Am-Pu-Cm alpha source.

The neutron gamma discrimination was achieved both by the Time of Flight and the Zero-Crossing method that rely on the longer tail of the neutron signals with respect to the gamma ones in liquid scintillators. Through the correlation between the Zero-Crossing and the deposited energy of the interacting radiation two different loci relative to neutrons and gammas can be distinguished. A neutron detection threshold of about 150 keVee was achieved with the PSA discrimination. This threshold correspond to a minimum neutron energy of about 0.5 MeV. The detection threshold determine the efficiency of the BC501 detectors that can be calculated by a Monte Carlo code as reported in ref. [35]. The calculated intrinsic efficiency for the BC501 used in this work as a function of the neutron energy is reported in Fig. 1. From two-boby kinematics calculations the energy range of the neutron coming from the $^6Li(^3He,n)^8B$ reaction at 5.77 MeV is from 0.8 MeV at the most backward angle to about 3 MeV for the most forward detector.

In Fig. 2 the neutron time-of-flight spectrum of the scintillator detector positioned at 15 degrees is shown after the proper neutron signal selection from PSA. One can easily identify the two ^8B peaks (ground state and the first excited state at 0.78 MeV that immediately de-

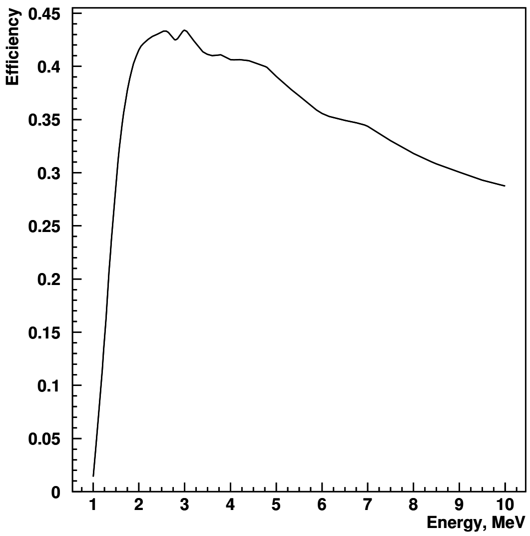

Figure 20. Absolute neutron detection efficiency calculated for one RIPEN detector.

cay by proton emission) and the peak from the reaction ^{12}C(^{3}He,n)^{14}O due to the Carbon deposited on the target. The overall continuum is due to the three-body reaction ^{6}Li(^{3}He,np)^{7}Be. Uncorrelated backgrond and continuum have been subtracted by using the Sensitive Nonlinear Iterative Peak (SNIP) clipping algorithm within the ROOT class TSpectrum.

From the area under the peaks of interest one can infer the differential cross section at the considered angles after correction for the detection efficiency and normalization to the Rutherford scattering on the gold backing. The experimental angular distribution obtained is shown in Fig. 3 for the ^{8}B ground state population. The error bars take into account all the uncertainties of the measure (solid angle of the detectors, target thickness, detection efficiency) and are of the order of 10%.

2. *Results and discussion*

Theoretical calculations [36] were performed in order to compare the results of the absolute cross section and angular distribution obtained experimentally for the ground state of ^{8}B. The evaluations of the differential cross sections of the reaction ^{6}Li(^{3}He,n)^{8}B have been done by means of ŞZero Range Knock-out Distorted Wave Born ApproximationŤ (ZR-KO-DWBA) [37] for two-nucleon transfer with microscopic Bayman-Kallio form factors [38] using the code DWUCK4 [39].

The differential cross section for the allowed combination of transferred angular momenta LSJ (L - orbital angular momentum transfer, S - spin transfer, J - total angular momentum transfer) is given by:

$$\frac{d\sigma}{d\Omega}(\theta) = N\left(\sum_L A_L^2 \frac{d\sigma_{LSJ}}{d\Omega}(\theta)\right). \tag{11a}$$

$$\frac{d\sigma_{LSJ}}{d\Omega}(\theta) = 10\frac{mb}{fm^2}\frac{(2I_B+1)}{(2I_A+1)(2J+1)}\sigma_{LSJ}^{DWUCK4}(\theta), \tag{11b}$$

where I_A and I_B are spins of the target and the product nuclei, respectively, N and A_L are renormalization factors that contains information about the unknown volume integrals and spectroscopic amplitudes of the corresponding configurations. The optical model parameters for entrance (^{3}He+^{6}Li) and exit (n+^{8}B) channels extrapolated from corresponding global optical potentials [40, 41] were used. Single-particle wave functions for two-nucleon transfer form factor in DWUCK4 were calculated by the Well-Depth-Procedure with geometrical parameters $r_0 = 1.25$ fm and $a = 0.65$ fm. All volume integrals are equal to 1. To estimate renormalization factors N and A_L^2 the calculations for the case of beam energy $E = 5.6$ MeV were performed and and the results were compared to the experimental data of ref. [34]. The resulting values used in our calculations were: $N = 16679$, $A_0^2 = 0.878$ and $A_2^2 = 0.122$.

In Fig. 3 the experimental differential cross section in the center of mass frame is compared with the above discussed theoretical predictions. We found a reasonably good agreement between measurement and calculations. The integrated measured cross section is 58±7 mb to be compared with the 75 mb calculated value.

The present result is also in good agreement with the findings of earlier measurements using the neutron time-of-flight method [34], thus confirming the disagreement with the positron counting results [24].

3. *Conclusions and outlook*

We measured angular distribution and cross section of the ^{6}Li(^{3}He,n)^{8}B reaction using the neutron time-of-flight method. The results of our experiment is in agreement with earlier measurement using the same technique [34] showing the same discrepancy with the data coming from positron counting and reported in the original paper by C. Rubbia et al. [**?**]. Model calculations based on the ŞZero Range Knock-out Distorted Wave Born ApproximationŤ for the ground state are able to reproduce our data. In order to understand the differences of the results using the two experimental method there is a strong need to perform other experiments at the ^{3}He beam energy above 10 MeV.

D. ^{8}Li cross section measurements

The two-body reaction $^{7}Li + d \rightarrow {}^{8}Li + p$ is the only possible channel that leads to the production of protons

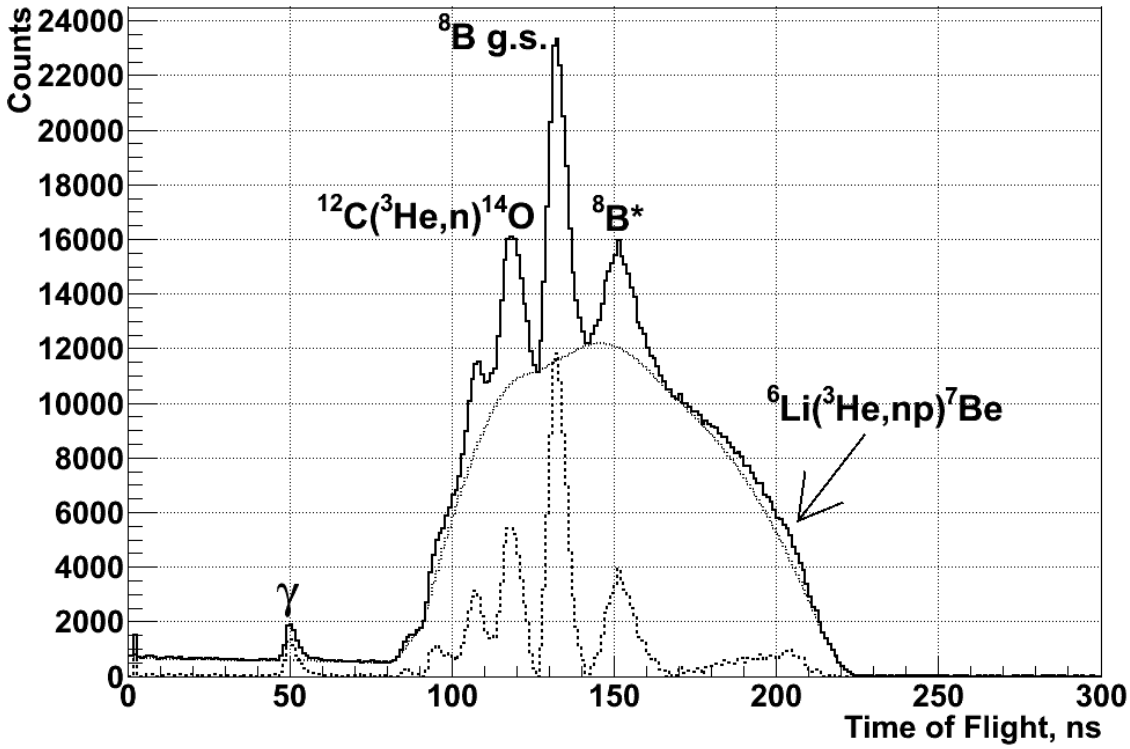

Figure 21. Neutron time-of-flight spectrum at 15 degrees in the laboratory reference frame from the reaction ^{6}Li(^{3}He,n)^{8}B at 5.77 MeV. The time calibration is 1 ns per channel. The distance from the target to detector is 200 cm. See text for details.

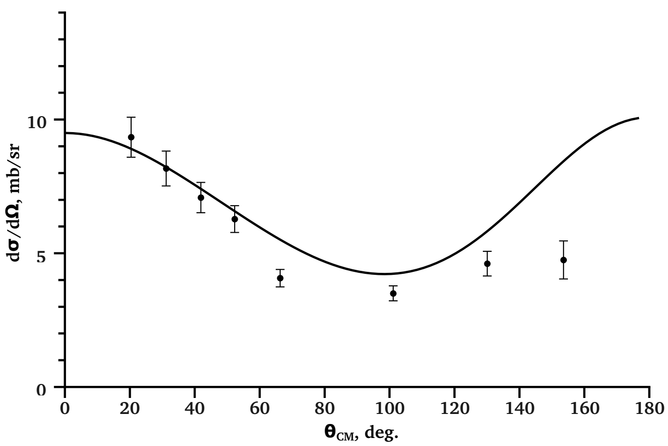

Figure 22. Neutron angular distribution in the center of mass frame of the ^{6}Li(^{3}He,n)^{8}B reaction. The solid line is the result of theoretical predictions based on the DWUCK4 code.

and ^{8}Li. Therefore, the angular distribution of ^{8}Li can be deduced from the angular distribution of the protons by using the conservation laws. The question that may remain open is whether the process is a transfer reaction (stripping reaction) or goes through an excited compound nucleus that eventually decays by proton evaporation (compound nucleus formation and decay). This question can possibly be disentangled by studying the simmetries of the protons angular distribution and the shape of the protons energy spectra which are supposed to be very different in those two opposite cases. However, the energetics is not affected by the details of the reaction process because it follows from the mass-energy conservation law.

Because of the reverse kinematics, ^{8}Li nuclei are strongly focused in the forward direction, while protons are spread out over 4π. The angular correlation expected by using linear momentum and energy conservation laws is shown in figure 23. The solid curve shows that the maximum laboratory angle expected for ^{8}Li with respect to the beam direction is $\approx 11°$, which corresponds to protons emitted at about 50°. Figure 24 shows the expected correlation E_{lab} vs. ϑ_{lab} (lab energy vs. angle with respect to the beam direction in the laboratory reference frame) for the case of ^{8}Li produced in its ground state. The curve shows that the laboratory energy of ^{8}Li is between 11 and 24 MeV. Protons can be produced instead with a maximum energy of about 13 MeV. From the above considerations, if follows that it is sufficient to measure the angular distribution of the protons to obtain the angular distribution of ^{8}Li, regardless of the kind of reaction process.

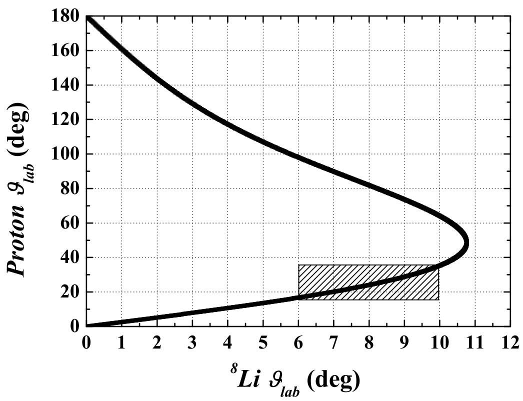

Figure 23. Correlation of the protons laboratory angle with respect to the laboratory angle of ^8Li. The hatches area highlights the region of maximum production of ^8Li

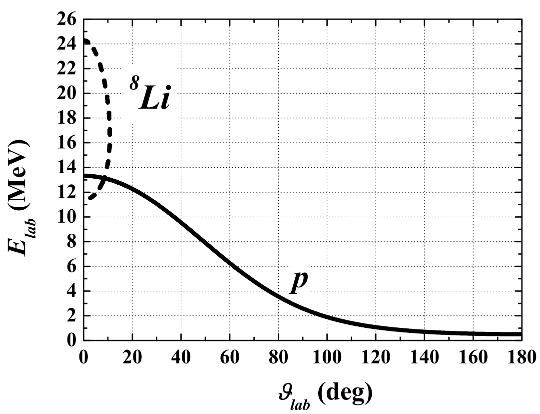

Figure 24. The expected laboratory energy vs. laboratory angle correlations for protons (solid line) and ^8Li (dashed line) from the two-body kinematics. The calculation is performed considering ^8Li in the ground state.

1. *Experimental method and results*

In the experiment performed at LNL, a pulsed beam of ^7Li of 25 MeV was produced by the XTU Tandem at LNL. The target was of the CD_2 type. Protons were detected by the $8\pi LP$ apparatus [42] which is a 4π detector made out of more than 300 two-stage $\Delta E - E$ telescopes. The main duty of $8\pi LP$ is to detect and identify light charged particles, namely, protons, deuterons, tritons and α particles.

In figure 25 the proton energy spectrum measured at the laboratory angle of 20.6° is shown. Five peaks can be readily seen. The lower energy peak is partially cut because of the energy threshold of the detector.

In order to interpret the origin of these five peaks it is necessary to consider the energy balance of the reaction, namely, the connection between the Q values and the known level scheme of ^8Li. The peaks correspond to the reaction in which ^8Li is in its ground state (consequently maximum allowed kinetic energy for the protons), 1st, 2nd and 3rd excited state. The highest is the energy of the excited state, the lowest is the kinetic energy of the protons. An additional peak is observed due to the elastic scattering of ^7Li on the hydrogen as a contaminant of the target.

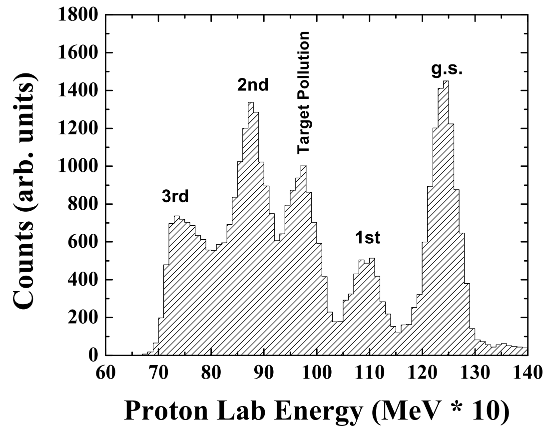

Figure 25. Proton laboratory energy spectrum measured at 20.6° with respect to the beam.

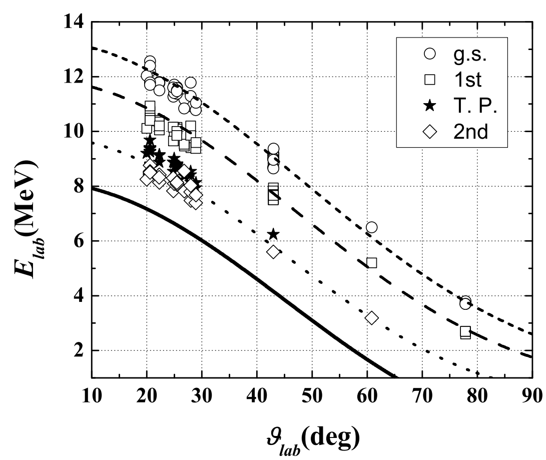

Figure 26. Comparison between the measured energy peak at different laboratory angles and the values (solid lines) expected from two-body kinematics and different excited states of ^8Li.

There are no experimental points for the 3rd exited state case because of the energy cut due to the detectors energy thresholds (see figure 25). The good agreement between the points and the curves supports the correct assignment of the origin of the peaks.

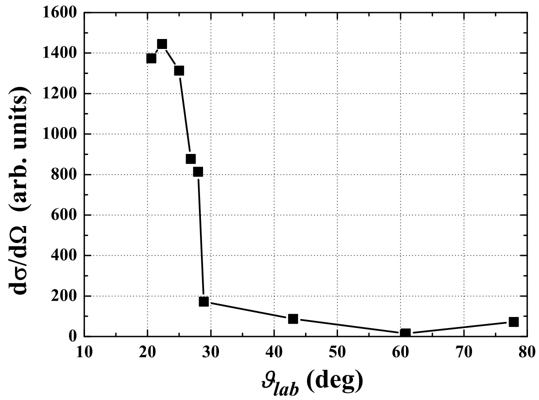

Figure 27. Angular distribution in the laboratory reference frame of the protons corresponding to ^{8}Li in the ground state.

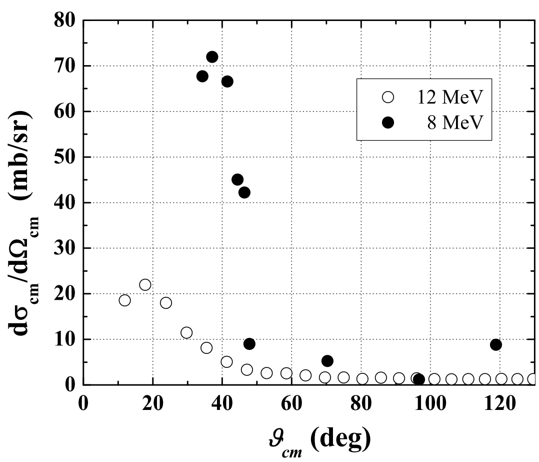

Figure 28. Center of mass angular distribution for the protons corresponding to ^{8}Li in the ground state.

The laboratory angular distribution of the protons correlated to ^{8}Li produced in the ground state is shown in figure 27. Protons are mostly produced in an angular range lower than 40°. By going back to figure 23, this means that ^{8}Li production is maximized at the laboratory angles between 6° and 10°. This region is highlighted with a hatched area.

In order to extract the absolute cross section, the lab angular distribution in 27 has been normalized to cross section units by using the elastic scattering and transformed into the center of mass (c.m.) frame. The c.m. distribution is shown in figure 28 along with the results of Ref. [43]. The label "8 MeV" is here used since a beam of 25 MeV of ^{7}Li on deuterons gives rise to the same reaction c.m. angular distribution of a deuteron beam of ≈8 MeV impinging on a ^{7}Li target (direct kinematics). The data from Ref. [43] refer to a deuteron beam of 12 MeV impinging on a ^{7}Li target. The angle integrated cross section is obtained by the following numerical integration:

$$\sigma = \int \frac{d\sigma}{d\Omega} d\Omega \tag{12}$$

For the present case, the integration was limited to the angular range of the data. This means that the total ^{8}Li cross section obtained of 89±18 mb is a lower limit. This datum is plotted in figure 29 (full square) along with the cross section from Ref. [44] (empty circles) and Ref. [43] (empty triangle). Considering that only the ground state of ^{8}Li has been included in the experimental cross section, the present datum is in rahter good agreement with the other data taken from literature.

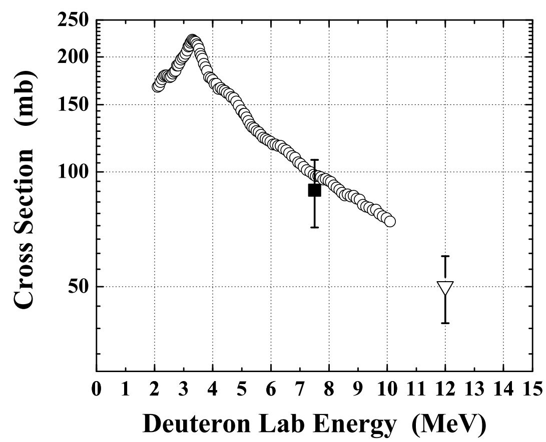

Figure 29. ^{8}Li production cross section compared with known data. Full square: present experiment; empty circles from Ref. [44]; empty triangles from Ref. [43]

2. Summary

The primary goal of this experiment was the measurement of the angular distribution of the ^{8}Li produced in the reaction $d(^{7}Li,p)^{8}Li$ at 25 MeV. The experimental method takes advantage of the two-body nature of the process. ^{8}Li angular distribution is obtained by measuring tha angular distribution of the protons. A by-product of this experiment is the total ^{8}Li production cross section. Considering that only the ground state is included, the cross section at 25 MeV is in good agreement with data from literature.

E. Summary of Isotope production for Beta Beam isotopes

Table III below shows the rates that can be achieved today. ^{6}He and ^{18}Ne have been experimentally verified. Rates for ^{8}Li and ^{8}B have been simulated, using available information on cross-sections and by optimizing the production ring target wedge and the incoming ion beam. We see that the Production Ring still needs some tuning to perform as specified. Considerations concerning the Collection Device and related problems (see III B) have not been considered for ^{8}Li and ^{8}B in the simulations.

Table III. The rate (r) extracted from the source (using different production methods (^{6}He estimated from experiments, for ^{18}Ne from experiments and calculations and rates for ^{8}Li and ^{8}B are estimated from calculations).

Isotope	^{6}He	^{18}Ne	^{8}Li	^{8}B
Prod.	ISOL(n)	ISOL	P-Ring	P-Ring
Beam	SPL(p)	Linac4(p)	d	^{3}He
I [mA]	0.07	7	0.160	0.160
E [MeV]	2000	160	25	25
P [kW]	140	1120	4	4
Target	W/BeO	^{23}Na, ^{19}F	^{7}Li	^{6}Li
r [10^{13}/s]	5	1.0	0.1	0.08

IV. IONIZATION: THE ECR SOURCE

The high frequency Electron Cyclotron Resonance (ECR) ion source is expected to accept an intense continuous flux of ^{6}He or ^{18}Ne, ionize the gas and bunch the ions with a high efficiency. As a continuation of the work started in the EURISOL Design Study, a compact, robust, innovative design was proposed for a 60 GHz ECR ion source prototype called SEISM: Sixty gigahertz ECR Ion Source using Megawatt magnets. Using high field magnets technology, the confinement structure was constructed and tested. Upcoming experiments at 28 GHz will allow an estimation of SEISM beam characteristics, compared to beams extracted from the known 28 GHz ECR ion sources.

A. Ion source specifications

As described previously (see section III E) radioactive ion beam intensities of up to $5{\cdot}10^{13}$ ions per second for ^{6}He (i.e. 8 pμA) are foreseen. The beam should be structured according to the postacceleration duty cycle (refer to V): as a working hypothesis one considered short pulses of 50 to 100 μs duration with a 10 to 25 Hz repetition rate.

Due to the high ionic densities in a classical Electron Cyclotron Ion Source (ECRIS) (up to 10^{13} charges per cm^3 for a 28 GHz plasma [45, 46]) and to its high ionization efficiency for noble gases (close to 100%), ECRIS allow the production of intense continuous beams and are considered as a promising solution.

Studies started within the EURISOL Design Study [47, 48] predicted that short bunches of 100 μs duration could be produced in the pulsed working mode called preglow (PG) [49], provided that the heating radiofrequency would be much higher than 28 GHz.

Experiments have been performed at LPSC Grenoble with a Phoenix V2 ECRIS in PG mode at 18 GHz and at 28 GHz, and a theoretical model has been developped in collaboration with IAP Nizhny Novgorod [50–52], confirming that increasing the heating frequency would allow the production of higher intensities in PG mode.

The location of the ion source, close to the target, will impact its lifetime due to the high radioactivity level, therefore the magnetic structure should be radiation hard.

A 60 GHz ECRIS prototype, the first in the world, was designed at LPSC Grenoble with the aim of fulfilling the specifications listed above.

B. Design choices

As a first design, the simplest magnetic configuration, a cusp structure, was chosen. Extensive simulations have shown that two sets of coils supplied with opposite currents of 30 kA could generate a closed 2.1 T iso-B surface for 60 GHz resonance (figure 30), with magnetic field values up to 7 T at the injection and 3.5 T at the extraction on a 100 mm axial mirror length, and 4.5 T for the radial mirror [53].

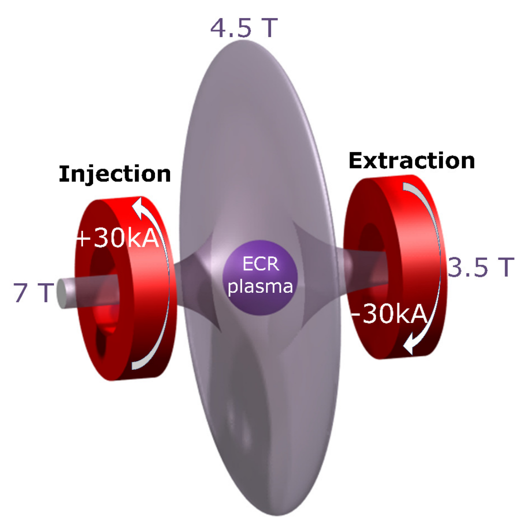

Figure 30. Schematic view of the SEISM cusp magnetic trap

In order to reach high magnetic field gradients on such short dimensions, radiation-hard coils using LNCMI polyhelix technology were used, accepting current densities up to 640 A/mm^2. Due to their low resistivity, the coils need 6 MW electrical power and can be cooled with de-ionized water. Following the magnetic field calculations, thermal and hydraulic calculations were performed using a general finite element solver program in order to optimize polyhelix cooling. The helices are radially cooled, so the windings are stuck together with 20 to 24 pieces of pre-impregnated fiberglass (prepreg, see figure 31), in between which the water flows through. At full power operation, temperature can locally reach 330°C and exceed the prepreg thermal resistance, so new insulator designs were investigated to prepare full power tests [54]. The cooling tanks (figure 32) were designed to bear the stress due to an internal water pressure of 43 bars and limit the lengthening due to the 300 kN magnetic repelling forces.

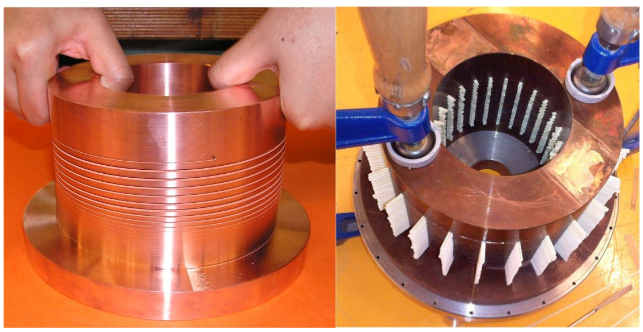

Figure 31. Insertion of the prepreg insulators between the helix windings

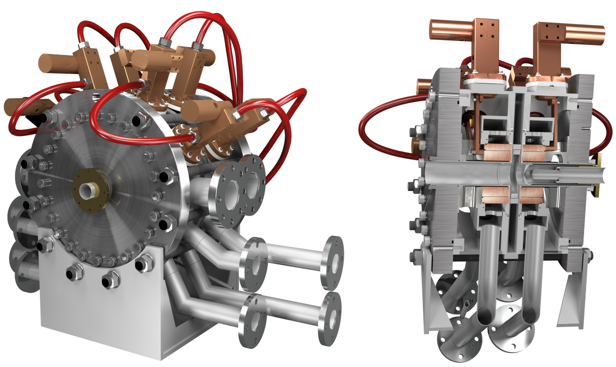

Figure 32. Three-dimensional view of SEISM prototype

The plasma chamber diameter is 60 mm due to the 80 mm helix inner diameter, with a shoulder at the center that allows the magnetic field lines to pass from axial to radial mirrors through the resonance zone without touching the chamber walls. A polarized ring was added to prevent radial particle leaks. The plasma chamber is insulated by 2 mm thick PEEK parts. As a first approach, conventional single-gap plasma and puller electrodes were designed. Depending on the first experimental results, a multielectrode design will be performed in order to extract high intensities at high voltage (above 50 kV).

C. Experimental validation

Tests were conducted at LNCMI to measure the magnetic field map of the SEISM confinement structure [55–58]. Axial and radial hall probes allowed 1 mm-step measurements, all along three axes parallel to the chamber central axis, at 0 mm, 15 mm and 30 mm radial distances. Precise positions of the helices magnetic centres relatively to the plasma chamber centre were verified by a flux variation integration experimental method. One could see that the 1 T iso-B surface corresponding to the 28 GHz resonance zone is closed at 15 kA (see figure 33).

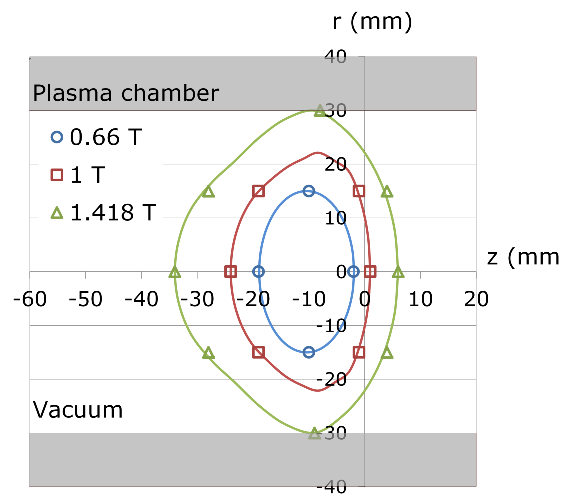

Figure 33. Magnetic field map for 15 kA current intensity on the coils

However, one observed that the peak to peak length was about 90 mm, so shorter than calculated. As a consequence, the maxima value is up to 20% lower than expected on the extraction side. Moreover the cusp point, where the magnetic field value is zero, is located 9 mm further towards the extraction. Such displacement could cause energetic electrons to follow the magnetic field lines and hit the chamber, rapidly creating a hole.

In order to solve this issue and to prepare plasma experiments, possible intensity operating ranges are under evaluation. The adjustment of the ratio of applied currents between injection and extraction coils is computed in order to bring back the zero field point at the centre of the plasma chamber (see figure 34). In the meantime, parametric simulations, including for example, the temperature gradient in the cooling water or mesh variations [59], were introduced to fit the discrepancies between the calculations and the measurements.

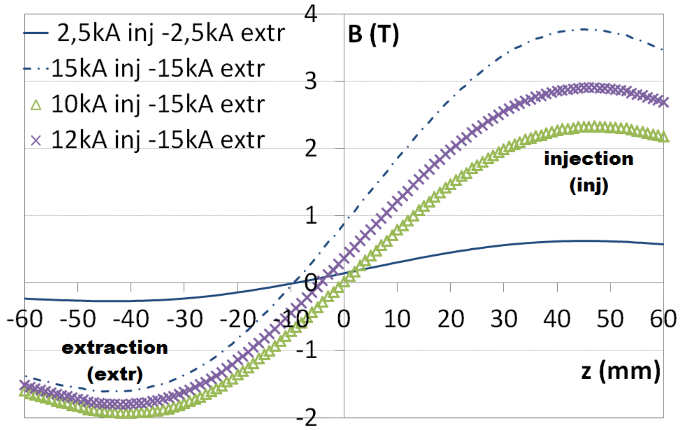

Figure 34. Position of the cusp point on the plasma chamber central axis for various values of the injection (inj) and extraction (extr) current intensities

D. Perspectives

Next step is to produce a 28 GHz plasma in order to compare SEISM cusp performances to existing minimum-B ECRIS [60, 61]. Figure 35 shows the beamline layout which is currently under construction at LNCMI.

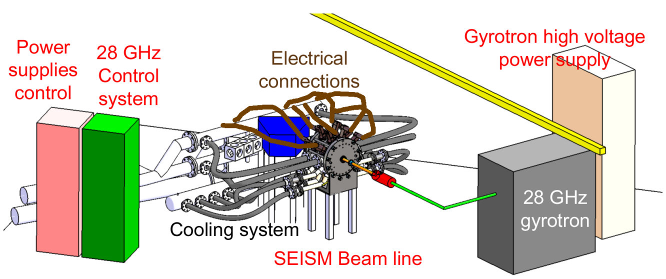

Figure 35. Schematic view of the beam experiment layout

Depending on the beam characteristics, the pertinence of producing a 60 GHz plasma with this first prototype will be evaluated. Developments are already ongoing to overcome the thermal limitation on the prepreg insulators. The design could also be complexified towards a minimum-B magnetic structure, as first preliminary design studies show the possibility to use poly-helix technology to produce multipolar radial field.

A 60 GHz - 300 kW gyrotron was developed at IAP within an ISTC contract [62] and should be available at LPSC-LNCMI end summer 2012. In the future, in the frame of the COLOSSECRIS excellency laboratory project, LNCMI power supplies may provide high intensity currents to magnet experiments at research facilities such as ILL, ESRF and LPSC. Possible 60 GHz experiments could then take benefit of a high intensity beamline currently developed at LPSC.

V. THE ION LINAC

Due to the low duty cycle of 0.05% and the high pulse beam current up to 13 mA as required for the Beta-Beam, the use of normal conducting RF-structures even up to the intended final energy of 100 MeV/u has been considered a favorable choice. Even at accelerating gradients between 3 and 6 MV/m the thermal load on the cavities is very moderate. For the desired maximum mass to charge ratio of $A/q = 3$ an operating frequency of 175 MHz at energies up to 10 MeV/u is well adapted, which then would be changed to 352 MHz for further acceleration [63].

Figure 36 shows a schematic layout of a possible ion Linac and the parameters are shown in Table IV. The first accelerating stage behind the ECR ion source would be a Radio-Frequency Quadrupole (RFQ). However the ions are not fully stripped as assumed in [63] but have charge state $+1$, therefor we may consider two RFQs and strip the ions fully before the DTL structure. The study of these RFQs still remains to be done. The transition energy between RFQ and the Drift Tube Linac (DTL) has been chosen to be 1 MeV/u, which can be adapted to DTL requirements during further optimization procedures.

Possible candidates for NC-DTLs are H-mode cavities (IH- , CH-DTL). In general, H-mode cavities have high shunt impedance. IH-structures are operated in the low energy regime between 0.1 MeV/u and 10 MeV/u with RF frequencies between 36 and 250 MHz. The IH-DTL structure has no competitor with respect to RF efficiency. The first DTL part could consist of three IH-structures operated at 176 MHz. The input energy is 1 MeV/u and the output energy 8 MeV/u. The total voltage gain is 22 MV with a length of about 7 m. The total required power per cavity including the beam loading is between 600 and 750 kW. The following DTL section from 8 MeV/u to 100 MeV/u could consist of NC-CH cavities. CH-cavities are operated in the H21 mode. The CH-section would be operated at 352 MHz. For this frequency cost-efficient klystrons in the MW range are available. To cover the voltage gain of 276 MV about 46 CH structures are necessary. The effective voltage per cavity varies between 5 and 7 MV. The total power per cavity is kept below 1 MW including the beam loading. The length of the CH-DTL is about 100 m. The total length is about 110 m. This corresponds to a real estate gradient of 2.73 MV/m.

Table IV. Beta-Beam requirements for the ion Linac.

Beta Beam Linac Parameters	
Duty cycle	0.05%
Beam current	š13mA
Mass to charge ratio A/q	š3
Input energy W_{in}	8 keV/u
Output energy W_{out}	100 MeV/u
Input emittance $\epsilon_{in,rms,normalized}$	0.2 π·mm·mrad

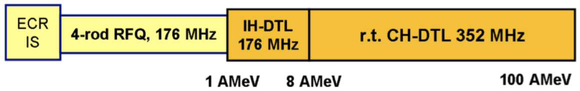

Figure 36. Schematic layout of an IH/CH-DTL for the production of b-beams

VI. THE RAPID CYCLING SYNCHROTRON

The work on the RCS [6] was done within the FP6 Framework Program (EURISOL Design Study) [2] and it is summarized here for completeness.

A. RCS general parameters

The RCS accelerates He and Ne ion beams from 100 MeV/u to a maximum magnetic rigidity of 14.47 Tm (that is the rigidity of 3.5 GeV protons, 787 MeV/u for $^{6}He^{2+}$ and 1.65 GeV/u for $^{18}Ne^{10+}$) with a repetition rate of 10 Hz. The threefold symmetry lattice proposed is based on FODO cells with missing magnets providing three achromatic arcs and three sufficiently long straight sections for accommodating the injection system, the high energy fast extraction system and the accelerating cavities. The number of dipoles have been optimized to obtain a transition energy allowing acceleration of protons up to 3.5 GeV. The dipoles have been split into two parts separated by a drift space to place absorbers to intercept the decay products. The physical radius has been adjusted to 40 m in order to facilitate the synchronization between the CERN PS and the RCS and therefore the transfer of bunches from one ring to the other. The ring is composed of 60 short dipoles and 48 quadrupoles. A schematic view of the RCS layout is shown in figure 37 and the main parameters are summarized in V.

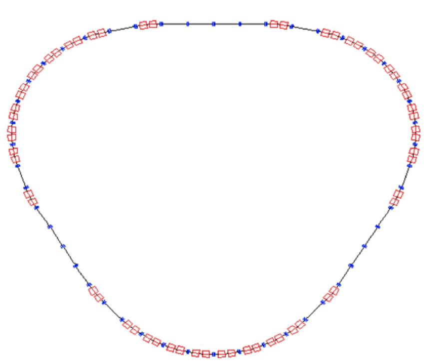

Figure 37. Schematic layout the RCS

B. Optical design

The RCS is partitioned into 24 FODO cells, 6 in arcs and 2 in a straight section. The betatron phase advance per cell (i.e quadrupole strength) and the length of the 2 sections without dipoles in the arcs have been adjusted so as to cancel the dispersion function in long straight sections and to obtain, with only two quadrupoles families, a working point located in a region of the tune diagram which is free of systematic resonances up to the fourth order. Dipoles are only 1.4 m long with a maximum magnetic field of 1.08 T to avoid a high ramping rate for the 10 Hz operation. The quadrupoles are 0.4 m long and have a maximum gradient of less than 11 T/m. The diluted transverse emittances in the RCS after multiturn injection are calculated from the emittances required in the PS at the transfer energy with a possible blow-up of 20%.

C. Injection

The ion source delivers a beam pulse of 50 μs . The revolution period at 100 MeV/u is 1.96 μs, and the injection process takes place over 26 turns (multiturn injection) in one of the long straight section by means of an electrostatic septum and 2 pulsed kickers. Optimum filling in the horizontal phase space is achieved when the incoming ions are injected with a position and a slope which minimize their Courant and Snyder invariant. In the vertical phase space the dilution is obtained by a betatron function mismatch and a beam position offset. The injection efficiency is 80%.

D. Acceleration

After injection the circulating beam is continuous and occupies a rectangle in the longitudinal phase space. To capture the injected beam, one stationary bucket is created. During trapping, the magnetic field is clamped at its minimum value for a period of a few ms and the synchronous phase is zero. The RF voltage is optimized to obtain a beam rotation of about 90° and a momen-

Table V. Beta-Beam requirements for the RCS

Beta Beam RCS Parameters	
Circumference	251 m
Superperiodicity	3
Injection Energy	100 MeV/u
Maximum magnetic rigidity	14.47 Tm
Repetition tate	10 Hz
Number of dipoles	60
Number of quadrupoles	48
Max ramping rate	24T/s
Emittance h/v	72/39 π·mm·mrad

tum spread as small as possible before the acceleration of the 20 bunches starts. The 20 bunches are then single turn extracted and transfered to the PS. The accelerating voltage is 100 kV over a frequency range of 0.51 MHz to 1.12 MHz. Ferrite loaded cavities developed at CERN or magnetic alloy cavities like those developed for SIS18 at GSI or at J-Parc could would be a possible choice.

E. Other beam optics aspects

Several beam dynamics studies have been investigated in order to assess the feasibility of the RCS, in addition to the results presented here. Unavoidable magnet misalignments and dipole field errors can affect the RCS closed orbit. Distortions to be expected have been statistically estimated assuming standard error tolerances and a correction system has been defined. In fast ramping machines such as the Beta-Beam RCS, eddy currents induced in metallic vacuum chamber walls by the time varying magnetic field produce various field components acting on the beam. In dipole vacuum chambers, one important component is a sextupole which modifies the natural chromaticity of the ring. The associated effects may be compensated for to guarantee the beam performance. The beam dynamics studies made on the RCS show that the ring can be realized using available technologies.

F. Vacuum System Requirements for the RCS

The vacuum decrease due to beam losses is a potential problem for all machines and it has been studied for the RCS. The required gas pressure for a good transmission is $1 \cdot 10^{-8}$ mbar.

The losses are dominated by radioactive decay. However, beam losses at injection are crucial for the transmission. Transmission calculations assume a beam loss at injection of 20%. Using $^{18}Ne^{10+}$ as projectile ion the pressure stays below $1 \cdot 10^{-8}$ mbar for pumping speeds greater than 2 m^3/s, reaching a maximum for effective pumping speed S_{eff} = 5 m^3/s of about $6.5 \cdot 10^{-9}$ mbar. The situation for $^6He^{2+}$ is different. For pumping speeds less than 10 m^3/s the pressure goes up exceeding the $1 \cdot 10^{-8}$ mbar limit. The pumping speed is not sufficient to remove enough of the gas desorbed at injection before the next cycle starts. As it is desirable to have a conventional pumping system installed in the RCS, the best way to work around this problem would be to reduce the beam losses at injection. If it is possible to reduce the losses to about 10% an effective pumping speed of 2 m^3/s would be sufficient to stay below the $1 \cdot 10^{-8}$ mbar limit. If the injection losses cannot be reduced one has to consider an increase of the pumping speeds for example by applying NEG-coating to a part of the vacuum chamber. This analysis was done for $^6He^{2+}$ only, since the pressure evolution for $^{18}Ne^{10+}$ is not critical. Because most beam losses occur within or close to the dipole magnets, NEG-coating should be applied the these dipoles. For all calculations the maximum residual gas pressure is $5 \cdot 10^{-9}$ mbar, while the effective pumping speed due to the NEG ranges from about 310 to 650 m^3/s for 8 and 20 coated dipoles respectively. One has to consider an ongoing saturation effect, which reduces the pumping speed of the NEG coating over time. If NEG-coating is needed all dipole magnets should be treated with NEG to ensure a stable residual pressure over the entire time of operation. It is important to remark that only beam losses inside the RCS ring are relevant for the calculation of the pressure bump at injection. In this sense a beam loss of 20% means that all particles are lost inside the machine. Losses outside the machine, e.g. inside a drift line just before injection do not contribute to the pressure rise and must be subtracted. In general it is hard to distinguish these two effects.

G. radiation protection studies

Detailed radiation protection studies were realized according to the different loss mechanisms within the RCS. They permitted to define the shielding required by the machine operation, the classification of the area and limits on the release of airborne activity. Beam losses can be divided into injection, decay and RF (capture and acceleration) losses, see Table VI. At injection 30% of the beam is lost on the septum. Decay losses are uniformly distributed in the dipoles and in the short straight sections in the arcs during all the magnetic cycle. RF losses are point losses that occur in the families of quadrupoles in the arcs as indicated in figure 38.

The areas around the RCS tunnel will probably be classified as supervised radiation areas during operation, with a dose rate constraint of 3 μSv/h: this would require concrete shielding thicknesses ranging from 3 to 5 m, depending on the position in the tunnel. In these places where different kinds of losses occur, the thickness imposed by the dominating mechanism was considered. In the released airborne activity study a constant rate of 10000 m^3/h was chosen for the ventilation system in the RCS tunnel. In this condition, the effective dose given to the reference population in one year of operation was estimated to be in the order of 0.7 μSv for the most critical ion, i.e. ^{18}Ne. It is well below the reference value for CERN emission. Figure 39 presents the contributions of the main radionuclides to the annual effective dose.

For the inhalation dose to workers that could access

Table VI. Beam loss for ^{6}He (^{18}Ne).

E [MeV/u]	Injection	Decay	RF
100	30%	0.10 (0.45) %	5.70 (9.40) %
400 (640)	-	0.80 (0.20) %	2.85 (8.50) %
787 (1650)	-	1.80 (0.70) %	4.75 (5.05) %

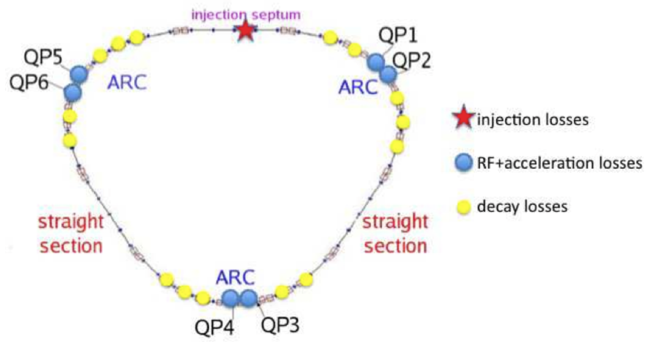

Figure 38. The different kinds of losses and their locations in the RCS ring.

the tunnel during shutdown periods a conservative assumption was made: the ventilation system is not operating. The intervention time depends on dose rates and on whether or not the ventilation system is on. For a one hour intervention, the integrated dose does not exceed the constraints, considerably below 1 μSv even without waiting time. Furthermore, if the ventilation system is working a waiting time before access of nearly 20 minutes is enough to completely change the air in the tunnel.

Dose rates from material activation were calculated for a 3-month continuous operation and 3 different waiting times of one hour, one day and one week. The results show that, according to CERN area classification, the RCS tunnel is likely to be classified as a limited stay area, accessible one week after the shutdown. The doses do not decrease significantly after one week because the residual radionuclides that mostly contribute to the total dose have half-lives longer than one week. The high activation of the machine elements that remains after one week may require a remote handling system for the maintenance.

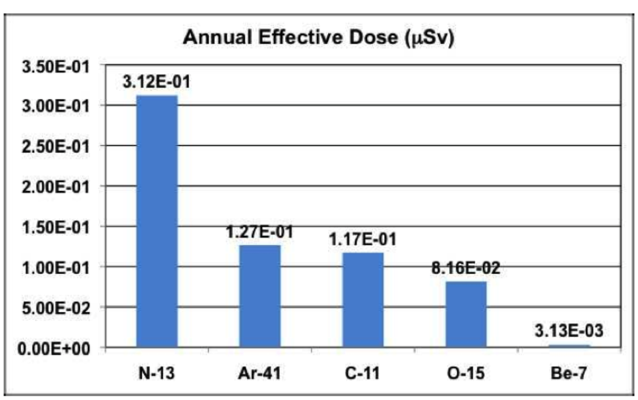

Figure 39. Annual effective dose to the reference population: contributions from the main radionuclides.

VII. THE CERN PS

Ion acceleration in the PS and SPS is a routine operation since many years. Different ion types from light ions such as sulfur up to heavy ions such as lead have been accelerated. Studies of a possible acceleration scenario and the PS vacuum were performed during the EURISOL design Study (see [2], for details). The recent measurements of the oscillation angle Θ_{13} show that the requirements for short and intense bunches in the final accelerator, the Decay Ring, can be relaxed now. The reason for the requirement for a small "duty factor" (the time during which the intensity is distributed with respect to the total time the machine is working) is the signal to noise (atmospheric neutrinos) relation in the detector. The new relaxed bunching conditions in the Decay Ring have only been studied partly and would need reconsidering of the RF also in the PS. The original scenario in the PS, that would give a sufficient rate of neutrinos for physics, will be summarized here.

Since the beta-decay lifetime at injection in the PS is much longer than the cycle time of the RCS, it has been chosen to operate the PS at the RF harmonic consistent with the 10 MHz upper frequency limit of the accelerating cavities and to transfer the maximum number of batches from the RCS. Thus, the PS harmonic of choice becomes h=21 and 20 bunches are accumulated one by one from the RCS. One RF bucket is left empty to accommodate the extraction kicker rise-time.

The beta-decay diminishes the number of ions accumulated on the PS injection plateau. Also the intensity of the first bunch injected into the PS will be less than the last. As little as 40% of the first helium bunch remains when the last one arrives. The situation is better in the neon case due to its longer half-life and more advantageous charge-to-mass ratio. The PS extraction kicker gap is positioned differently within the bunch train, from batch to batch, in order to even out the bunches that are ultimately stored in the decay ring. The longitudinal emittance that the PS must deliver is 0.80 eV·s in the case of helium ions and 1.8 eV·s for neon. This implies matching voltages of $\cong$ 30 kV and $\cong$10 kV, respectively, in order to provide the required bunch length of 20 ns at ejection. No bunch shortening gymnastics are required due to the proposed addition of a 40 MHz RF system in the receiving SPS (see section VIII).

A. Vacuum System Requirements for the PS

Particle losses are dominated by radioactive decay. Losses due to charge exchange are negligible, as the cross sections for electron capture are very small. For both $^{6}He^{2+}$ and $^{18}Ne^{10+}$ the losses are spread over the whole ring. The transmission was checked by using an ideal cycle assuming the maximum number of particles coming from the RCS. Given these numbers there were $4.29 \cdot 10^{12}$ particles ejected. This is close to the desired number of $4.31 \cdot 10^{12}$.

There are 147 vacuum pumps along the PS ring, which were assumed to be equally distributed. Together with the given total pumping speed of 38 m^3/s, the simulation program StrahlSim calculates an effective pumping speed of about 11.5 m^3/s. The pressure stays well below $10 \cdot 10^{-8}$ mbar for both $^6He^{2+}$ and $^{18}Ne^{10+}$ when a pumping speed of 11.5 m^3/s is assumed.

At an accelerator operation with $^6He^{2+}$ and $^{18}Ne^{10+}$ as projectile ions an effective pumping speed of 11.5 m^3/s in the PS ring is sufficient. This pumping speed is delivered by the existing vacuum system of the PS. The minimum effective pumping speeds needed for a stable operation were estimated to be 9 m^3/s and 7 m^3/s for $^6He^{2+}$ and $^{18}Ne^{10+}$ respectively.

B. CERN PS radiation protection studies

Preliminary work within the EURISOL study has focused on two radiation protection aspects related to the operation of the PS as part of a Beta-Beam facility, namely the induced radioactivity in the magnets and the air activation. A complete study would also include an analysis of the existing shielding (in particular with respect to those points, where the shielding is relatively thin), the prediction of induced radioactivity in hot components like septum magnets and the activation of the cooling water of the magnets. At this stage it is not possible to perform such a detailed study because of the lack of information on the operation conditions and on the exact particle loss distribution. Nevertheless, during this study it was possible to assess the impact that the Beta-Beam operation would have on the radiation level expected during maintenance and on the release of radioactivity to the environment.

The PS bridge (the SS42 region of the CERN PS, near Goward Road) has been studied using the same geometry models as for the 2GeV proton beam, studied for a possible upgrade of the injector complex, for LHC [64]. The conclusion is that dose rates for Beta Beams are lower by a factor 3 for ^{18}Ne and by a factor 16 for ^{6}He compared to full proton intensities. The energy deposition on the septum blade (SMH42) is $1.0 \cdot 10^{-4}$ [GeV/cm3/primary] for ^{18}Ne. The energy deposition on the blade of the septum SM16 is higher by a factor of 3.7. No show-stopper has been found for the Beta Beam, neither for radioprotection nor for the equipment.

At the beginning of the annual shutdown period in 2008, radiation survey measurements of ambient dose equivalent rate were performed to gain information about the present radiation levels in the CERN PS. The survey measurements are done at 40 cm distance from the object of concern, usually the vacuum chamber. The average dose rate along the PS ring is about 250 μSv/h, with 40% of the measured points below 100 μSv/h and only 5% above 1 mSv/h. Simulations with 3-month continuous irradiation of ^{6}Li and ^{18}F and 1-week waiting show that the dose rate at 40 cm distance from a PS magnet would range between 60 μSv/h and 2 mSvh which is relatively high compared to the present level of induced radioactivity. This indicates that the tunnel would remain accessible with limited stay during maintenance, as long as the maintenance operations are well planned and optimized in order to reduce doses to workers. These values also suggest that there might be magnets whose levels of induced radioactivity require remote handling. This can only be confirmed or ruled out by a detailed study with precise and realistic scenarios of beam losses and with the implementation of the exact material composition (including traces). The effective dose given to the reference population in a 1-year operation of the PS, due to the air release in the environment, is 0.37 μSv for the He-operation and 0.35 μSv for the Ne-operation. For comparison, the total effective dose given to the population by all CERN installations must not exceed 10 μSv.

C. Q-scans in the PS

The Beta Beam will be injected into the PS (2.0 GeV proton equivalent). Tune scans in the PS (2 GeV protons) without chromaticity correction have been performed to identify the dangerous lines and measurements with correction are ongoing to avoid vertical tails [65]. Measurements show that the ^{6}He beam (ΔQ_x,ΔQ_y)=(-0.22,-0.31) should survive and the ^{18}Ne beam (ΔQ_x,ΔQ_y)=(-0.28,-0.38) still needs more work (probably resonance compensation). Studies on Head-Tail effects are also needed as well as optimization of the bunch structure in the PS and the SPS (beam stability) taking into accont a possible duty factor release in the Decay Ring.

VIII. THE CERN SPS

A. The RF of the SPS

Studies of the the Beta Beam in the SPS within the EURISOL design Study (see [2] for more information and references) will be briefly summarized here for completeness. Rather than consider a new machine, the space charge bottleneck at SPS injection has been addressed by adding a ‘modest’ 40 MHz RF system to the existing infrastructure. This would allow much longer bunches to be transferred from the PS, the matching voltage for 20 ns bunches being about 120 kV and 5 kV for helium and neon, respectively. Near transition when the bunches are short enough, the standard 200 MHz system of the SPS would take over. However, buckets have very different aspect ratio which means that mismatch of the bunches is unavoidable.

1 MV at 40 MHz is at the limit of what might be considered as ‘modest’ and constrains the maximum ramp rate to around 0.1 T/s in the early part of the cycle. Even so, the ramp rate must be slowed down still further

for the re-bucketing because even a small ramp rate reduces the 200 MHz bucket length and buying this back with voltage is costly in terms of mismatch. Assuming a ramp rate of 0.02 T/s and that the emittance the SPS is supposed to deliver is already established before transition, proximity to transition (γ_{tr}=23) reduces the 200 MHz voltage that is required to accommodate the bunch length accelerated in the proposed new 40 MHz bucket. Performing RF gymnastics close to transition is bound to be a delicate matter, but it incurs no penalty in mismatch because the aspect ratios of the two buckets scale identically with Lorentz γ.

Despite a larger emittance, the situation is easier in the neon case due to its advantageous charge-to-mass ratio. Although re-bucketing must still be performed at the same small ramp rate of 0.02 T/s, proximity to transition can be decreased to $\gamma = 20$ and still have 1 MV at 40 MHz changing over to 1.75 MV at 200 MHz. 7.8 MV at 200 MHz is needed to rematch. 1 MV is the minimum 40 MHz voltage requires. It also costs cycle time because of the need to slow the ramp rate down to permit re-bucketing. However, since the 40 MHz system sees almost all the frequency swing during acceleration, more voltage would be expensive. Alternatively, one could consider re-bucketing at zero ramp rate as this reduces slightly the problem of matching. The longitudinal emittance that the SPS must deliver is 1.0 eV·s in the case of helium ions and 2.2 eV·s for neon. These values are derived from the known performance for protons and, allowing an emittance budget of some 25% for blow-up during each acceleration stage, they also fix those in all the upstream machines. The injection scheme proposed for the decay ring requires the beam to be delivered off-momentum into the nonlinear region of the receiving bucket. Consequently, the bunch is deliberately mismatched before extraction from the SPS by a step down in 200 MHz voltage. This bunch tilting is a first-order attempt to increase the capture efficiency at the end of a quarter of a synchrotron turn in the decay ring. The fine detail of capture will depend on the large-amplitude distribution created in the SPS.

B. Vacuum System Requirements for the SPS

The losses in the SPS are dominated by radioactive decay. Losses due to charge exchange are negligible, as the cross sections for electron capture are very small. For both ^{6}He^{2+} and ^{18}Ne^{10+} the losses are peaked behind the quadrupole magnets. The transmission was checked by using the proposed cycle assuming the maximum number of particles coming from the PS. The resulting number of particle ejected from the SPS are arguably identical with the desired numbers of $9.0{\cdot}10^{12}$ and $4.26{\cdot}10^{12}$for ^{6}He^{2+} and ^{18}Ne^{10+} respectively.

Every SPS magnet has an ion pump with a pumping speed of 20 l/s. Considering the main magnets only, a conductance corrected effective pumping speed of S$_{eff}$=2.6 m^3/s was calculated. Placing pumps at the positions where there are no dipoles in the ring, leads to S$_{eff}$=2.8 m^3/s . All simulations carried out for the SPS assume S$_{eff}$=2.8 m^3/s.

Ionization of residual gas particles by the revolving beam, called target ionization, is the dominant effect that causes a pressure rise in the SPS during Beta-Beam operation. The ionized gas particles are accelerated away from the beam by its space charge potential. When these particles hit the vacuum chamber, a low energy desorption process takes place. The desorption rate, η, for this process is considered to be in the range between 1 and 10 desorbed particles per ionized gas particle hitting the vacuum chamber. The pressure evolution strongly depends on the assumed desorption rate. For ^{6}He^{2+} the residual gas pressure is not stable when a desorption rate greater than 5 is assumed, while for ^{18}Ne^{10+} even in case of η = 1 the pumping speed is not sufficient to stabilize the pressure.

One possibility to reduce the pressure buildup is to reduce the acceleration time within the SPS. The acceleration time can be shortened from 2.54 s to 1.58 s for ^{6}He^{2+} and from 1.42 s to 0.90 s for ^{18}Ne^{10+}, when using the maximal available ramping rate of the SPS of 0.74 T/s. Furthermore the cycle time of the ^{18}Ne^{10+} cycle was extended to 6 s in order to give the vacuum more time to relax. This would slow down the pressure rise for ^{6}He^{2+}operation with $\eta = 10$ and stabilize the ^{18}Ne^{10+} operation with $\eta = 1$. In this scenario accelerating ^{18}Ne^{10+} ions with $\eta > 1$ is still not feasible.

As shown before the operation with ^{6}He^{2+} is stable for η=5. At a pumping speed of 4 m^3/s the pressure is stabilized below $1 \cdot 10^{-8}$ mbar. For ^{18}Ne^{10+} various combinations of η and S$_{eff}$ have been calculated assuming the maximal ramping rate and an extended cycle time of 6 s. For each η=1, 3 and 5 the required pumping speeds were estimated to be 2.8 m^3/s, 7.5 m^3/s and 12.0 m^3/s respectively. Simulations show, that during SPS operation with ^{6}He^{2+} or ^{18}Ne^{10+}, there is a massive pressure build up due to ionization of residual gas particles induced by the circulating beam. It could be shown, that an operation with ^{6}He^{2+} ions is possible, if the desorption rate for ionized gas particles hitting the vacuum chamber is less or equal to 5. In this case the residual gas pressure stays below $1{\cdot}10^{-8}$. Should the desorption rate be greater than five, the pressure can be stabilized by reducing the acceleration time from 2.54 s to 1.58 s by using the maximal available ramping rate of 0.74 T/s and increasing the total effective pumping speed to approximately 4 m^3/s. An operation using ^{18}Ne^{10+} ions with the proposed cycle is not possible without adjusting the cycle or the pumping speed. In case of a desorption rate $\eta = 1$ either the effective pumping speed has to be increased to about 7.5 m^3/s or the acceleration time has to be minimized by using the maximal available ramping rate of the SPS, while the cycle has to be extended to 6 s in order to give the vacuum enough time to relax. The increased ramping rate reduces the acceleration time from 1.42 s to 0.90 s. If the desorption rate is greater than one, the higher ramping rate and the extended cycle of 6 s have to be combined with a higher effective pumping speed. For desorption rates $\eta = 1$, 3 and 5 effective pumping speeds of 2.8 m^3/s, 7.5 m^3/s and 12.0 m^3/s have to be applied.

Losses occurring in the PS and the SPS for the Beta-Beam operation are in the same order of magnitude as CNGS for nominal intensities of ^{6}He and ^{18}Ne and are therefore not a show-stopper for the project.

The studies of the PS and the SPS have to be reconsidered in the case the cycling and the RF needs modification to get better conditions for the overall beta Beam in the CERN accelerators: recent measurements values of the oscillation angle θ_{13} may permit relaxation bunching constraints in the Decay Ring, which may give more flexibility in the preceding machines).

IX. THE DECAY RING

The Decay Ring parameters are summed up in Table VII.

After presenting the latest version of Beta-Beam decay ring (DR), the scheme to inject and accumulate the ions and the losses which occur in the decay ring will be discussed. The required RF system to handle the very large peak intensities in the decay ring bunches that are needed to have sufficient signal/noise ratios in the detectors. Collective effects put an upper limit on the intensities that can be stored in the Decay Ring. Some design features have to be optimized to permit a maximum number of ions to be stored in the Decay Ring.

A. Optics

1. *First order optics of the DR*

The circumference of the Decay Ring was chosen to be the same as for the SPS (6911.5 m) to keep the same temporal structure at the injection. The Decay Ring is racetrack-shaped to permit neutrinos to obtain a γ-boost in the direction of the detector. The long straight sections must be as long as possible to maximize the neutrino flux towards the detector. The length of the long straight section is equal to 2572 m, which corresponds to 37.2% of the total length and the length of the arcs is then 876 m with a compaction of about 50%. The dipoles are 7 m long with an angle of $\pi/70$ rad, which corresponds to a curvature radius of 156 m and a magnetic field of 6 T. Five functional parts can be distinguished in the ring [66–68]:

- a long straight section which is directed to the detector
- regular FODO lattices in the arcs
- dispersion suppressors at the arc bounds. They are used to extract the decay products coming from the straight section
- a collimation section in energy
- an insertion for the injection

Improvements of the lattice [69, 70] has been made within EUROnu to locate the injection in a chicane in the straight section which is not directed to the detector [71]. Moreover, the momentum collimation is located in the chicane which makes it possible to have only FODO lattices in the arcs. Another advantage of the chicane is to enlarge the momentum compaction of the ring, which relaxed the head tail instabilities, as explained in the subsection about the collective effects IX F. The drawback of this solution is to require extra dipoles for the injection and to increase the needed total RF voltage because of a larger slip factor.

In order to keep a large dynamic aperture, the arcs are symmetric and are realized as 2π insertions. The working point of the ring is then determined by the optics of the long straight sections. The working point, $Q_x = 18.228$ and $Q_z = 18.16$, was chosen far from the second and third order resonances as shown on the tune diagram given on Figure 40.

The periodicity of the decay ring is 1 because of the chicane in one of the long straight sections. A schematic layout of the decay ring is given in figure Figure 41.

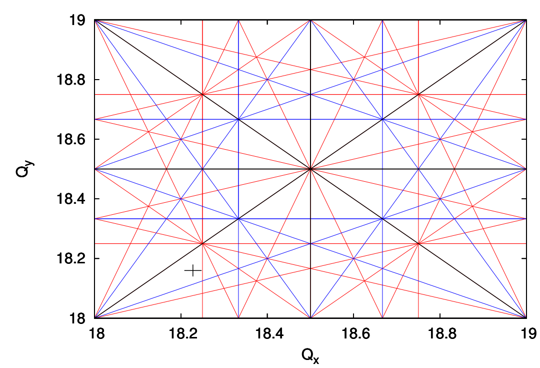

Figure 40. Working point (in black). In black, second order resonances, in blue third order and in red fourth order.

The optical functions of the decay ring are given on Figure 42 at the reference energy and at the injection energy ($\delta = 5‰$). The stored beam will be assumed to be collimated in energy at $\delta_C = 2.5‰$. The beam sizes at 6(5) standard deviations for the stored (injected) beam are given on Figure 43 for the injected and stored beams. The global parameters of the decay ring are summed up in Table VIII. The parameters at the injection point into the decay ring are summed up in Table IX. Excepted near the extraction and injection points, a half-aperture of 60 mm is sufficient in all elements, as Figure 43 shows it. Most super conductiong magnets would preferably have coil free mid-planes to prevent magnet quenching

Table VII. Beam parameters

	Units	$^{6}He^{2+}$	$^{18}Ne^{10+}$	$^{8}Li^{3+}$	$^{8}B^{5+}$
Atomic mass $A_{\rm eff}$	u	6.019	18.006	8.022	8.025
$E_{\rm rest}$/ion	GeV	5.606	16.772	7.471	7.473
γ	-	100	100	100	100
β	-	1.00	1.00	1.00	1.00
$\beta\cdot\gamma$	-	99.995	99.995	99.995	99.995
Half-life at rest τ	s	0.807	0.167	0.840	0.770
$B\rho$	T.m	934.87	559.27	830.64	498.50
Ring length	m	6911.5	6911.5	6911.5	6911.5
Revolution time	μs	23.06	23.06	23.06	23.06
Number of bunches	-	20	20	20	20
Norm. ϵ_x (1 σ)	π mm.mrad	14.8	14.8		
Norm. ϵ_z (1 σ)	π mm.mrad	7.9	7.9		
Injection cycle time	s	6.0	3.6	4.8	3.6
Nominal annual ν flux	10^{18}	2.9	1.1	14.5	5.5
STORED BEAM					
Number of stored ions	10^{13}	9.346	7.178	48.18	16.70
Number of ions/bunch	10^{12}	4.673	3.589	24.09	8.35
Full energy of the beam	MJ	8.3937	19.282	57.668	19.984
Average beam current	A	1.30	4.99	10.04	5.80
Peak beam current	A	227.9	875.0	1762	1017
Longitudinal emittance (full)	eV.s	14.4	43.3	19.3	19.3
Bunch length	m	1.97	1.97	1.97	1.97
Momentum spread (full)	10^{-3}	2.5	2.5	2.5	2.5
INJECTED BEAM					
Relative energy difference	10^{-3}	5	5	5	5
Number of ions/bunch	10^{11}	5.57	2.70	27.6	9.17
Full energy of the beam	MJ	0.475	2.99	6.61	2.20
Longitudinal emittance (full)	eV.s	1.0	2.2	1.33	1.33
Bunch length	m	1.197	1.197	1.197	1.197
Momentum spread (full)	10^{-3}	0.4	0.4	0.4	0.4

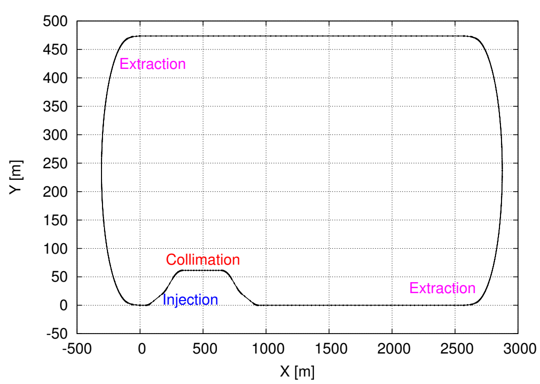

(a) Decay ring

Figure 41. Layout of the Beta-Beam decay ring.

due to high energy deposition from decay products impinging the superconducting coils [72]. Studies with thick stainless steel liners to protect the magnets (similar to the LHC insertion quadrupoles) indicate that reasonably thick liners would probably not be sufficient to fully protect the coils, but could be further investigated for other equipment protection [73]. The operational dipole field is 6 T and the maximum gradient for the quadrupoles should be 42 T/m for such apertures[74]. Special care was taken to keep the gradients of the quadrupoles as low as possible; they are less than 35 T/m (Figure 44).

Table VIII. Parameters of the decay ring.

Length	m	6911.5
Machine radius	m	1100
α	10^{-3}	3.555
$\gamma_{\rm tr}$	-	16.772
Q_x	-	18.228
Q_y	-	18.160
$Q'_{\rm x,nat}$	-	-22.871
$Q'_{\rm y,nat}$	-	-25.867
$\beta_{\rm x,max}$	m	262.750
$\beta_{\rm y,max}$	m	306.123
$D_{\rm x,max}$	m	10.544
Maximum dipole field	T	5.984
Number of dipoles	-	176
Maximum quadrupole gradient	T/m	36.049
Number of quadrupoles	-	235

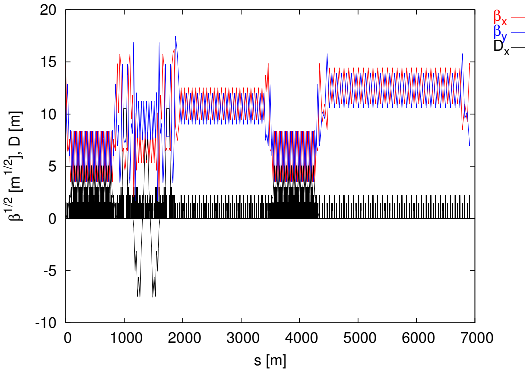

(a) δ=0

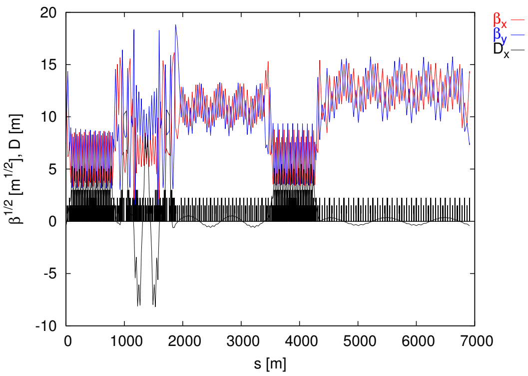

(b) δ=5‰

Figure 42. Optical functions in the beta-beam decay ring at the reference energy and at the injection energy.

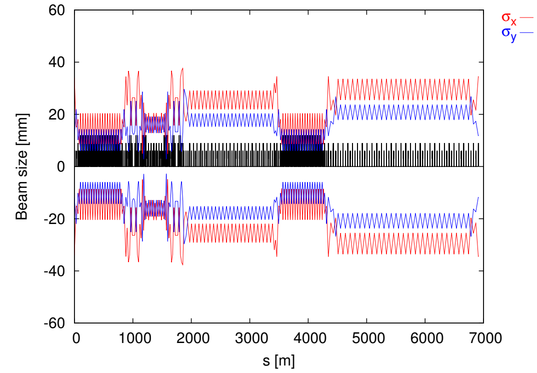

(a) δ=0

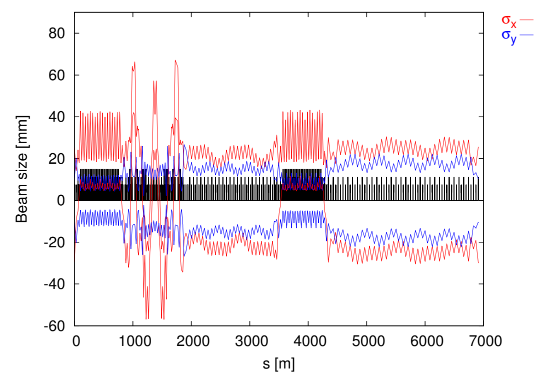

(b) δ=5‰

Figure 43. Beam sizes at 6σ and 5σ in the decay ring respectively at the reference (top) and injection energy (bottom).

Table IX. Optical parameters at the injection point.

-	Units	Stored beam	Injected beam
β_x	m	25.0	26.1
β_z	m	54.1	64.2
α_x	-	-0.43	-0.45
α_z	-	-0.17	-0.02
D_m	m	10.54	10.46
$\Delta E/E_0$	10^{-3}	0	5
σ_E/E_0	10^{-3}	2.5	0.4
ϵ_x	π mm.mrad	0.15	0.15
ϵ_z	π mm.mrad	0.08	0.08
n	-	6	5
Beam size	mm	26.4	10.7
e_S	mm	15	
X_{CO}	mm	36.5	

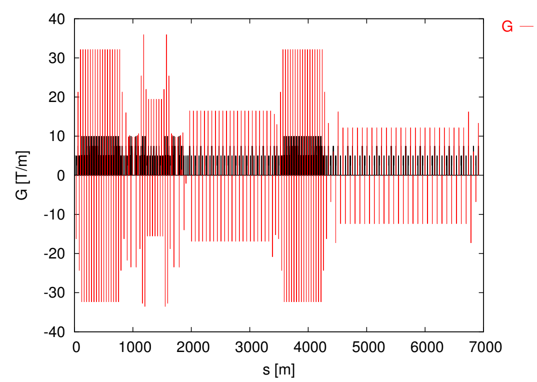

Figure 44. Gradients of the quadrupoles in the beta-beam decay ring.

2. *Dynamic aperture*

The natural chromaticity in the decay ring is $Q'_x = -22.871$ (or $Q'_x/Q_x = -1.255$) and $Q'_y = -25.867$ (or $Q'_y/Q_y = -1.424$). In order to accept the injected beam at $\delta = 5‰$, the natural chromaticity must be corrected by sextupole families in the dispersive areas. Two sextupole families located in the arcs are used. The phase advance per FODO lattice in the arcs is $\pi/2$ in both planes, which enables to compensate some geometric aberrations due to the presence of sextupoles. The dynamic aperture for 10,000 turns at the center of the chicane in the energy range of the stored beam can be seen in Figure 45). The RMS beam size in the horizontal and vertical planes is respectively 1.782 mm and 2.054 mm. The dynamic aperture is large enough to accept the whole beam (more than 20 σ).

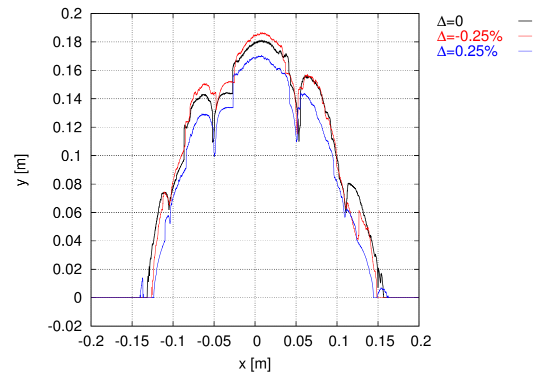

Figure 45. Dynamic aperture around the chromatic orbit for 10,000 turns at the middle of the injection insertion.

B. Correction of the closed orbit.

Unavoidable magnet misalignments and errors of the main magnetic field occur in the magnetic elements in the arcs. One of the consequences is a distortion of the closed orbit [75, 76]. The code *BETA* [77] enables to calculate the RMS closed orbit in presence of these defects. The assumed tolerances for the misalignments are given in Table X according to the values for LHC [78] and RHIC [79]. The standard deviation of the residual closed orbit without correction is then given on Figure 46. The BPMs are assumed to be ideal. It appears that the r.m.s. error on the closed orbit is a few centimeters, which makes the closed orbit correction necessary. 120/117 horizontal/vertical dipole correctors were inserted near focusing/defocussing quadrupoles in the whole structure and 120/117 horizontal/vertical BPMs were needed. After correction, the r.m.s. error of the closed orbit is less then 0.7 mm (see Figure 46). The maximum of the distortion is in the chicane; no corrector near the injection point was inserted. The angular distortion of the closed orbit in the long straight section is less than 0.01 mrad and very small compared to $1/\gamma$. The contribution to the divergence of the neutrino flux is then negligible. The maximum r.m.s. value is respectively 0.046 mrad for a horizontal dipole corrector and 0.070 mrad for a vertical dipole corrector. It is assumed that the closed orbit can be corrected up to three standard deviations. Finally, the integrated field in the dipole correctors must be respectively 0.128 T $\cdot$ m and 0.195 T $\cdot$ m.

1. *Case of a decay ring at γ = 350*

New scenarios for the Beta Beams were proposed by the EUROnu physics workpackage [80] to increase the physics reach of the Beta Beam facility. One of the proposals is to accelerate the Helium and Neon ions to higher $\gamma = 350$. The required neutrino flux is kept the same (this is compatible with estimated possible production rates): 2.9×10^{18} anti-neutrinos per year from the decay of $^6He^{2+}$ and 1.1×10^{18} neutrinos per year from the decay of $^{18}Ne^{10+}$. The alternative scheme to get high energy neutrinos is to use $^8Li^{3+}$ and $^8B^{5+}$ but for the same flux in the alternative scheme is to get a flux of neutrinos and anti-neutrinos from $^8Li^{3+}$ and $^8B^{5+}$. The required annual flux is 2×10^{18}. Actually, the highest γ value which can be reached with the SPS is 450 for protons, which means a $\gamma = 150$ for Helium (by scaling with Z/A). Injecting ions at $\gamma = 350$ implies that the SPS has to be upgraded to higher energies.

The aim is to quantify some of the implications of a

Table X. Assumed tolerances for magnetic elements.

Defect type	Units	RMS value
DIPOLES		
$\frac{\Delta B}{B}$	10^{-3}	0.5
Horizontal misalignment	mm	0.5
Vertical misalignment	mm	0.5
Longitudinal misalignment	mm	0.5
Rolling error	mrad	1
QUADRUPOLES		
$\frac{\Delta k}{k}$	10^{-3}	1
Horizontal misalignment	mm	0.4
Vertical misalignment	mm	0.4

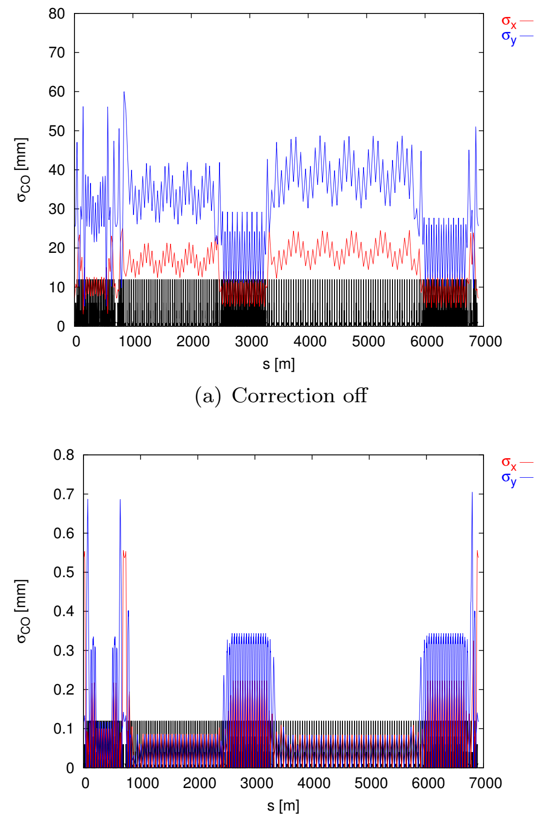

(a) Correction off

(b) Correction on

Figure 46. Closed orbit distortion (RMS value) without and with correction (in red, horizontal distortion and in blue vertical one).

higher γ decay ring, and to compare with the $\gamma = 100$ case and with the LHC [81]. For a decay ring at $\gamma = 350$, the acceleration scheme has not been studied. In order to make the comparison relevant, we have made some assumptions:

- The ramping speed of the upgraded SPS is the same as the SPS. Therefore, more time is needed to reach $\gamma = 350$ for the ions, which implies an increase the repetition time T_{rep}.
- The normalized transverse emittance is the same as for the $\gamma = 100$ case. The acceleration scheme before injecting into the upgraded SPS is assumed to be the same.
- The RF system of the decay ring is not changed; it is assumed that the same voltage and the same RF frequency are kept.
- The bunch length is not changed. The longitudinal emittance of the beam is then deduced from this constraint.
- The merging is assumed to occur without any errors and with the same RF program. In other terms, the number of merges n_{merges} before losing the ions is the ratio between the longitudinal emittance of the stored beam and the one of the incoming beam. The longitudinal emittance of the incoming beam is assumed to be the same as in FP6. The number of stored ions N_{tot} can be deduced from the number of injected ions N_{inj} by:

$$N_{\text{tot}} = N_{\text{inj}} \frac{1 - 2^{-\frac{n_{\text{merges}} T_{\text{rep}}}{\gamma \tau}}}{1 - 2^{-\frac{T_{\text{rep}}}{\gamma \tau}}}$$

- The theoretical single bunch intensity limit from collective effects due to transversal mode coupling is calculated from the formula (see Eq. Eq. (21))[82]:

$$N_{bx,y}^{th} = \frac{32}{3\sqrt{2}\pi} \frac{R|\eta|\epsilon_l^{2\sigma}\omega_r}{\langle\beta\rangle_{x,y} Z^2 \beta^2 c R_\perp}$$

  where R is the average ring radius, η the slip factor, $\epsilon_l^{2\sigma}$ the longitudinal emittance at 2σ in eV.s, ω_r the cut pulsation linked to the beam pipe radius (6 cm) and $R_\perp$ is the transverse wall impedance (assumed to be 1 MΩ/m for the decay ring). In reality, that is an optimistic upper limit and generally, the instabilities are excited for a smaller beam intensity. For the LHC, the given impedance is without any collimator and for two frequencies (8 kHz and 20 MHz).

The reference case (noted **ref**) at $\gamma = 100$ is compared to two scenarios at $\gamma = 350$. In the first case (noted **1**), the circumference is kept the same and the field of the dipoles is scaled with the magnetic rigidity. In the second case (noted **2**), the circumference is scaled to keep the same magnetic field in the magnets. The results are summarized in Table XI. In order to make the comparison easier, we have added in the last columns the parameters of the proton beam in the LHC after acceleration.

In the first scenario, the required magnetic fields are high. The technical feasibility of such magnets has to be studied. In the R&D program for the LHC, an ultimate upgrade would be to double the energy of the protons (DLHC). The magnetic field of the dipoles for the DLHC is about 20 T, which is outstanding. Other challenging items are the stored beam energy, which is about the same as in the LHC and the collective effects. Higher intensities have to be stored in the Decay Ring to keep the production rates and the flux the same for the increased life times of the isotopes at higher γ. The high intensities stored in the Decay Ring needs additional studies concerning the safety and the and beam control.

In the second scenario, the circumference is almost like the LHC circumference and the magnets are less than those of the LHC, however, the cost of a larger ring with a large number of elements is likely to be higher. The stored beam energy is a concern.

The presence of collimators in the decay ring will increase the impedance seen by the beam, which will change the collective effect issues.

To conclude, the parameters for a decay ring at $\gamma = 350$ are outstanding and require constraints similar to the ones of the LHC. The stored beam energy increases by a factor of about 12.

C. Merging of the injected and stored beams

One of the main issues of the Beta-Beam complex is the production of the ions. Moreover, the space charge effects limit the maximum intensity we can accelerate in the PS [69]. That is why it is necessary to use an accumulation scheme in the decay ring to increase the stored intensities and then to reach the required neutrino fluxes. The injection compensates the losses which occur between two injection cycles.

In conventional schemes, a cooling scheme is used to damp the emittances between two successive injections, which enables to keep the emittance of the stored beam constant [83, 84]. Unfortunately, it is not possible to use such a system for the decay ring. Electron cooling would require an electron beam of more than 50 MeV [85] and electron capture would introduce a severe loss mechanism. Stochastic cooling [83] rates at the bunch intensities envisaged are orders of magnitude too slow and laser-ion cooling is neither possible because the ions are necessarily fully stripped and also there is no significant synchrotron radiation to provide damping.

Table XI. Comparisons of a decay ring at $\gamma = 350$ with the reference case.

	Units	He	Ne	Li	B	LHC p
Nominal annual ν flux	10^{18}	2.9	1.1	14.5	5.5	-
γ		100 350 350	100 350 350	100 350 350	100 350 350	7460.523 7460.523 7460.523
Half-life time	s	81.0 283.5 283.5	167.0 584.5 584.5	83.8 293.3 293.3	77.0 269.5 269.5	∞ ∞ ∞
Magnetic Rigidity	T.m	934.87 3272.2 3272.2	559.27 1957.5 1957.5	830.64 2907.4 2907.4	498.50 1744.8 1744.8	23349 23349 23349
Decay ring circumference	m	6911.5 6911.5 24190	6911.5 6911.5 24190	6911.5 6911.5 24190	6911.5 6911.5 24190	26659 26659 26659
Dipole magnetic field	T	5.984 20.95 5.984	3.580 12.53 3.580	5.317 18.61 5.317	3.191 11.17 3.191	8.327 8.327 8.327
Repetition time	s	6.0 15.6 15.6	3.6 9.6 9.6	4.8 14.4 14.4	3.6 9.6 9.6	- - -
Total number of stored ions	10^{13}	9.346 32.50 32.50	7.178 25.08 25.08	48.18 168.2 168.2	16.7 58.20 58.20	32.29 32.29 32.29
Number of stored ions/bunch	10^{12}	4.673 16.25 16.25	3.589 12.54 12.54	24.09 84.08 84.08	8.35 29.10 29.10	32.29 32.29 32.29
Stored beam energy	MJ	8.3937 102.15 102.15	19.282 235.79 235.79	57.668 704.45 704.45	19.984 243.87 243.87	362.16 362.16 362.16
Average intensity	A	1.30 4.52 1.29	4.99 17.428 4.749	10.04 35.06 10.02	5.80 20.22 5.78	0.582 0.582 0.582
Peak intensity	A	227.9 792.3 792.3	875.0 3057 3057	1762 6150 6150	1017 3547 3547	0.582 0.582 0.582
Power lost by decay	W/m	9.872 34.78 9.938	11.41 40.00 11.43	66.18 232.3 66.37	25.20 88.54 25.30	- - -
Limit Collective Effects/bunch	10^{12}	38.6 139 485	4.64 16.7 584	23.0 82.5 289	8.27 29.7 104	- - -

1. *Dual RF system*

In the case of the beta-beam decay ring, the losses by β decay are compensated by regular injections in presence of the stored beam. The ions are injected at an energy slightly different from the one of the stored beam on their chromatic orbit. Besides, they are merged to the stored beam by varying the voltage and the phase of two cavity families, of which one is at the frequency 40 MHz and the other at the double frequency 80 MHz [86]. Such a system has already been used to create halos or change the distribution of ions in the longitudinal phase space [87, 88]. The principle was experimentally tested by injecting a hollow bunch [89].

The injection consists in three steps.

- The stored beam is deflected to the blade of a septum magnet by using a system of four kickers. The fresh beam is injected "off momentum" and deflected by the septum magnet. The kickers are then switched off.
- Whereas the main RF cavity family, at the harmonic number $h = 924$ (40 MHz), is on, the secondary family is still off. After a quarter turn in the longitudinal phase space, the injected beam is at the same energy as the stored beam but is late.
- The secondary cavity family, at the harmonic number $h = 1848$ (80 MHz), is switched on. The RF program is then run to merge both beams.

The beta-beam RF system uses two cavity families, of which one is at double frequency. The reference particle, which corresponds to one of the synchronous particles, is not accelerated. In the injection scheme for the beta-beam, a fresh beam is injected off momentum into the decay ring. One turn after the injection, two beams are then circulating into the decay ring: the stored beam at the nominal energy and the injected beam with an offset in energy. The aim of the RF program is to merge both beams to get a unique beam at the reference energy. Four main steps which will be detailed in the following, can be identified [86, 90]:

1. rotation of a quarter turn in the longitudinal phase space;
2. asymmetric merging with a constant area for the capture bucket;
3. symmetric merging;
4. progressive switching off of the second cavity family.

The whole RF program was calculated by using *Mathematica* [91]. We will respectively note V_1, ϕ_1, V_2, and ϕ_2 the voltage and phase of the first and second cavity. We will use $r = V_2/V_1$ the ratio between the voltages of the two cavities and $\phi_{21} = \phi_2 - 2\phi_1$ the phase difference.

2. Rotation of a quarter turn in the longitudinal phase space

First, only the first cavity is on and its maximum voltage is 54 MV for $^6He^{2+}$. The distribution of the incoming beam is assumed to be parabolic in the longitudinal phase space. Moreover, the beam is injected with a phase offset and tilted to optimize the capture at the injection. The fresh beam makes then a quarter turn (31 turns) in the longitudinal phase space. The capture bucket should be then centered on this phase to maximize the capture of the fresh beam.

3. Asymmetric merging with a constant area for the left bucket

The second cavity family is then switched on and the maximum voltage of the first cavity family is then decreased from 54 MV to 35 MV for $^6He^{2+}$ [92]. The voltages of both cavity families and their phases were calculated to maximize the number of ions trapped in the capture bucket. For synchronism reasons with the CERN-SPS, the azimuthal position of the center of the stored beam must stay the same from an injection to another.

The area of the capture bucket is taken equal to the full longitudinal emittance of the injected beam and will be kept constant along this process. If we choose a larger area for the capture bucket, the gain on the number of trapped ions at the injection is mitigated by the quicker blow up of the stored beam. We have chosen to reduce adiabatically the voltage of the second cavity, keeping the voltage of the first cavity constant. At the end of the asymmetric merging, the areas of both buckets are equal with ϕ_{21}=0°. The merging becomes symmetric.

4. Symmetric merging

During this step, the area of the left bucket is not kept constant whereas the buckets are kept symmetric ($\phi_{21} = 0$). At the end of the symmetric merging, $r = 0.5$ and the synchrotron frequency is zero. We would need then an infinite time to perform an iso-adiabatic merging. Therefore, it was chosen to linearly decrease ϕ_1 up to 180°. The merging symmetric stops when r=0.5.

5. Progressive switching off of the second cavity

We linearly increase the voltage of the first cavity whereas we adiabatically switch off the voltage of the second cavity. The total time of the merging is 143 ms. The variation of phases and voltages while the RF merging is given on Figure 47 for $^6He^{2+}$.

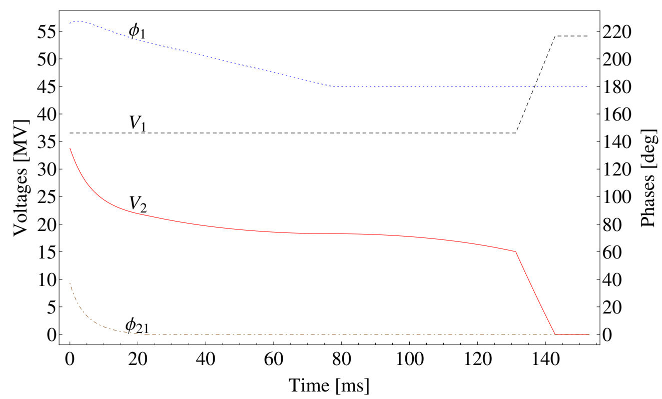

Figure 47. Variations of the phases (in blue dotted for ϕ_1 and in brown dot-dashed for ϕ_{21}) and voltages (in red for V_1 and in black dashed for V_2) of the two cavity families during the RF program for Helium.

6. Simulation of the merging

To illustrate the different steps of the merging, we have drawn the injected beam at different moments. The simulation was performed after applying the RF program illustrated on Figure 47 [93]. First of all, the fresh beam is injected with an offset of 5‰ in energy. This energy offset was determined to enable the insertion of a septum blade between the stored and injected beams at the injection [69]. In order to optimize the capture, the beam does not enter exactly in phase with the stored beam and was tilted. The longitudinal emittance of the entering Helium 6 beam was taken equal to 1 eV.s according to the FP6 database [94]. The beam is shown on Figure 48 for several steps while the merging process. After one quarter turn, the beam is on momentum but is late compared to the stored beam. Since the beam is injected in a non linear region, the beam shape is strongly modified and has lost its initial elliptical shape. The second cavity is switched on and the asymmetric merging occurs. At the end of the asymmetric merging, most ions are still in the capture bucket. Some of them have generated a halo, which corresponds to the ions which were not initially in the capture bucket. The symmetric merging is then performed to go on the merging. At the end of the symmetric merging, the center of the fresh beam is at the origin. The area of the beam seems to have doubled. In fact, during the symmetric merging, the capture bucket is merged with its symmetric centered on the origin. At the end of the merging, both buckets have merged and according to Liouville's theorem, the area has doubled. The second cavity is then progressively switched off to obtain the final beam. The beam is then stored until the RF merging is performed again for the next injection.

7. Barrier Buckets

An alternative injection scheme was studied in [95]. The idea is to use voltage barriers to squeeze all incoming ions from SPS into one so called Barrier Bucket. A high intensity of ions inside the bucket increases the neutrino flux and thereby also the sensitivities of the experiment. The time spread of the bucket would however decrease the sensitivities since that would worsen the suppression factor of the experiment. The question was then to study whether it is possible to optimize between the ion intensity kept inside the bucket and the duty cycle that the bucket occupies so that the sensitivities comply with the requirements for the Beta-Beam.

The conclusion was that for a bucket with a size corresponding to 4% (2%) duty cycle of the DR, barriers with filling times 1/2 (or 300 ns) (1/4 or 150 ns) of the SPS cavities are necessary so that not more than 80% of the ions escape the bucket before they decay. By additionally assuming an ion production rate of 10^{14} ions/s for both ^{8}B and ^{8}Li and no charge intensity limit in the SPS a much too optimistic (anti) neutrino flux of (7.57×10^{18}) 3.25×10^{18} was estimated. Even with these fluxes sensitivity plots of δ_{CP} and θ_{13} show that a suppression factor for the atmospheric background less than 1% would be needed. Since that suggests unrealistic RF cavities in the DR the conclusion is that the Barrier Bucket method is not optimal for the FP7 framework. The Barrier Bucket scheme would be interesting again only if the SF could be significantly enlarged.

D. Decay Ring RF System Design

In order to merge the stored bunches with the injected bunches in the decay ring 40 MHz RF is required in quadrature with the beam, as well as 80 MHz RF [92]. The required voltage is 55-35 MV in both systems for Helium. The stored current is 227 A hence the beam induced voltage is larger than can be controlled effectively with a realistic RF power. In order to reduce the beam loading it is necessary to modify the RF system to either detune the cavity or use a lower R/Q cavity. Both have been considered for the decay ring and each have their own challenges which shall be addressed.

1. Detuning

As the beam is in quadrature with the RF the beam-loading is strongly capacitive, adding additional inductance to the cavity, by detuning it, can compensate for this [69]. In principle the phase shift due to the RF being run at the wrong frequency is equal and opposite to the phase shift caused by the beam. For a cavity of frequency, f, geometric shunt impedance, R/Q, gap voltage, V_g, and a beam of current, I_b, the phase shift is

$$\Delta\phi = \arctan\left(\frac{I_b R}{V_g Q}\right) \tag{13}$$

Hence the detuning in frequency should be

$$\Delta\omega \approx g = \omega_0\left(\frac{I_b R}{V_g Q}\right) \tag{14}$$

For the beta beam decay ring ($I = 200\ A$) using a cavity similar to the PS 40 MHz cavity [96] ($R/Q = 25\ \Omega$), and using a 300 kV gap voltage the required detuning is around 0.8 MHz. This results in a required RF power of 90 kW to keep the cavity on voltage compared to 5 MW required without detuning. As the beam-loading is forced at the bunch rep rate of 40 MHz and the cavity is filled at a detuned frequency there is a small phase shift of 6 degrees, correcting this phase shift requires 270 kW. Calculations have been performed to study the effect of beam current fluctuations on the RF amplitude and phase. As the current varies from the design value the required RF power increases sharply, as can be seen in Figure 49.

However problems arise due to the pulsed nature of the decay ring. The beam comprises of 20 bunches each separated by 25 ns, giving a pulse length of 500 ns. However as the decay ring is around 7 km long there is a large gap between pulses of over 20 μs. The cavity is detuned hence when the beam is not present we must fill at the detuned frequency, while running at 40 MHz when the beam arrives. In order to switch the frequency of the RF source by 0.8 MHz in 25 ns we would require a very wide bandwidth, low output Q tetrode. Such systems do exist but typically not at high power or gain, hence it would be necessary to use two separate amplifiers.

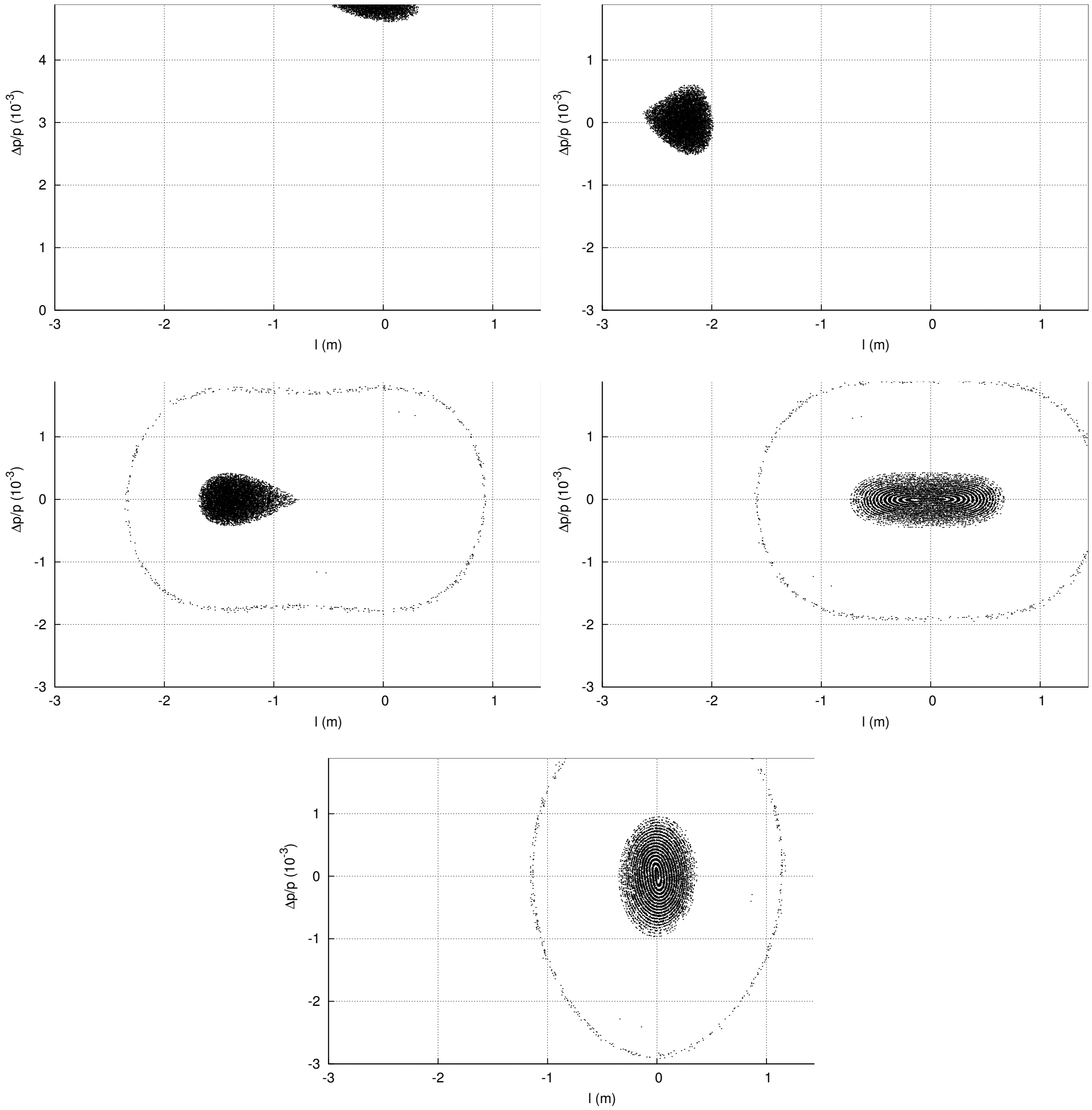

Figure 48. Fresh Helium beam in the longitudinal phase space after entering into the decay ring , after one quarter turn, before the symmetric merging, while the symmetric merging, at the end of the merging.

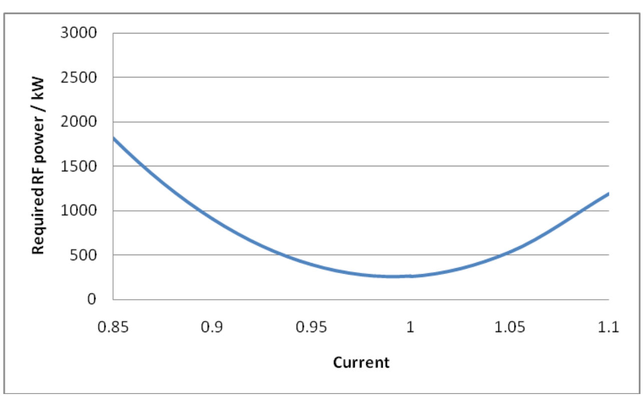

Figure 49. RF power required as a function of current fluctuations

A further challenge comes from the stacked filling pattern of the decay ring. It is proposed that the ring will be stacked in 20 A shots, hence the current will vary with time. There will however be a large time gap between shots. If the cavity frequency is kept constant at the value calculated for the maximum current, then the beam will detune the cavity more than expected and the cavity will be resonant at a third frequency, with its frequency increased by a 20^{th} of the full cavity detuning. The RF amplifier will have to fill the cavity at this frequency until the cavity can be mechanically detuned back to the correct frequency, unless the cavity bandwidth is larger than the detuning. The required power to keep the cavity at the correct phase and amplitude will be higher, as shown previously. As the required detuning is proportional to beam current the cavities resonant frequency will have to vary when the beam current varies as running the cavity as the frequency shift would cause a very large phase transient during the train (8 degrees for a single shot). The typical response time for cavity tuners is on the order of milliseconds, hence it would be several cycles before the cavity could be powered by the RF leading to large phase and amplitude transients (although it could probably be filled when the beam is not present). The tetrode would also have to alter its frequency as well. In order to keep the RF phase and amplitude under control it would be necessary to increase the bandwidth of the cavity such that it is greater than the change in the cavity frequency due to the beam in one shot. One method of increasing the bandwidth is to load the cavity with ferrite however this would significantly limit the voltage per cavity and hence requires hundreds of RF cavities. The alternative is to drop the cavity Q, either through losses or external damping. A 20 A change in beam current changes the cavity frequency by 100 kHz, hence a Q of at most 400 is required. When the beam is present the RF power requirement for a 300 kV is 200 kW, however it requires 3.5 MW to fill the cavity. Reducing the cavity voltage to 80 kV reduces the power requirement to 900 kW but this again requires more than 500 40 MHz cavities to reach 55 MV.

2. *Low R/Q design*

An alternative approach is to reduce the R/Q of the cavity to reduce the beam loading. This will also reduce the shunt impedance hence the cavity can be made superconducting to reduce the power requirements. Detuning is now only a few tens of kHz, however the cavity bandwidth is much narrower due to the higher Q factor hence we will still have to run at the detuned frequency when the bunch arrives. However as the beam induced power is much lower we are better able to cope with the additional power demands.

Reducing the R/Q by reducing the voltage experienced by the beam means we need to increase the stored energy to achieve a given cavity voltage. However we eventually run in to problems as we reach the peak surface electric and magnetic fields. For an R/Q of 2 Ω the maximum achievable voltage is 600 kV, hence for a 55 MV total voltage we would require 92 cavities.

As we are still using detuning we must also deal with the issue of the beam current changing. When a new bunch is injected and merged the current changes and hence so does the detuning. The detuning for a low R/Q system is much smaller and hence running at the wrong frequency for a few bunch trains does not cause a significant phase shift.

In order to determine the ideal R/Q we need to consider the maximum voltage, and hence number of cavities required, as well as the power required when the beam arrives. As the R/Q decreases the voltage decreases proportional to the square root of the R/Q. The power required to fill the cavity is only inversely proportional to the Q of the cavity as the voltage and R/Q scale together. A Q of 106 requires a power of 22.5 kW to fill the cavity or maintain the cavity voltage when the beam is not present. For the R/Q of 2 Ω the maximum voltage is 600 kV hence we require 92 cavities for 55 MV and an RF power per cavity of 480 kW. For an R/Q of 0.5 Ω we would need 184 cavities at 240 kW per cavity, hence the total power requirements as very similar.

3. *Recirculating Beam*

As the beam is recirculating the RF needs to be at the correct phase when the train returns. The revolution frequency of the decay ring is 43 kHz which is larger than the detuning. This makes it impossible to choose a harmonic for the detuned frequencies, hence a phase advance must be added to the RF phase at the end of the train in order for the phase to return to the correct value when the train returns to the cavity.

The RF system will have to run at several different frequencies depending on the stored current and this will complicate the LLRF system. It is proposed that the LLRF system would operate using a 40 MHz reference and digitally add a phase advance correction to the measured phase to correct for the detuned frequencies of operation.

4. *Beta Beam RF System proposed*

A SRF quarter wave cavity with an R/Q of 2 Ω is proposed. This allows an operating voltage of 0.6 MV, hence 92 cavities are required. The loaded Q of the cavity should be 10^6, hence the power required to fill the cavity is 90 kW. If the beam current is 227 A then the required detuning should be 32 kHz, hence after injection the cavity will have to run at a frequency 1.6 kHz higher until the cavity can be detuned, hence the phase shift due to this is 0.3 degrees which is acceptable. When running on resonance the required power to keep phase and amplitude on spec is 250 kW, however as the stored current increases from 95% of the maximum to the full stored current, the additional beam capacitance requires a power of 480 kW to keep the cavity on phase. However this power is only required during the pulse which is 500 ns long, the other 98% of the time, between the trains, is only 22.5 kW is required hence the total average power per cavity is only 35 kW which is more reasonable.

A low R/Q cavity can be realized by using a conventional quarter wave resonator and moving the point where the beam traverses the cavity to a location of lower voltage. This can be achieved by moving the beam towards either end of the cavity. This will unfortunately also provide a transverse electric or magnetic field that will provide a transverse kick to the bunch as the accelerating and deflecting fields are 90 degrees out of phase with each other. This however can be canceled by flipping the cavity orientation every other cavity. An alternative approach is to reduce the transit time factor for the cavity by reducing the radii of the inner and outer conductor of the resonator. As the field flips on either side of the inner conductor reducing the transit time factor also reduces the voltage, however reducing the inner conductor size also increases the peak electric field so it cannot be reduced too far. In addition making the cavity wider in the plane perpendicular to the beam velocity will increase the stored energy but it will also increase the voltage hence the shunt impedance goes up. However if we assume that we can move the beam axis to reduce voltage and shunt impedance then what we want to optimize is $V_{\max} \times \sqrt{2Q/R}$, which is the maximum voltage at the beam axis position that give R/Q=2 Ω. This voltage is maximum at when the width is a factor of 2 larger than the length.

It would seem more practical to have the quarter wavelength in the longitudinal direction in order to reduce the cavities transverse size, however in practice to achieve the design voltage and R/Q reduces a large transverse size so the widths ends up being very similar in both cases.

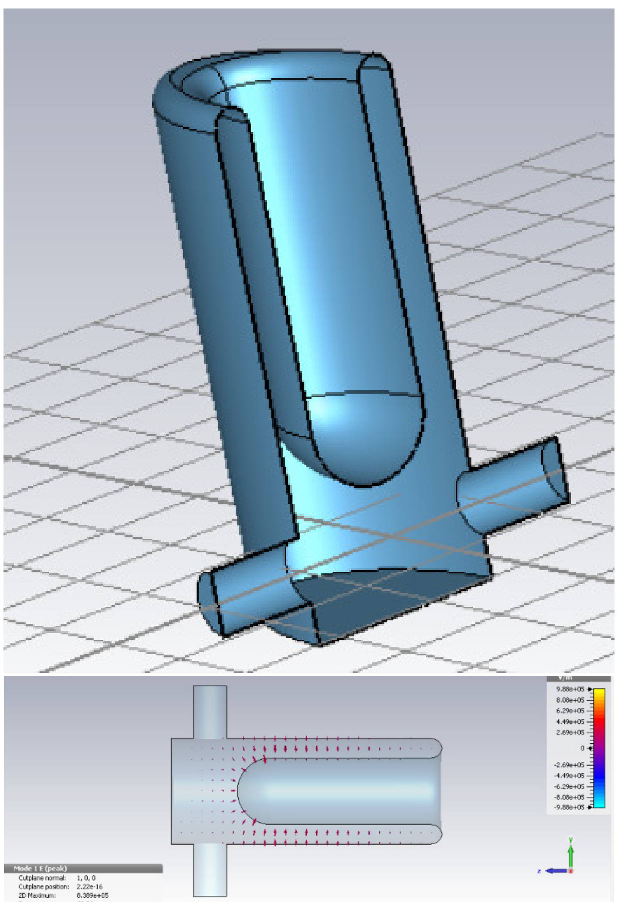

Figure 50. The cavity geometry, top, and the cavity electric field profile for the decay ring 40 MHz RF system, bottom.

The final cavity design, shown in Figure 50, has been simulated using CST Microwave studio [97]. It is 452 mm long and has a height of 1.9 m. However as the cavities must flip orientation every other cavity the total width will be twice this at 3.8 m, making the total cryostat width around 4.5-5 m wide. The peak electric field at the design voltage of 600 kV is 30 MV/m. The R/Q is 2 Ω, and the peak magnetic field is 67.5 mT. The geometry factor is 33.3 Ω so the BSC Q at 4.2 K is 3×10^9.

5. *Decay Ring RF System, Conclusion*

A solution is proposed for the Decay ring 40 MHz RF system. The proposed system requires 92 cavities, and a total RF peak power of 9 MW and a total average power of 3.2 MW. However this system is based on phase quadrature but the decay ring will require the phase to be linearly increased during bunch merging which is likely to increase the required RF power further. The total cavity width is 1.9 m hence a cryostat is likely to be 4.5-5 m wide and 1.5 m wide. Each cavity is 0.452 m long. If we assume a packing factor of 1.5 and 92 cavities the total RF section length will be about 62 m long.

E. Beam losses

For this study, only two beam losses were looked at:

- losses due to the β-decay of the radioactive ions;
- losses due to the RF merging after the injection. Some injected ions are not captured and are then lost while the merging. Moreover, the merging process blows up the longitudinal emittance which makes some particles be collimated at the end of the injection.

The decay losses occur continuously and anywhere in the ring whereas the losses due to the RF merging occur mostly after the injection and where the momentum acceptance is the lowest.

1. *Decay losses*

The aim of the decay ring is to store high intensity and high energy beams of β radioactive ions until their decay. A first study was realized in order to quantify the average activation of the concrete walls and their impact on the public health [98]. First estimations show that these values are under the allowed ones. Nevertheless, since the superconducting magnets may be sensitive to the beam losses losses, the deposition of the decay products in the vacuum pipe walls. Protection of the superconducting coils is an issue that should be considered early in the lattice and magnet design.

When an ion decays, its momentum variation is negligible (the energy taken by the electron and the antineutrino is low compared to the energy of the secondary ion) whereas its charge number increases or decreases by 1. Therefore, its magnetic rigidity changes. In this part, we shall respectively use the subscripts 0 and 1 to refer to the primary and secondary ions. We shall consider as a decay product only the secondary ion which comes from the decay of the radioactive ions. The relative difference of magnetic rigidity between the secondary ion and the primary ion is then:

$$\delta = \frac{\Delta(B\rho)}{B\rho} = \frac{Z_0}{Z_1} - 1 \tag{15}$$

The ions $^{6}He^{2+}$, $^{18}Ne^{10+}$, $^{8}Li^{3+}$ and $^{8}B^{5+}$ respectively decay into $^{6}Li^{3+}$, $^{18}F^{9+}$, $^{8}Be^{4+}$ and $^{8}Be^{4+}$ and the magnetic rigidity variation is respectively $\delta = -1/3$, $\delta = +1/9$, $\delta = -1/4$, and $\delta = +1/4$. The variation is so large that the decay products are quickly lost after deflecting in the dipoles, which makes the extraction impossible in the arcs.

Since the revolution time (23 μs) is low compared to the half-life time of the stored ions in the laboratory frame ($\approx$ 100 s), we can assume that the number of ions lost per meter is the same anywhere in the structure. The probability $P(t)$ that an ion did not decay after t seconds is then:

$$P(t) = 2^{-\frac{t}{\gamma\tau}}$$

where τ is the half-time of the ion at rest.

With an initial number of ions of N_0, the number of ions which decay per second is then $-N_0P'(t)$. The maximum power lost by decay per meter $\mathcal{P}_m$ is then:

$$\mathcal{P}_m = \frac{\gamma - 1}{\beta\gamma}\frac{N_0 E_0 \ln(2)}{2\pi R\tau} \tag{16}$$

By using the stored intensities given in Table VII, we obtain the power lost by decay per meter in the structure are respectively 9.872 W/m, 11.41 W/m, 66.18 W/m and 25.20 W/m for Helium, Neon, Lithium and Boron.

The first approach handle the decay losses in the arcs was to insert absorbers after the dipoles. The lack of flexibility and the significant impedance increase, suggested that other solutions should be studied.

Since the decayed ions are deflected essentially only in the magnet mid planes, it was decided to use coil free dipoles and quadrupoles as shown in figure Figure 51. By this way, the decay products will impinge a region without any superconducting coil.

Since the RMS vertical beam size is about 2.5 mm and the magnet aperture is 60 mm, the opening angle can be 5°. First studies of such a dipole for the beta-beam decay ring were shown in [99, 100]. First designs of open mid-plane quadrupoles were shown on [74].

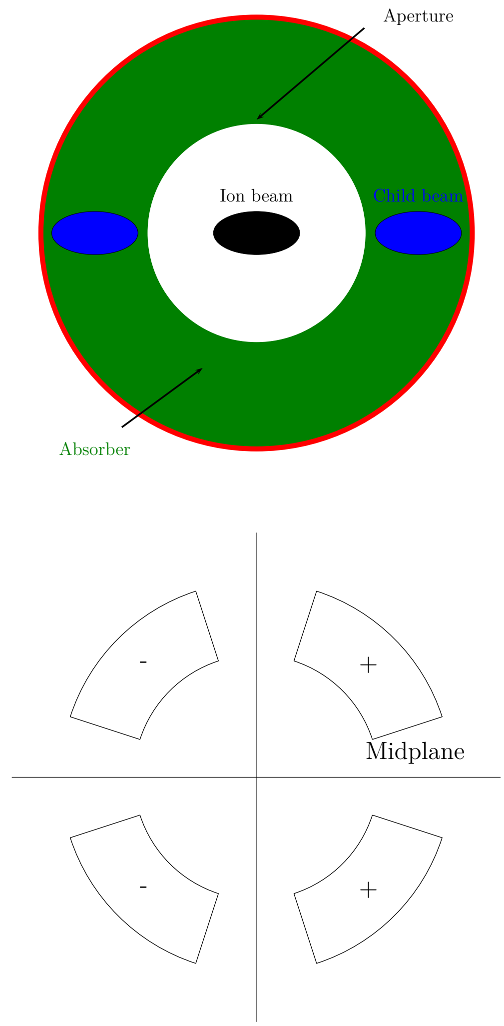

Figure 51. Schematic repartition of the losses in the dipoles (top). The solution is to open the coils on the mid plane (bootom).

2. *Injection losses*

After each merging, the beam blows up in the longitudinal phase space due to Liouville's theorem. Since there is no cooling quick enough to compensate the growth of the longitudinal emittance, it is necessary to collimate in energy between two successive injections. Since some particles with a relative momentum difference of 2.5‰ hit the septum blade at the injection, it was decided to collimate at $\delta_C = 2.5$‰. Because of the large average power to collimate, it was decided to use a multi-staged collimation section.

Since the particles have a betatron amplitude, some of them will hit the collimator although their energy difference is lower than the energy at which we want to collimate. We have evaluated the efficiency of the collimation by tracking a large number N of particles in the longitudinal phase space for 40 merging processes. At the end of the merging, the voltages and phases of the cavities do not vary. We consider a particle P_i of the beam. The coordinates of the particle in the longitudinal phase space after n injections is $(l(n), \delta(n))$. We calculate then the maximum relative energy difference $\delta_i(n)$ that P_i can reach while the synchrotron motion before the next merging. If $\delta_i(n) > \delta_C$ then P_i is lost. If $\delta_i(n) < \delta_C$ then P_i hits the collimator if its normalized betatron amplitude is greater than $k_i(n) = (\delta_C - \delta_i(n))\frac{D_{n,x,C}}{\sqrt{\epsilon_x}}$ where $D_{n,C,x} = \frac{D_x}{\sqrt{\beta_x}}$ at the collimation point. Since we know the transverse distribution, we know the probability $p(k_i(n))$ that P_i has a normalized betatron amplitude smaller than $k_i(n)$. The number of ions $N_{\text{ion}}(D_{n,x,C}, n)$ which survived after n injection cycles can be then evaluated by:

$$N_{\text{ion}}(n) = \frac{1}{N}\sum_{i=1}^{N} N_{\text{inj}} p(k_i(n)) 2^{\frac{-nT}{\gamma\tau}} \tag{17}$$

The total number of ions lost by decay $N_d(D_{n,x,C})$ and the one lost by momentum collimation $N_C(D_{n,x,C})$ between two injections is then:

$$N_d(D_{n,x,C}) = \left(2^{\frac{T}{\gamma\tau}} - 1\right)\sum_{n=0}^{\infty} N_{\text{ion}}(n+1) \tag{18a}$$

$$N_C(D_{n,x,C}) = \sum_{n=0}^{\infty}\left(N_{\text{ion}}(n) - N_{\text{ion}}(n+1)2^{\frac{T}{\gamma\tau}}\right) \tag{18b}$$

That enables to plot the repartition of the losses between two injections versus $D_{n,x,C}$ (Figure 52). The losses approach an asymptote for $D_{n,x,C}$ equal to a few $\text{m}^{1/2}$.

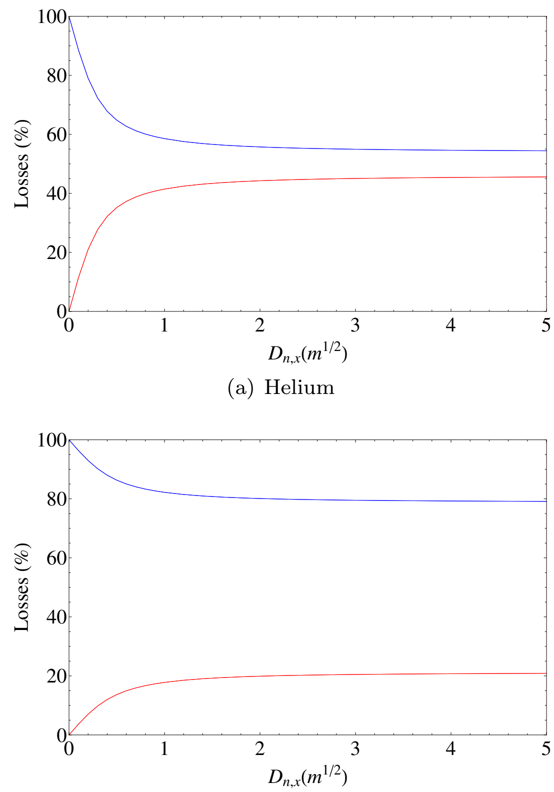

(a) Helium

(b) Neon

Figure 52. Sum of the losses by collimation (red) and by decay (blue) versus the normalized dispersion at the primary collimator for a Gaussian beam.

F. Collective Effect Studies

High intensity ion beams are foreseen for the Beta Beam project. High intensity bunches can have non-negligible amount of charges which could cause the particles to interact with each other and with the vacuum chamber, so called "Collective Effects". Collective effects could limit the final performance of the accelerators. The studies of instabilities of all machines in the Beta Beam complex is therefore a crucial part of the project.

1. *Direct space charge effect*

Although the beam is relativistic, the direct space charge is not negligible due to a charge of several microcoulombs per bunch. For a beam with a Gaussian transverse distribution and a parabolic longitudinal distribution, the incoherent tune shift is [101]:

$$\Delta Q_{x,y} = -\frac{3}{4}\frac{Z^2}{A}\frac{N_{\text{bunch}} r_0 R}{L_{\text{beam}}\beta^2\gamma^3\epsilon_{x,y}\left(1+\sqrt{\frac{\epsilon_{y,x}Q_{x,y}}{\epsilon_{x,y}Q_{y,x}}}\right)} \tag{19}$$

where $\epsilon_{x,y}$ is the transverse RMS emittance and r_0 the classical proton radius.

The tune shifts for the different ion species are summed up in XII. Since Neon ions have the largest charge number, their tune shift is the greatest. The tune shift is then at the limit we can manage for a storage ring. A special care should be taken to verify if the beam is perturbed by its own potential. This study has not been pursued yet. A solution to mitigate the direct space charge effects could be to inject a beam with a larger transverse emittance or a mismatched beam.

2. *Transverse Broadband Resonance Impedance*

The electric field lines from the bunch causes an image charge to travel along with the bunch in the vacuum chamber [102]. Geometrical or material variations of the vacuum chamber cause the image charge to radiate electro magnetic fields called wake fields. The beam then looses energy that heats the chamber and feeds the wake fields that could be trapped and remain oscillating for some time. If the wake fields last for the duration of the bunch (≈100 ps) particles in the "tail" of the bunch can interact with the wake fields due to the particles in the "head" of the bunch and cause *single bunch instabilities*. Wake fields that last until the next bunch (≈ns) could cause *multi bunch instabilities*. For the studies shown in

Table XII. Laslett tune shifts for the different ion species in the decay ring.

	Units	He	Ne	Li	B
Charge number Z		2	10	3	5
Mass number A		6	18	8	8
Rest energy	GeV	5.606	16.77	7.471	7.472
γ		100.0	100.0	100.0	100.0
Horizontal tune	m	18.23	18.23	18.23	18.23
Vertical tune	m	18.16	18.16	18.16	18.16
Number of ions/bunch	10^{12}	4.673	3.589	24.09	8.35
Number of stored ions/bunch	10^{12}	4.457	3.423	3.162	2.895
Hor. RMS emittance	μm.rad	0.110	0.110	0.110	0.110
Vert. RMS emittance	μm.rad	0.079	0.079	0.079	0.079
Total bunch Length	m	1.933	1.933	1.933	1.933
Laslett tune shift		-.025	-.164	-.204	-.213

this report we have focused on single bunch instabilities only.

The action of the wake fields are described by the wake potential, $W(t)$, in the time domain and by the impedance, $Z(\omega) = \mathcal{F}[W(t)]$, in the frequency domain. If the wake fields are caused by resistivity of the vacuum chamber material the impedance is called resistive wall impedance, $Z^{rw}(\omega)$, but is beyond the scope of this study. Here we will report on studies of impedances caused by wake fields trapped in cavities of the vacuum chamber, so called resonance impedances, $Z^{res}(\omega)$. If the quality factor is $Q = R\sqrt{C/L}$ and the resonance frequency is $\omega_r = 1/\sqrt{LC}$ the resonance impedance can be modeled as an RLC circuit [103] in the transverse plane as

$$Z_{\perp}(\omega) = \frac{R_{\perp}\frac{\omega_r}{\omega}}{1 + iQ\left(\frac{\omega_r}{\omega} - \frac{\omega}{\omega_r}\right)} \tag{20}$$

where $R_{\perp}$ is the *transverse shunt impedance.* $R_{\perp}$ is a value indicating the total divergence from a perfectly smooth vacuum pipe around the whole ring. The value for SPS is about 20 MΩ/m but for the DR this is an unknown value since the DR is yet a non-existing machine. Since the DR is a modern machine we can assume it will have a smooth vacuum pipe design and since it will not be as general machine as SPS it will also have less number of kickers. We can therefore assume a factor 20 better transversal shunt impedance; $R_{\perp}^{DR} \approx 1$ MΩ/m [104]. So far we have only studied short lived resonance wake fields, i.e. *broadband* ($Q = 1$) impedances in the transverse plane. There are many different types of collective effects that could lead to beam instability and limit the maximum number allowed ions per bunch, N_b^{th}, but this study is constrained to transverse broadband resonance impedances.

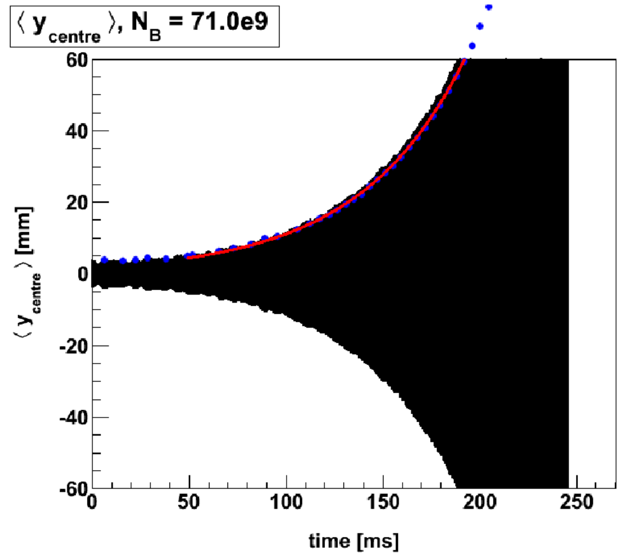

(a) Vertical oscillation

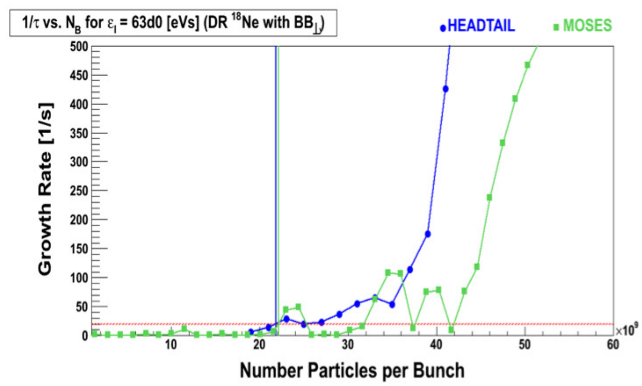

(b) Growth rate

Figure 53. **(a)** Vertical oscillation of the mean of the bunch from tracking simulation in HEADTAIL. Growth rate is given by exponential least square fit of the envelope of the oscillation. **(b)** Growth rate according to HEADTAIL (blue) and MOSES (green) as a function of bunch intensity.

3. *Methods to Estimate Bunch Intensity Limits*

Three different methods have been used to estimate N_b^{th}, the maximum number ions that could populate a bunch without too big chance for severe beam instability.

One approach is to use the peak current values of the bunch current and momentum spread as input to a coasting beam formula. This gives an expression for the intensity limit that we will call the coasting beam equation [82];

$$N_{b_{x,y}}^{th} = \frac{32}{3\sqrt{2}\pi}\frac{Q_{x,y}|\eta|\varepsilon_l^{2\sigma}\omega_r\left(1 + \omega_{\xi_{x,y}}/\omega_r\right)}{cZ^2\beta^2 R_{\perp}} \tag{21}$$

Here c is the speed of light in vacuum, $\omega_{\xi_{x,y}} = \xi_{x,y}Q_{x,y}\omega_{rev}/\eta$ and all other parameters are given in table XIII.

MOSES [105] solves an integral equation in the frequency domain to give the rise time, τ, of the instabilities for different head-tail modes as a function of the bunch intensity. The limit, I_b^{th}, is given by the most crucial head-tail mode after defining the maximum allowed growth rate, $(1/\tau)^{th}$. To reach the ion equivalent intensity threshold we divide by a factor Z; $\bar{I}_b^{th} = I_b^{th}/Z$. The maximum allowed number of ions per bunch is then given by the conversion $N_b^{th} = T_{rev}\bar{I}_b^{th}/Ze$. The green curve in figure 53**(b)** shows growth rates, $1/\tau$, as a function of bunch populations, N_b, from MOSES. The maximum allowed number ions per bunch, N_b^{th}, according to MOSES, is indicated by the green vertical line, for this example when $(1/\tau)^{th}$ was chosen to 20 Hz (indicated by red dotted line).

The third method uses the multi-particle tracking code HEADTAIL [106] where a bunch of macro-particles is sliced longitudinally and the impedance is assumed to be localized at a few positions around the ring. At each impedance location, each slice leaves a wake field behind and gets a kick by the field generated by the preceding slices. The bunch is then transferred to the next impedance location via a transport matrix. For the Beta Beam studies the possibility of bunches with ^{18}Ne and ^{6}He was added to the code. One of HEADTAIL's output, the vertical mean position of the bunch, is shown in figure 53**(a)** (black curve). Exponential least square fit [107] (red curve in figure 53**(a)**) to the envelope of the vertical oscillation gives the growth rate of the instability. The blue curve in figure 53**(b)** shows growth rates, $1/\tau$, as a function of bunch populations, N_b, from HEADTAIL. Same as for MOSES the bunch intensity limit, N_b^{th}, (blue vertical line in figure 53**(b)**) is reached when the rise time is shorter than allowed, i.e. $1/\tau > (1/\tau)^{th}$ (red dotted line).

4. Decay Ring Scans

With the three methods, mentioned above, we studied the effect on the bunch intensity limit, N_b^{th}, on the longitudinal bunch size by changing slightly the longitudinal emittance, ε_l, (figure 54**(a)**) and assuming $R_\perp = 2$ MΩ/m and $(1/\tau)^{th} = 400$ 1/s (see discussions below). We see that according to MOSES, HEADTAIL and the Coasting Beam equation (CB Eq.), see eq. (21), increasing ε_l the allowed number of ^{18}Ne per bunch increases but this also means an undesired increase in SF and momentum spread (also indicated in fig. 54 **(a)**). It is clear from fig. 54**(a)** that the bunch intensity limit for ^{18}Ne, $3.4 \cdot 10^{12}$, is far out of reach when $R_\perp = 2$ MΩ/m is assumed.

Since impedance could improve in modern machines compared to old accelerators a scan over the shunt impedance was performed to see the impact on N_b^{th} (figure 54**(b)**). This was done for transverse broadband resonance impedance with all the parameters used shown in table XIII.

Table XIII. Input parameters above the first line. Assumed transversal impedance parameters between the lines. Calculated parameters below the last line. These parameters are the same for the different isotopes.

Parameters	Description	DR
N_B	*Number Bunches*	20
h	*Harmonic Number*	924
C [m]	*Circumference*	6911.6
ℓ_{eff}	*Eff. Straight Sec.*	37.2%
ρ [m]	*Magnetic Radius*	155.6
γ_{tr}	*Gamma Transition*	16.772
γ	*Relativistic Gamma*	100.0
Q_x	*Horizontal Tune*	18.23
Q_y	*Vertical Tune*	18.16
$\langle\beta\rangle_x$ [m]	*Av. x-βtron Func.*	111.18
$\langle\beta\rangle_y$ [m]	*Av. y-βtron Func.*	106.63
$\langle D\rangle_x$ [m]	*Av. Dispersion*	0.936
$\xi_{x,y}$	*x,y Chromaticity*	0.0
b_x [cm]	*x Pipe Size*	12.0
b_y [cm]	*y Pipe Size*	12.0
$Q_\perp$	*Quality Factor*	1.0
f_r [GHz]	*Resonance Freq.*	1.0
$R_\perp[\frac{M\Omega}{m}]$	*Shunt Impedance*	1.0
$\beta = \sqrt{1-\gamma^{-2}}$	*Relativistic Beta*	1.00
$\eta = \gamma_{tr}^{-2} - \gamma^{-2}$	*Phase Slip Factor*	3.455e-3
$T_{rev}[\mu s] = \frac{C}{\beta c}$	*Revolution Time*	23.06
$f_{rev}[Hz] = \frac{1}{T_{rev}}$	*Revolution Freq.*	0.27e6
R [m] $= C/2\pi$	*Machine Radius*	1100
$\omega_c[GHz] = \frac{\beta c}{b_{x,y}}$	*Cut-Off Ang. Freq.*	2.50

Figure 54 **(b)** shows that for a shunt impedance at the level of SPS, $R_\perp^{sps} = 20$ MΩ/m, maximum number ^{18}Ne allowed per bunch, according to HEADTAIL, MOSES and CB Eq., is not more than $200{\cdot}10^9$. For $N_b = N_{b_{sat}}^{nom} = 3.4 \cdot 10^{12}$ ^{18}Ne per bunch $R_\perp < 0.2$ MΩ/m is needed, which is easiest seen in figure 54 **(c)**. It could be argued that instabilities with the longest rise times should define N_b^{th}, i.e. $(1/\tau)^{th} \to 0$. However in in figure 54**(b)** and **(c)** an optimistic approach was taken. It was assumed that slow instabilities can be damped with sextu- and octupoles, so $(1/\tau)^{th}$ was defined to 400 1/s for both MOSES and HEADTAIL. Also, defining $(1/\tau)^{th} \to 0$ makes our approach more sensitive to systematic uncertainties. This is shown in figure 54**(d)**, which is the same as figure 54**(c)** except for that $(1/\tau)^{th} = 0.2$ 1/s. For some $R_\perp$ very slow instabilities for very small intensities are probed by our method which causes the discontinuity in the HEADTAIL results. Since this happens much more for MOSES than for HEADTAIL it is clear that this is due to systematics in the methods and the MOSES results were chosen not to be included in this plot.

Attempts to damp instabilities, and thereby allow more ions per bunch, have been made. Instabilities can be damped by avoiding resonances, i.e. making sure particles in the bunch oscillates with different frequencies. Tune spread in the bunch can be introduced by two different type of magnets; sextupole and octupole magnets.

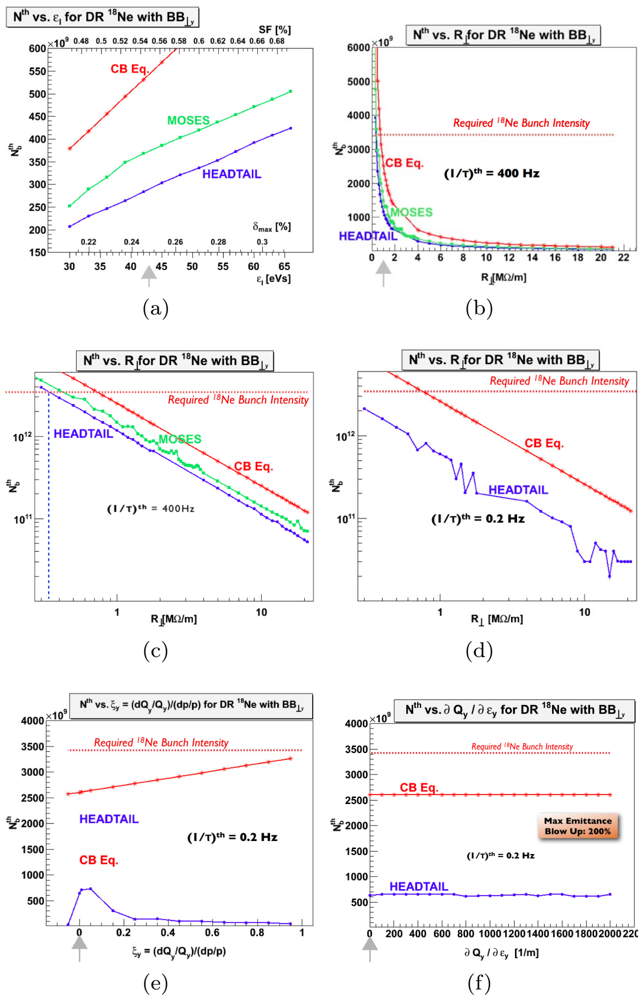

Figure 54. N_B^{th} as a function of **(a)** the longitudinal emittance and **(b, c, d)** the transversal shunt impedance according to the C.B. eq. (21), MOSES [105] and HEADTAIL [106]. Only the case for the neutrino emitter, ^{18}Ne, in the Decay Ring is shown. With the log-log scale in **(c)** we see that $R_\perp < 0.2$ MΩ/m is needed to allow $3.4 \cdot 10^{12}$ ^{18}Ne per bunch. Instability dampings were attempted with chromaticity **(e)** and amplitude detuning **(f)**, both without success.

With sextupoles it is possible to introduce a tune dependence on the momentum offset. The achieved tune spreads follow $\Delta Q_{x,y} = \xi_{x,y} Q_{x,y} \frac{\Delta p}{p}$ where $\Delta p/p$ is the momentum spread and ξ is the "chromaticity". By changing the chromaticity we investigated if the bunch intensity limit could be relaxed by increasing the sextupole magnet strength. It is known that the "rigid bunch mode" (n = 0) is stable for negative (positive) chromaticity below (above) transition, and unstable otherwise. So since $\eta > 0$ for the DR and since n = 0 is the most crucial mode (most likely to cause beam loss) we scanned $\xi \in [0, 1]$ (where the unity is chosen as a normal chromaticity scale according to [108]). The simulation results are shown in figure 54**(e)** for $(1/\tau)^{th} = 0.2$ 1/s since when damping is studied we do not assume any other damping. Also with damping it turned out that our methods were less vulnerable to systematics. It is evident that increasing the chromaticity would not help the intensity limit and it also confirms more instabilities for $\xi < 0$. Octupole magnets can introduce a tune dependence on the oscillation amplitude of the bunch particles. The achieved tune spreads follow $\Delta Q_{x,y} = \frac{\partial Q_{x,x}}{\partial \varepsilon_{x,y}} a_x + \frac{\partial Q_{x,y}}{\partial \varepsilon_{y,y}} a_y$ where the single particle "action" $a_\alpha = \frac{\alpha^2 + \alpha'^2 \beta_\alpha}{\beta_\alpha}$, $\alpha = x, y$, and $\frac{\partial Q_x}{\partial \varepsilon_x}$, $\frac{\partial Q_y}{\partial \varepsilon_x}$, $\frac{\partial Q_x}{\partial \varepsilon_y}$ and $\frac{\partial Q_y}{\partial \varepsilon_y}$ are the "amplitude detuning coefficients". By changing one of the amplitude detuning coefficients, $\frac{\partial Q_y}{\partial \varepsilon_y}$, we explored the dependence on the bunch intensity limit octupole magnets could have. The other coefficients are then fixed to $\frac{\partial Q_x}{\partial \varepsilon_x} = 424.9$ m^{-1}, $\frac{\partial Q_{x,y}}{\partial \varepsilon_{y,x}} =$ -878.0 m^{-1}. These values are taken from SPS measurements [109] where also $\frac{\partial Q_y}{\partial \varepsilon_y} = 1155.0$ m^{-1} was given. Amplitude detuning does damp instabilities in the DR, however for every instability damping, there is an unacceptable transversal emittance growth of the beam. This is shown in figure 54**(f)** where a scan over $\frac{\partial Q_y}{\partial \varepsilon_y} \in [0, 2000] m^{-1}$ was performed but no relaxing in N_b^{th} could be claimed due to a parallel check in emittance growth. Even if as much as double transversal emittance growth was allowed the damping due to amplitude detuning had no impact.

Table XIV. First four columns show the ion pair, assumed yearly neutrino fluxes, number of years for run and the θ_{13} sensitivities, from [80]. The fifth column show single bunch ion intensity limit compared to nominal intensity necessary for the neutrino fluxes in the 2nd column. These results are based on transverse resonance broad band impedance studies for the DR (assuming $R_\perp = 1$ MΩ/m).

Ions	ν-Flux $[10^{18}]$	Years	$(\sin^2\theta_{13})_{min}$	N_b^{th}/N_b^{nom} in DR
^{18}Ne	$\phi_0 = 1.1$	5	$5{\cdot}10^{-4}$	0.20
^{6}He	$\bar{\phi}_0 = 2.9$	5		1.31
^{18}Ne	$\phi_0/2$	8	$6{\cdot}10^{-4}$	0.41
^{6}He	$\bar{\phi}_0 \times 2$	2		0.65
^{8}B	$\phi_0 \times 5$	5	$2{\cdot}10^{-4}$	0.15
^{8}Li	$\bar{\phi}_0 \times 5$	5		0.15

5. *Results for All Ions*

From equation (21) we can extract that $N_b^{th} \propto \frac{A}{Z^2}$. This is used for estimations of bunch intensity limit for all the different radioactive ions investigated for the Beta Beams. For example, figure 54**(d)** gives that maximum $7{\cdot}10^{11}$ Neon ions can populate each bunch in the DR assuming $R_\perp^{DR}$=1 MΩ/m. This gives then that maximum number of Helium ions allowed per bunch is estimated with equation (21) to be $N_b^{th} = 7{\cdot}10^{12}(6/18)/(2/10)^2 = 5.8{\cdot}10^{12}$. The required number of ions per bunch, N_b^{nom}, necessary to reach nominal neutrino flux, ϕ_0, is for the DR given by;

$$N_b^{nom} = \frac{\phi_0 T_C}{N_B \ell_{eff} T_{eff}} \left(1 - 2^{-\frac{T_C}{\gamma t_{1/2}}}\right)^{-1} \quad (22)$$

where T_{eff}=10^7 seconds and all other parameters are given in table XIII. We get from Table VII that $N_b^{nom} = 4.7{\cdot}10^{12}$ number ^{6}He per bunch is necessary in the DR to achieve $\phi_0 = 2.9{\cdot}10^{18}$. So the bunch intensity limit for ^{6}He, taking into account a transversal shunt impedance of $R_\perp = 1$ MΩ/m, is actually bigger than necessary; $N_b^{th}/N_b^{nom} = 1.3$. This is however not the case for ^{18}Ne as can be seen in table XIV; only 20% of required bunch intensities would be possible before collective effects would cause instabilities and beam loss. To use the excess of allowed ^{6}He ions and mitigate the deficiency of allowed ^{18}Ne it was suggested to aim for double ^{6}He intensity and half ^{18}Ne intensity. This turned out to have similar physics reach but only half the required bunch intensities would in that case be possible for both ions (see the middle setup in table XIV). One way to solve this would be to make the DR a two bore machine [110]. The larger deficiencies for high Q ion pair, ^{8}B and ^{8}Li, in the DR are however not as easily solved.

6. Stability of Beam, Conclusions

Collective effect studies for the Beta Beam Decay Ring and SPS have been performed taking into account transversal shunt impedance of $R_\perp^{DR} \approx 1$ MΩ/m and $R_\perp^{SPS} = 20$ MΩ/m respectively. The DR study indicates that there will be large challenges due to requirements of seemingly low transverse broadband impedance. The bunch intensity limits in the SPS indicates that completely new solutions are necessary, possible even a "green-field" Beta-Beam.

The analysis software developed for these Beta Beam studies are general, object oriented and can easily be used for any beams [111].

G. Conclusion

Several aspects of the Decay Ring were studied in EUROnu. A new lattice was proposed enlarging the momentum compaction to push the intensity limits. An important advantage of this optics is to have very regular FODO lattices in the arcs, however more RF power and more dipoles are needed. In the case of a $\gamma = 100$ Decay Ring, the required superconducting magnets with coil free mid-planes (arcs and injection section) may profit of existing technology; however development times are about 10 years. An alternative solution to the merging, barrier buckets, is not promising in the range of parameters we use. A first design of the 40 MHz cavities for the decay ring has been presented and a solution to the beam loading generated by the high beam intensities could be proposed. Collective effects, in particularly the head tail effects, will not permit the decay ring with its present design to store the required ion intensities. Some solutions using multipoles to mitigate the head tail effects were investigated without success. However, with the new values measured of the neutrino oscillation angle θ_{13} the duty factor of the Decay Ring may be relaxed, see section X below.

X. POSSIBLE OPTIMIZATIONS IN VIEW OF BETTER PHYSICS

The Beta Beam is essentially limited by the production and the beam stability. According to simulations, where only known losses are taken into account (decay losses, looses at the transfer from one machine to another, losses from merging in the Decay Ring), the presently achieved results for the production will give the number of neutrinos used by the physics evaluations to make the performance cost comparison. However, the fact that the oscillation angle θ_{13} is relatively large means that the suppression of atmospheric neutrinos could be relaxed. Preliminary simulations show that the duty factor of the Decay Ring (the distribution of the available intensity in the bunches) may be increased from 0.5 % to 2% without significant loss in physics potential, assuming that the same intensity is delivered to the experiments. For the machines however, this may give better possibilities to have a stable beam by having more bunches with lower intensities, implying however that the bunching of the Beta Beam in all machines may need to be reconsidered. Losses will be reduced and the longitudinal merging at injection into the Decay Ring could be optimized to mitigate losses. This work remains to be done.

XI. COSTING

The costing is an important ingredient to be able to select a way to proceed in preparing the strategic work to place (or not) these facilities in a global planning for the future.

The costing has been done in close collaboration between the three facilities to arrive at comparable costing scenarios. The lack of available technical expertise for this non trivial task has made it necessary to make many assumptions and apply scaling. For the Beta Beam we are grateful for the help we could get from different groups at CERN in spite heavy work-load for other activities. The result of the costing will be a separate document, common for the 3 facilities, the Super Beam, the Beta Beam and the Neutrino Factory.

XII. CONCLUSION AND FOLLOW UP

The work on Beta Beams within EUROnu has essentially addressed the following topics

- design of a small storage ring for isotope production
- development of a new approach to production using a molten salt loop
- cross section measurement for the production of the high-Q isotopes
- collection of the produced isotopes
- possible use of barrier buckets to gain intensities at injection into the Decay Ring
- simulations of the beam in the CERN machines: Q-scan in the PS and stability calculations in the Decay Ring and the SPS
- development of a 60GHz Electron Cyclotron Resonance Source
- tuning of the Decay Ring lattice for beam stability
- optimization work on the decay ring and the cycling of the machines using the information on θ_{13}

The work has shown that the Beta Beam is now feasible, however work remains to produce a technical design: a list of the most important items for the Beta Beam baseline option (^{6}He and ^{18}Ne) would be

- a Linac 160 MeV, 1.2 MW, technical design
- ^{6}He production full scale prototype with acceleration
- ^{18}Ne full scale prototype
- some adjustments of the magnetic field shape for the 60 GHz ion source before design and construction
- technical design of the two RFQs and stripping
- technical design of the RCS
- technical design of the Decay Ring, including beam dumps and instrumentation
- the PS injection system
- PS space charge measurements
- collective effects and RF-studies of the SPS
- technical design of the safety related equipment and radio protection studies in all machines
- shielding in all machines

XIII. TIME LINE FOR THE CONSTRUCTION OF A BETA BEAM

To give a minimum time scale, the most time-demanding item should be pulled out; this is the Decay Ring magnet development. The construction of an ion Linac and the RCS are also major projects. The other research topics could be made simultaneously. Initial R&D is necessary, however the research topics are very different and can be done by different groups and laboratories simultaneously. The validity of this approach depends on available resources and the how they can be deployed. The Decay Ring magnet design and model construction are estimated to 2.5 years: magnet full length prototype would be 2 years, tendering for series production (materials, superconductor and assembly contracts) would take 0.75 year. Tooling construction for production (superconductors and material deliveries) would be one year and to produce 152 magnets would take 3 years. In total 9.25 years from the start of the magnet design. The resistive magnets (series of 30 magnets) would in principle be possible to produce simultaneously during 3 years. In figure 55 is shown the time-line of the civil engineering work. It is assumed this can be done in parallel to magnet development.

Installation and commissioning time have been estimated to one year each.

Figure 55. Time-line for the civil engineering of the Beta beam facility

In table XV estimated shortest time taken for different parts of the construction installation is shown.

XIV. SAFETY ASPECTS FOR THE BETA BEAM

The work on safety for the EUROnu Beta Beam is limited to a brief overview of aspects of safety and a list of presently known items to care about.

The long acceleration time, 3.6 s in the PS for both ^{6}He and ^{18}Ne and 3.6 s in the SPS for ^{6}He and 6 s for

Table XV. Beta Beam development and construction

Initial R&D	3	years
Decay Ring Magnets	10	years
Installation	1	year
Commissioning	1	year
Total	**15**	**years**

^{18}Ne, causes decay losses of about 50 % for ^{6}He and 20 % for ^{18}Ne before the beams are accelerated to $\gamma = 100$.

For the PS and the SPS machines no specific modifications concerning the safety aspects can be seen. Some radio protection issues are specific to beta Beams and have to be further investigated in particular localized losses; the overall radio protection has been studied for the RCS, the PS and the Decay Ring, see **??**. Areas of controlled access or remote handling identified.

For the new machines, the Cryogenic Decay Ring, the RCS and the new beam lines it is assumed that the experience for the LHC can be used. A tentative list of items, valid for all machines, would be the following:

- access system
- fire detection system
- evacuation alarm system
- gas detection system
- oxygen deficiency hazard detection (cold machine)
- ventilation
- electrical risks (powering interlocked with Access System)
- cryogenic risks (cold machine)
- civil engineering and construction
- lifting and handling

Radio Protection is well established at CERN for all what are environmental and legal issues. The following items need special attention.

Environment (dose to public):

- stray radiation
- releases of radioactivity into the environment (air & water)

Workers:

- shielding
- air & water activation Induced radioactivity in accelerator components:
- activated fluids and contamination risk (closed circuits, etc.)
- optimized design of components (material composition)
- optimized design for maintenance and repair
- optimized handling of devices, remote handling
- ventilation and pressure cascades

A few items in the Decay Ring need special attention

- momentum collimators
- SC-magnets in radioactive environment, how to deal with losses in the arcs, maintenance (remote handling?)
- impedance considerations for absorbers and collimators

A radiation monitoring system (likeRAMSES) is needed as well as buffer zones for cool down and a repair workshop (access control, filters and fire proof areas have to be installed). Operational dosimetry systems and closed loops for cooling water, as well as remote systems for maintenance & remote handling need to be investigated as well and will add to the cost of the facility. An expensive item not to forget is provision for the dismantling and waste handling; these costs are in general high.

The ECR Breeder in the production area creates high magnetic fields and high voltages. Microwaves and x-rays have to be monitored and need controlled access. The safety conditions for the production in the ISOLDE area (^{6}He and ^{18}Ne) will follow already known procedures (ISOLDE at CERN and and SPIRAL2 at GANIL). If the high-Q option is used the high pressure in the gas jet target would be a safety item, Lithium in contact with water has to be avoided, and the collection device has an oven of high temperature which also has to be put on th list of safety related items.

ACKNOWLEDGMENTS

We acknowledge the financial support of the European Community under the European Commission Framework Program 7 Design Study: EUROnu, Project Number 212372. The EC is not liable for any use that may be made of the information herein.

We would like to thank L. Maran, S. Marigo, A. Minarello, and L. Pranovi for the excellent technical support during the experiment at LNL for the measurements of 8Li and cross section and we are grateful to Prof. S.A. Goncharov for the theoretical ZR-KO-DWBA calculations and the fruitful discussions.

We also acknowledge the help for costing of the different pieces of equipment, given by the expert groups at CERN (L. Bottura, G. de Rijk, E. Todesco, D. Tommasini, L. Tavian, A. Perin, J.-P. Burnet, J. Osborne, C. Waaijer, A. Kosmicki, L. Scibile, T. Pettersson, R. Catherall, H. Schmickler)

[1] P. Zucchelli, Phys. Lett., **B532**, 166 (2002).

[2] Final report of the EURISOL design study (2005-2009),

a Design study for a European Isotope-Separation-On-Line radioactive ion beam facility, EU Contract 515768 (2009).

[3] C. Rubbia, A. Ferrari, Y. Kadi, and V. Vlachoudis, Nucl. Instrum. Meth., **A568**, 475 (2006), arXiv:hep-ph/0602032.

[4] T. Stora, in *CERN Yellow Report, CERN-2010-003* (2010).

[5] F. P. An *et al.*, Phys. Rev. Lett, **108:171803** (2012).

[6] A. Lachaize and A. Tkatchenko, EURISOL DS task note 12-25-2008-0012 (2008).

[7] A. Chancé, PhD thesis, Université Paris Sud (2007).

[8] FP7 INFRA-2007-2.1-01, ref. 212343.

[9] J. Osborne, A. Kosmicki, and C. Waaijer, https://edms.cern.ch/document/1223890/1.

[10] *Final Report of the EURISOL Design Study*, Tech. Rep. (J. Cornell Ed, GANIL, 2009).

[11] H. Ravn and B. Alardyce, *"On-line mass separators", Treatise on heavy-ion science*, edited by D. Bromley (Plenum Press, New York, 1989).

[12] T. Stora, E. Noah, R. Hodak, T. Hirsch, M. Hass, V. Kumar, K. Singh, S. Vaintraub, P. Delahaye, H. Franberg-Delahaye, M.-G. Saint-Laurent, and G. Lhersonneau, European Physics Letters, **98**, 32001 (6pp.) (2012).

[13] *ENDF Database, http://www-nds.iaea.org/exfor/endf.htm*.

[14] T. Stora, E. Bouquerel, and J. Lettry, *EURISOL-DS, TN03-25-2006-0003*, Tech. Rep. (2006).

[15] L. Penescu, R. Catherall, J. Lettry, and T. Stora, Review of Scientic Instruments, **81**, 02A906 (2010).

[16] M. Lagunas-Solar, Nuclear Instruments and Methods in Physics Research B, **69**, 452 (1992).

[17] D. Williams, *Assessment of candidate molten salt coolants for the NGNP/NHI heat-transfer loop, ORNL/TM-2006/69*, Tech. Rep. (Oak-Ridge National laboratory, 2006).

[18] D. Williams, L. Toht, and K. Clarno, *Assessment of candidate molten salt coolants for the advanced high-temperature reactor, ORNL/TM-2006/12*, Tech. Rep. (Oak-Ridge National Laboratory, 2006).

[19] *www.haynesintl.com/pdf/h3142.pdf*.

[20] V. Parkhomchuk and A. Skrinsk, Sov. J. Nucl. Phys., **12:3** (1981).

[21] D. Neuffer, Nucl. Instrum. Methods Phys. Res. A, **532:26** (1981).

[22] M. Schauman, CERN-THESIS-2009-128, EUROnu-WP4-004 (2009).

[23] E. Benedetto, IPAC10 (2010).

[24] D. B. R.E. Marrs and E. Adelberger, Phys. Rev. C, **8**, 427 (1973).

[25] C. McClenahan and R. Segel, Phys. Rev. C, **11**, 370 (1975).

[26] C. Amsler *et al.*, Physics Letters B, **1**, 667 (2008).

[27] O. Boine-Frankenheim *et al.*, Nuclear Instruments and Methods in Physics Research Section A, **560(2)**, 245 (2006).

[28] D. Neuffer, Nucl. Instrum. Methods Phys. Res. A, **585(3):109-116** (2008).

[29] M. S. E. Benedetto and J. Wehner, Proceedings European Strategy for Future Neutrino Physics Workshop, CERN (2009).

[30] E. Benedetto, CERN ATS/Note/2011/094 TECH (2011).

[31] M. Boucheron *et al.*, CERN-PS-90-15-RF (1990).

[32] E. V. et al., Phys. Rev. ST (2012).

[33] W. W. et al., Phys. Rev. Lett., **91**, 252501 (2003).

[34] P. V. der Merwe et al., Nucl. Phys. A, **103**, 474 (1967).

[35] N. Colonna *et al.*, Nucl. Inst. Meth. A, **381**, 472 (1996).

[36] S. Goncharov, Private Communication.

[37] G. Satchler, Clarendon Press, Oxford, **833** (1983).

[38] B. Bayman and A. Kallio, Phys. Rev., **156**, 1121 (1967).

[39] P. Kunz, The Code DWUCK4.

[40] X. L. C.T. Liang and C. Cai, Journ. Phys. G, **36**, 085104 (2009).

[41] J. Dave and C. Gould, Phys. Rev. C, **36**, 2212 (1983).

[42] E. Fioretto *et al.*, IEEE Trans. Nucl. Sci., **44**, 1017 (1997).

[43] J. Schiffer *et al.*, Phys. Rev., **164**, 1274 (1967).

[44] S. Abramovich *et al.*, Jour. Izv. Rossiiskoi Akademii Nauk, **50**, 65 (1986).

[45] R. Geller, "Specified elements of plasma physics applied to electron cyclotron resonance ion sources (*ECRIS*)," in *Electron cyclotron resonance ion sources and ECR plasmas*, edited by B. IOP (1996) Chap. 1, pp. 1–146.

[46] T. Thuillier, J. Bouly, J. Curdy, E. Froidefond, and T. Lamy, in *Proceedings of the EPAC 2002* (2002) pp. 1744–1746, http://accelconf.web.cern.ch/AccelConf/e02/PAPERS/THPRI015.p

[47] T. Thuillier, T. Lamy, L. Latrasse, I. Izotov, A. Sidorov, V. Skalyga, V. Zorin, and M. Marie-Jeanne, Review of Scientific Instruments, **79**, 02A314 (2008).

[48] T. Lamy, L. Latrasse, T. Thuillier, M. Marie-Jeanne, C. Trophime, F. Debray, P. Sala, J. Dumas, C. Fourel, J. Giraud, I. Izotov, A. Sidorov, V. A. Skalyga, and V. Zorin, *Bunched efficiency advanced study - 60 GHz*, Final report on task 9: beam preparation (EURISOL Design Study, 2009).

[49] O. Tarvainen, T. Ropponen, V. Toivanen, T. Kalvas, J. Komppula, *et al.*, in *Proceedings of the VIIIth international workshop on Strong Microwaves and Terahertz Waves: Sources and Applications* (2011).

[50] I. V. Izotov, A. V. Sidorov, V. A. Skalyga, V. G. Zorin, T. Lamy, L. Latrasse, and T. Thuillier, IEEE Transactions on Plasma Science, **36/4**, 1494 (2008).

[51] V. Zorin, V. Skalyga, I. Izotov, S. Razin, A. Sidorov, *et al.*, in *XIXth International Workshop on ECR Ion Sources (ECRIS 2010)* (2011).

[52] V. Zorin, V. Skalyga, I. Izotov, S. Razin, A. Sidorov, *et al.*, in *8th International Conference on Open Magnetic Systems for Plasma Confinement (OS2010)* (2010).

[53] L. Latrasse, M. Marie-Jeanne, T. Lamy, T. Thuillier, J. Giraud, C. Fourel, C. Trophime, F. Debray, P. Sala, and J. Dumas, Review of Scientific Instruments, **81**, 02A324 (2010).

[54] F. Debray, J. Dumas, C. Trophime, and N. Vidal, IEEE Transactions on Applied Superconductivity - MT22 proceedings special issue, **22/3** (2012).

[55] M. Marie-Jeanne, J. Jacob, T. Lamy, L. Latrasse, F. Debray, J. Matera, R. Pfister, and C. Trophime, in *Proceedings of the XIXth ECRIS workshop* (2011).

[56] T. Lamy, F. Debray, I. V. Izotov, M. Marie-Jeanne, A. V. Sidorov, V. A. Skalyga, P. Sortais, T. Thuillier, C. Trophime, E. Verney, N. Vidal, and V. G. Zorin, in *Proceedings of the VIIIth international workshop on Strong Microwaves and Terahertz Waves: Sources and Applications* (2011).

[57] T. Lamy, M. Marie-Jeanne, P. Sortais, T. Thuillier, I. Izotov, *et al.*, in *13th International Workshop on Neutrino Factories, Super Beams and Beta Beams (NUFACT 11)* (2011).

[58] T. Lamy, L. Latrasse, M. Marie-Jeanne, F. Debray, P. Sala, and C. Trophime, IEEE Transactions on Applied Superconductivity - MT22 proceedings special issue (2011).

[59] B. Pardo, C. Trophime, S. Veys, and C. Prud'homme, *Toward robust and reliable numerical modeling of the radially cooled helices*, Annual Report (LNCMI Grenoble, 2011).

[60] M. H. Rashid, C. Mallik, and R. K. Bhandari, in *XVIIIth International Conference on Cyclotrons and Their Applications (CYCLOTRONS07)* (2011).

[61] D. Leitner, M. L. Galloway, T. J. Loew, C. M. Lyneis, I. Castro Rodrigue, and D. S. Todd, Rev. Sci Instrum., **79**, 02C710 (2008).

[62] M. Bakulin, A. Chirkov, G. Denisov, A. Eremeev, Z. Gasajniev, *et al.*, in *24th Joint Russian-German Meeting on ECRH and Gyrotrons* (2012).

[63] A. Bechtold and H. Podlech, European Particle Accelerator Conference (EPAC) (2006).

[64] E. Benedetto, S. Damjanovic, S. Gilardoni, and E. Wildner, BetaBeams in the CERN-PS: 2011 studies, note in preparation.

[65] E.Benedetto, IPAC2011 (2011).

[66] A. Chancé, *Étude et conception de l'anneau de désintégration d'une usine à neutrinos utilisant les décroissances β des noyaux Hélium 6 et Néon 18 produits par un faisceau intense de protons frappant diverses cibles.*, Ph.D. thesis, Université Paris Sud (2007), dapnia-07-06-T.

[67] A. Chance and J. Payet, Conf.Proc., **C060626**, 1933 (2006).

[68] A. Chancé, in *Proc. of Science* (Pos(Nufact08)088).

[69] M. Benedikt *et al.*, Eur. Phys. J., **A47**, 24 (2011).

[70] A. Chancé *et al.*, *Decay Ring Design*, Tech. Rep., 12-25-2009-0019.

[71] A. Chance and J. Payet, in *International Particle Accelerator Conference, 2011. PAC 2011. Proceedings of the* (2011).

[72] E. Y. Wildner and F. W. Jones, Particle Accelerator Conference PAC07 25-29 Jun 2007, Albuquerque, New Mexico.

[73] E. Bouquerel, A. Meregetti, and V.Vlachoudis, CERN.

[74] F. Borgnolutti, "Decay ring open mid plane quadrupole magnet design," (2009), 9th Beta-beam Task Meeting.

[75] G. Leleux and P. Nghiem, *Défauts dipolaires et quadripolaires dans une ligne de transport*, Tech. Rep. (Laboratoire National Saturne, 1991).

[76] J. Payet, *Correction des défauts dipolaires*, Tech. Rep. (Laboratoire National Saturne, 1993).

[77] J. Payet, "Code beta, lns version,".

[78] S. Fartoukh and O. Brüning, *Field Quality Specification for the LHC Main Dipole Magnets*, Tech. Rep. (LHC Project Report 501, 2001).

[79] J. W. *et al.*, in *Proc. of EPAC'96* (1996).

[80] A. Donini, (2011), Summary on Beta Beams.

[81] "Lhc design report," (CERN) Chap. BEAM PARAMETERS AND DEFINITIONS.

[82] E. Metral, in *Prepared for 1st CARE-HHH-APD Workshop on Beam Dynamics in Future Hadron Colliders and Rapidly Cycling High-Intensity Synchrotrons, Geneva, Switzerland* (8-11 Nov 2004).

[83] S. van der Meer, Rev. Mod. Phys., **57**, 689 (1985).

[84] S. Myers, *SIMULATION OF SYNCHROTRON ACCUMULATION FOR LEP*, Tech. Rep. CERN-LEP-NOTE-344 (CERN, Geneva, 1981).

[85] S. Nagaitsev, in *19th Particle Accelerator Conference (PAC 2001)* (2001) pp. 715–719.

[86] M. Benedikt and S. Hancock, Nuclear Instruments and Methods in Physics Research A, **550**, 1 (2005).

[87] C. Carli, *Creation of Hollow Bunches using a Double Harmonic RF system.*, Tech. Rep. CERN-PS-2001-073-AE (CERN, Geneva, 2001).

[88] C. Carli and M. Chanel, *Creation of Hollow Bunches by Redistribution of Phase Space Surfaces.*, Tech. Rep. CERN-PS-2002-019-AE (CERN, Geneva, 2002).

[89] M. Benedikt, S. Hancock, and J. L. Vallet, *A Proof of Principle of Asymmetric Bunch Pair Merging*, Tech. Rep. AB-Note-2003-080-MD (CERN, Geneva, 2003).

[90] A. Chance and J. Payet, in *Particle Accelerator Conference, 2005. PAC 2005. Proceedings of the* (2005) pp. 3221 – 3223.

[91] I. Wolfram Research, "Mathematica, version 8.0, champaign, il," (2007).

[92] A. Chance and S. Hancock (2006) pp. 1699–1701.

[93] D. C. Heinrich, C. Hansen, and A. Chance, AIP Conf.Proc., **1382**, 211 (2011), arXiv:1109.1777 [physics.acc-ph].

[94] European Commission, CORDIS, "Homepage of the Sixth Framework Package,".

[95] C. Hansen, E. Wildner, and E. F. Martinez, in *American Institute of Physics Conference Series* (2010) pp. 455–458.

[96] R. Garoby, D. G. Grier, E. Jensen, A. Mitra, and R. L. Poirier, *The PS 40 MHz bunching cavity.*, Tech. Rep. CERN-PS-97-039-RF (CERN, Geneva, 1997).

[97] M. Studio, "Cst gmbh,".

[98] M. Magistris and M. Silari, *Parameters of radiological interest for a beta-beam decay ring*, Tech. Rep. (TIS-2003-017-RP-TN, 2003).

[99] J. Bruer and E. Todesco, IEEE Trans. Appl. Supercond., **19**, 1191 (2009).

[100] J. Bruer, "Open midplane designs based on sector coils in superconducting dipole magnets," (2008).

[101] K. Schindl, , 305 (2003).

[102] A. Chao, "Physics of Collective Beam Instabilities in High Energy Accelerators,".

[103] Y. H. Chin, in *Proceedings of the 8th Joint School on Accelerator Physics* (1998).

[104] G. Rumolo, (2011), Private discussions.

[105] Y. H. Chin, *USER'S GUIDE FOR NEW MOSES: VERSION 2.0 (MODE COUPLING SINGLE BUNCH INSTABILITY IN AN ELECTRON STORAGE RING)*, cERN-LEP-TH/88-05.

[106] Rumolo, Giovanni et al, *Practical user guide for HEADTAIL*, cERN-SL-Note-2002-036-AP.

[107] Weisstein, Eric W., "Least Squares Fitting–Exponential." From MathWorld–A Wolfram Web Resource.

[108] S. Lee, *Accelerator physics* (1999).

[109] R. Thomas et al, AB-Note-2003-025-MD.

[110] E. Wildner, Conference Proceedings for NEUTEL2011 (2011).

[111] C. Hansen, "BBCollective,".